Doctoral Dissertation

Academic Year 2023

Development of the metabolomic analysis method for extracellular vesicles and its application to cancer cell profile analysis

Graduate School of Media and Governance

Keio University

Ryosuke Hayasaka

Doctoral Dissertation

Development of the metabolomic analysis method for extracellular vesicles and its application to cancer cell profile analysis

Abstract

Small extracellular vesicles (sEVs), including exosomes released by cancer cells, play an important role in cancer progression via angiogenesis and the formation of the premetastatic niche. sEVs are lipid bilayer-bound vesicles that contain a variety of molecules, including proteins, lipids, and nucleic acids such as deoxyribonucleic acid (DNA), messenger ribonucleic acid (mRNA), and micro ribonucleic acid (miRNA). Although the relationship between sEVs and cancer has been analyzed extensively, the hydrophilic metabolites contained in sEVs remain unknown. In this study, I constructed a metabolome analysis system for sEVs released by cultured cancer cells to elucidate whether the cancer microenvironment or genetic mutations alter the metabolite content in sEVs. Metabolomic analysis of sEVs recovered from the human pancreatic cancer cell line PANC-1 by ultracentrifugation (UC) revealed that the sEVs contained 140 hydrophilic metabolites and 485 lipids (Chapter 2). The metabolomic profile of the cells differed from that of the sEVs. Hypoxic stress under 1% O_2 altered the metabolite profile of sEVs and increased the loading of angiogenesis-associated metabolites (Chapter 2). However, UC requires a large amount of medium and is unsuitable for the pretreatment of multiple samples. Therefore, I established a semi-automated preparative method based on size-exclusion chromatography (SEC) to improve the recovery of sEVs (Chapter 3). This SEC method, followed by UC, was used to recover sEVs from the human colon cancer cell line HT29 cells. I found that differences in the recovery method resulted in variations, mainly in purine-pyrimidine metabolism, in the sEVs. Furthermore, sEVs derived from mutant strains of isocitrate dehydrogenase 1 (IDH1) contained large amounts of 2-hydroxyglutaric acid (2-HG), an oncometabolite involved in carcinogenesis and cancer progression, suggesting that sEVs may contain oncometabolites (Chapter 4). These results indicate that the metabolite profile of cells and sEVs differ and that the metabolite profile of sEVs is altered by genetic mutations and microenvironments, such as hypoxia. This study contributes to a better understanding of the mechanism of sEV-mediated oncogenic transformation.

Keywords: Cancer, Small extracellular vesicles, Metabolomic analysis, Lipidomic analysis, Hypoxic stress, Isocitrate dehydrogenase 1 mutation

Graduate School of Media and Governance, Keio University
Ryosuke Hayasaka

博士論文題目

細胞外小胞のメタボローム解析系の構築と
がん細胞におけるその代謝物質プロファイル解析への応用

論文要旨

がん細胞が放出するエクソソームをはじめとする小型細胞外小胞 (small Extracellular vesicles ; sEVs) は血管新生や前転移ニッチの形成などがんの進展に重要な役割を担っている. sEVs は脂質二重膜構造をした小胞であり, DNA や mRNA, micro ribonucleic acid (miRNA) のような核酸やタンパク質, 脂質が内包されており, それらとがんの関係性について精力的に解析が行われてきた．その一方，sEVs 中に含まれる親水性代謝物質に関しては不明点が多い現状にあった．本研究では，がんの培養細胞が放出する sEVs を対象にしたメタボローム解析系を構築し，がん微小環境や遺伝子変異による，sEVs 中の代謝物質変化について解析を実施した．膵臓がん細胞株 PANC-1 の培養上清より超遠心法を用いて sEVs を回収し，メタボローム解析を行った．sEVs 中には親水性代謝物質 140 種類，脂質 485 種類が含有しており，これは sEVs の代謝物質解析において定量的に明らかにした最大の同定数であった (第 2 章)．また，細胞と sEVs では異なった代謝物質プロファイルをしていた．1% O_2 の低酸素ストレスによって sEVs 中の代謝物質プロファイルが変化し，血管新生に関与する代謝物質の搭載量の増加が確認された (第 2 章)．一方，超遠心法においては大量の培地が必要であり，かつ多検体の前処理には適さない．そこで，これに代わる新たな sEVs の回収法として，サイズ排除クロマトグラフィー法 (size-exclusion chromatography , SEC) を用いた半自動分取法を構築した．構築した SEC 法と超遠心法を用いて大腸がん細胞株 HT29 細胞より sEVs を回収し，SEC 法で回収した sEVs は sEVs の特徴的な代謝物質をより多く含有することが明らかになった (第 3 章)．さらに，発がんやがんの進展に関与する代謝物質であるオンコメタボライトの 1 つである, 2-hydroxyglutaric acid (2-HG) を多量に産生するイソクエン酸脱水素酵素 1 の変異株由来の sEVs を構築した SEC 法で回収し、2-HG を多量に含んでいることを明らかにした (第 4 章)．本成果は，sEVs に，オンコメタボライトが含まれている可能性を示唆した初めての論文である．これらの結果から，細胞と sEVs の代謝物質プロファイルは異なっており，sEVs の代謝物質プロファイルは，低酸素のような微小環境や遺伝子変異によって変動することが明らかになった．本研究は，sEVs を介したがんの悪性化機構の一端の解明に繋がる可能性がある.

キーワード：がん, 小型細胞外小胞, メタボローム解析, リピドーム解析, 低酸素ストレス, イソクエン酸脱水素酵素 1 変異

慶應義塾大学大学院　政策・メディア研究科

早坂亮祐

Contents

List of figures

List of tables

Chapter 1 Introduction

1.1 Small extracellular vesicles

Exosomes are vesicles with a lipid bilayer structure 50–150 nm in diameter and are released from cells (Théry et al., 2018). They are found in the supernatant of cultured cells and body fluids, such as blood, urine, saliva, tear fluid, amniotic fluid, and bile (Bellio et al., 2021; Erdbrügger et al., 2021; Hefley et al., 2022; Ikeda et al., 2021; Iwai et al., 2016; Muraoka et al., 2022). In 1983, Pan et al. showed that erythrocytes released vesicles with a lipid bilayer structure (Pan & Johnstone, 1983) and named these vesicles exosomes in 1987 (Johnstone et al., 1987). Initially, these vesicles were thought to be "garbage bags" that remove transferrin receptors that are not required by erythrocytes for maturation. From 1999 to 2001, a comprehensive proteomic analysis of dendritic cell-derived exosomes revealed that these exosomes contained various proteins (Théry et al., 1999, 2001). In 2007, exosomes were shown to contain nucleic acids, such as messenger ribonucleic acid (mRNA) and micro ribonucleic acid (miRNA) (Valadi et al., 2007). In addition, the mRNA in exosomes is translated into other incorporated cells (Valadi et al., 2007). In 2010, it became clear that exosomal miRNAs function in other cells (Kosaka et al., 2010; Pegtel et al., 2010; Y. Zhang et al., 2010). Exosomes have been actively studied as tools for intercellular signaling.

Exosomes derive from endosomes (Février & Raposo, 2004). Early endosomes are formed via endocytosis. Early endosomes mature into late endosomes by decreasing the pH, and the late endosomes become distended to form intraluminal membrane vesicles (ILVs). Exosomes are secreted when ILV-rich multivesicular bodies (MVBs) fuse with plasma membranes.

There are two suggested pathways for the uptake of released exosomes into cells: endocytosis and protein-mediated uptake. Exosome uptake can be inhibited by endocytic pathway inhibitors or by low-temperature conditions, suggesting that temperature is important for endocytosis (Escrevente et al., 2011; Morelli et al., 2004). Tetraspanins [e.g., tetraspanin 8 (TSPAN8), cluster of differentiation 9 (CD9), cluster of differentiation 81 (CD81), and cluster of differentiation 49d (CD49d)] (Morelli et al., 2004; Nazarenko et al., 2010; Rana et al., 2012), intercellular adhesion molecule 1 (ICAM-1) (Morelli et al., 2004; Rana et al., 2012), C-type lectin receptors (Barrès et al., 2010), integrins (Hoshino et al., 2015), and other proteins have been implicated in protein-mediated exosome uptake.

However, there are still many unknowns as inhibiting these pathways does not necessarily inhibit uptake.

Vesicles as small as 100–1000 nm that bud directly from the cell membrane are called microvesicles (Raposo & Stoorvogel, 2013). Other vesicles released from cells have various names, including 1–5 μm apoptotic vesicles (Bergsmedh et al., 2001), which are formed by the degradation of cell nuclei and debris from apoptotic cells; prostasomes (Ronquist & Hedström, 1977), which consist of 40−500 nm lipid bilayer membrane vesicles released by prostate epithelial cells; and ectosomes (Stein & Luzio, 1991), which are derived from protoplasmic membranes. Because these particles cannot be strictly distinguished, the International Society for Extracellular Vesicles (ISEV) recommends the use of a collective name extracellular vesicles (EVs). In this study, the terms EVs and small EVs (sEVs, < 200 nm) conform to this definition. The ISEV published guidelines for EV research in 2014 (MISEV2014) (Lötvall et al., 2014), which were revised in 2018 (MISEV2018) (Théry et al., 2018). ISEV defines EVs as a generic term for particles naturally released from the cell that are delimited by a lipid bilayer and cannot replicate, that is, they do not contain a functional nucleus (Théry et al., 2018).

The recovery of EVs presents several problems. Ultracentrifugation (UC) is the gold standard for recovering EVs. However, this method encounters problems such as low recovery rates and damage to the recovered EVs. Other methods include size-exclusion chromatography (SEC), sucrose density gradient centrifugation, precipitation, and affinity purification of membrane-enriched components of EVs [CD9, cluster of differentiation 63 (CD63), CD81, phosphatidylserine (PS)]. The degree of purification and recovery rates for each method of EV recovery differ, and the methods are still under development. In addition, the composition of many buffers is not disclosed, and they may damage the mass spectrometer (MS) and require caution. Fetal bovine serum (FBS) is added to the culture medium during cell culture. However, FBS also contains large amounts of EVs, which must be suppressed. Therefore, it is necessary to use a unique medium without FBS or FBS from which the EVs have been removed.

EVs contain nucleic acids such as deoxyribonucleic acid (DNA), mRNA, miRNA, and non-coding RNA, as well as proteins and lipids (Jeppesen et al., 2019) (Figure 1-1). Their constituents are listed in databases of EV constituents such as

ExoCarta, Vesiclepedia, and EVpedia (Kalra et al., 2012; Keerthikumar et al., 2016; Kim et al., 2015). As of July 2023, Vesiclepedia had 1,254 registered studies with approximately 350,000 proteins, 28,000 mRNAs, 11,000 miRNAs, and 640 lipids (Kalra et al., 2012). These include proteins that are frequently enriched in EVs compared to those in cells, such as CD9, CD63, and CD81, which are four transmembrane proteins; Alix and tumor susceptibility 101 (TSG101), which are multivesicular body-associated proteins involved in EV release, and Syntenin-1, which supports endosomal membrane intraluminal budding (Baietti et al., 2012; Kalra et al., 2012; Keerthikumar et al., 2016; Kim et al., 2015). Conversely, proteins in the nucleus (histones, Lamin A), mitochondria [inner membrane mitochondrial protein (IMMT), cytochrome C, and translocase of outer mitochondrial membrane 20 (Tomm20)], and endoplasmic reticulum or golgi apparatus [Calnexin, heat shock protein 90 beta family member 1 (HSP90B1), heat shock protein family A (hsp70) member 5 (HSPA5), and golgin A2 (GM130)] are absent in the EVs. The absence of one or more of these proteins should be confirmed to check the quality of EV recovery (Théry et al., 2018).

EVs are associated with malignant transformation in many diseases. Compared with normal cells, cancer cells release more EVs. Kilinc et al. investigated the effects of nine oncogenes in releasing EVs in MCF10A cells (Kilinc et al., 2021). They found that myc proto-oncogene protein (MYC) and aurora kinase B (AURKB) release many EVs and alter their protein and miRNA compositions via different mechanisms (Kilinc et al., 2021). Another oncogene, cellular proto-oncogene tyrosine-protein kinase Src kinase (*c-Src*), promotes the release of EVs through the endosomal sorting complex required for transport (ESCRT) (Hikita et al., 2019). EVs are one of the factors involved in the distant metastasis of cancer. In 1889, Paget proposed the "seed and soil" hypothesis, which states that, just as plant seeds grow only on compatible soil, in the distant metastasis of cancer, a specific environment (soil) is vital for cancer cells (seeds) to spread and multiply (Paget, 1889). In addition, interactions between cancer cells and the host organ environment are essential for establishing cancer metastasis. Hoshino et al. identified a subtype of integrin, a membrane protein present on the membrane of EVs that plays the role of a zip code in determining the destination of EVs released by cancer cells (Hoshino et al., 2015). EVs taken up by normal organs form a pre-metastatic niche where cancer cells take up the vesicles and cancer metastasis is complete. The destination of EVs is involved in

determining organ-specific metastasis. Other EVs released by cancer cells are involved in the malignant transformations in cancer, such as angiogenesis (Umezu et al., 2014), proliferation (McCready et al., 2010), treatment resistance (Wei et al., 2014), and immunosuppression (Ye et al., 2016).

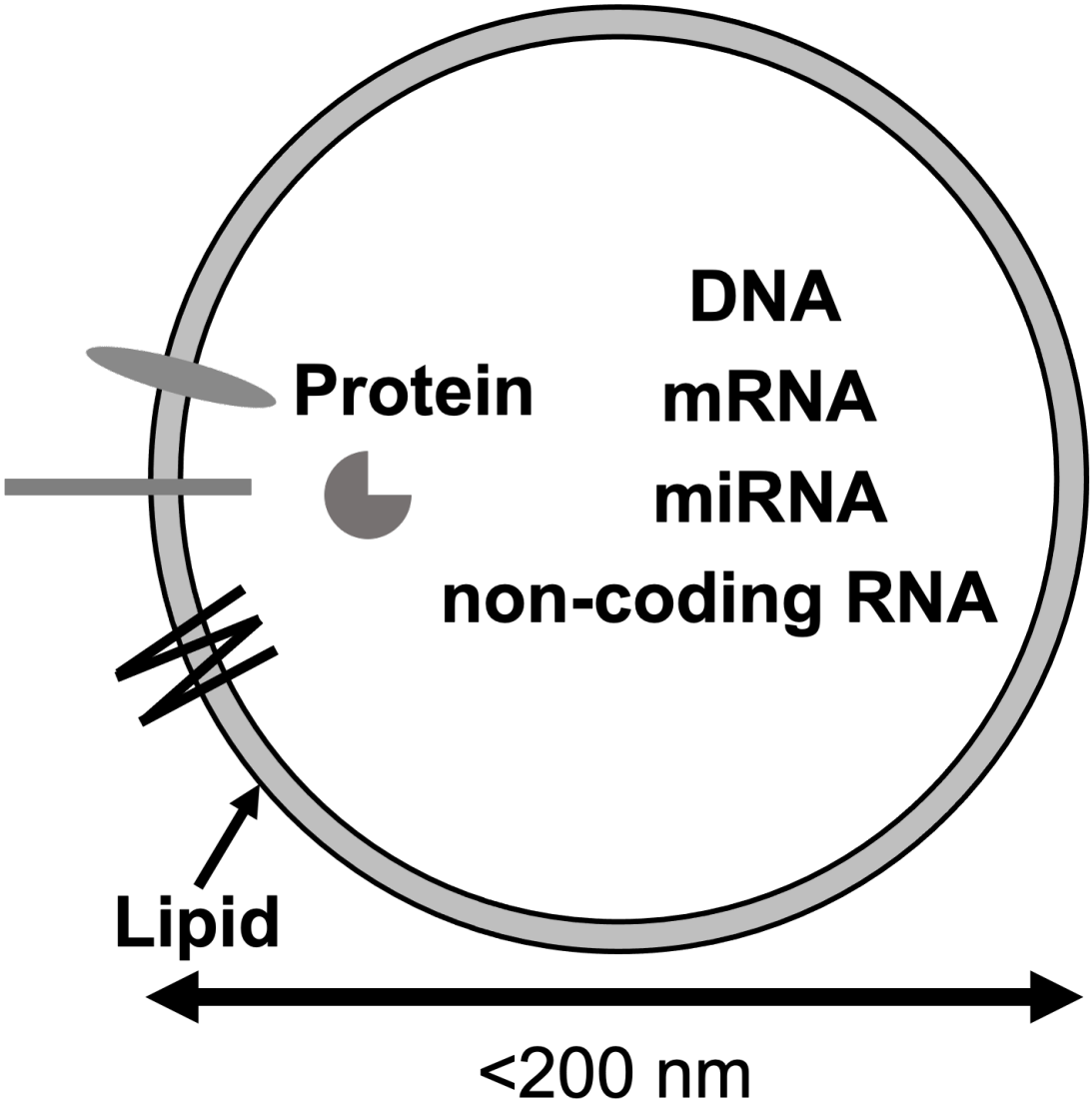

Figure 1-1. Components of small extracellular vesicles (sEVs).

This figure represents the constituents in sEVs analyzed so far.

1.2 Metabolomic analytical methods

1.2.1 Overview of metabolomic methods

Metabolomics is a method for comprehensively analyzing metabolites (1 kDa or less) in samples and is an omics technology, along with genomics, transcriptomics, and proteomics. Metabolomic analysis is performed using nuclear magnetic resonance (NMR) and MS.

Metabolite concentrations *in vivo* range from the order of mmol/L to pmol/L. Two approaches have been used to analyze metabolites: non-target and target analyses. In non-target analysis, metabolites are determined without prior selection and then identified against a database. This method has the advantage that a wide range of metabolites can be measured, and unexpected metabolites can be included. However, this method has the disadvantage that only metabolites with relatively high concentrations can be analyzed, and metabolites with relatively low concentrations are difficult to detect. Targeted analysis is a method in which the metabolites are selected in advance. Although the number of metabolites to be measured is limited, each metabolite can be quantitatively analyzed in samples with a wide range of concentrations *in vivo*. According to the Human Metabolome Database (HMDB), which focuses on metabolites in the human body, approximately 220,000 metabolites have been registered (Wishart et al., 2022). It is impossible to identify metabolites using mass spectrometry alone because metabolites with the same mass-to-charge ratio exist. Therefore, the metabolites have to be separated before MS.

1.2.2 Hydrophilic metabolomic analysis

Three primary metabolomic methods are used to analyze hydrophilic metabolites: amino acids, organic acids, and nucleic acids. The first method, gas chromatography/mass spectrometry (GC/MS), uses gas in the mobile layer and the difference in the desorption temperature between the column and the solid phase to enable measurements with good separation from low to high boiling points. GC/MS is suitable for the analysis of volatile metabolites. When GC/MS is used to measure metabolites that do not vaporize, derivatization, such as trimethylsilylation, is required to vaporize them in a thermally stable manner.

Second, capillary electrophoresis-mass spectrometer (CE-MS) can measure ionic metabolites with good separation without derivatization. Most metabolites in the glycolytic and tricarboxylic acid cycles, which are the central metabolic pathways, are water soluble and can be measured by CE-MS in two ways (Soga et al., 2009; Soga & Heiger, 2000). However, the measurement time easily sifting is a disadvantage of CE-MS. In addition, there is a decrease in sensitivity owing to approximately 200-fold dilution by the mobile phase solution during ionization, and various improvement methods are being considered (Hirayama et al., 2012; Kawai et al., 2019).

The third method is liquid chromatography-mass spectrometer (LC-MS), a general-purpose analytical method that uses a liquid in the mobile layer. LC-MS can separate hydrophilic and hydrophobic metabolites depending on the combination of columns and mobile layers. Various columns are commercially available, including the reversed-phase mode using OctaDecylSilyl, C8, and C4 as packing materials, and the normal-phase mode using silica gel as packing materials. Hydrophilic interaction chromatography (HILIC) is a separation method that has gained popularity in recent years. HILIC separates polar metabolites that are difficult to retain in reversed-phase columns. HILIC uses columns with packing materials modified with highly polar functional groups, such as amide groups and amino acids, and mobile phases, such as water and acetonitrile, utilizing hydrophilic interactions between the stationary phase and polar metabolites. It is suitable for the separation of amino acids.

Capillary ion chromatography-mass spectrometer (IC-MS) has been used since first performed in 2015 by Hu *et al* (Hu et al., 2015). Because of the problems related to the high concentration of potassium hydroxide (KOH), such as ionization suppression and elevated background, the connection with MS has seldom been made. With the development of suppressors, IC-MS has also been used in the field of metabolomics because cations can be efficiently exchanged with hydrogen ions and treated as water. Capillary IC-MS features good retention of highly hydrophilic molecules and good retention time reproducibility, and is a highly sensitive method for separating and measuring anionic metabolites such as nucleotides, sugar phosphates, and organic acids.

1.2.3 Lipidomic analysis

Lipidomic analysis (hydrophobic metabolite analysis) is a comprehensive method of targeting lipids. Lipids play an essential role in living organisms as a source of energy, bioactive substances, and their precursors, in addition to serving as components of the various cellular membranes. A wide variety of lipids exist, including different types of polar groups, lengths of fatty acids, number and location of double bonds in the fatty acids, and combinations of fatty acids. Therefore, efforts are underway to understand the lipid diversity through lipidomic analyses. GC/MS and LC-MS are used for lipid analysis. Recently, supercritical fluid chromatograph-mass spectrometer (SFC-MS) has become popular for lipid analysis. Supercritical fluid (SCF) refers to the state of matter at temperatures and pressures above a critical point. Supercritical fluid chromatography (SFC) uses SCF as mobile phase. In SFC, supercritical CO_2 is formed by applying 7.38 MPa at 31.18°C to CO_2, and SFC is achieved by gradually adding methanol (MeOH) to supercritical CO_2 in the mobile phase. In SFC, supercritical CO_2 is separated from the mobile phase. In the case of SFC-MS, because the retention times are different for each lipid class, the matrix effects can be suppressed using one internal standard for each lipid class. A triple quadrupole mass spectrometer allows quantitative analysis that differentiates between fatty acid side chains by calculating and setting up multiple reaction monitoring (MRM) transitions for each lipid *in silico* that can be used in the field (Si-Hung & Bamba, 2022).

1.3 Metabolomic analysis of EVs

1.3.1 Lipidomic analysis of EVs

The study of lipids in EVs has been ongoing. In 1989, Vidal *et al*. showed that EVs derived from guinea pig membranous erythrocytes contained phospholipids (Vidal et al., 1989). Subsequently, cholesterol, sphingomyelin (SM), PS, and glycosphingolipids were shown to be enriched in EVs relative to cells in many cancers, whereas phosphatidylcholine (PC) and phosphatidylinositol (PI) are diluted (Chapuy-Regaud et al., 2017; Llorente et al., 2013; Phuyal et al., 2015). Cholesterol and SM are enriched, suggesting the formation of lipid rafts, a functional domain of the plasma membrane, on the EV membrane (de Gassart et al., 2003; Simons & Sampaio, 2011). The relationship between the release mechanisms of EVs and lipids has also become evident. A relationship between neutral sphingomyelinase (nSMase), which is involved in the degradation of SM in lipid rafts, and the number of EVs released has been suggested (Trajkovic et al., 2008). Other relationships between intracellular lipid metabolism and EV release have also been reported (Mitani et al., 2022). Lipoproteins with similar diameters are rich in cholesterol ester and triacylglycerol (TAG) (Feingold, 2000) and are known to have a different lipid profile than EVs, with decreased percentages of PC and lysophosphatidylethanolamine (LPE) and increased percentages of alkyl-acyl phosphatidylcholine (ePC), alkyl-acyl phosphatidylethanolamine (ePE), and ceramide (Cer) (Y. Sun, Saito, & Saito, 2019). Recently, EV recovery kits such as the MagCapture™ exosome isolation kit have been developed that use T-cell immunoglobulin and mucin domain-containing protein 4 (TIM4), which binds to PS, a lipid enriched in EVs (Nakai et al., 2016; Skotland et al., 2020).

1.3.2 Hydrophilic metabolomic analysis of EVs

Few studies have been conducted on the hydrophilic metabolites of EVs. In 2015, Vallabhaneni et al. analyzed EVs derived from bone marrow mesenchymal stem/stromal cells and reported the content of lactic and glutamic acids (Vallabhaneni et al., 2015). In 2016, Zhao et al. reported a metabolomic analysis of hydrophilic metabolites in EVs released by cancer-associated fibroblasts (CAFs) in pancreatic and prostate cancer (Zhao et al., 2016). CAFs are major cellular constituents of the tumor microenvironment. EVs

derived from CAFs were recovered with a kit (total exosomes isolation reagent for cell culture media) and the GC/MS metabolomic analysis showed 34 metabolites, including amino acids and organic acids. They also used ^{13}C isotope-labeled amino acids to demonstrate that cancer cells take up and metabolize EVs. Although several other reports have been published (Altadill et al., 2016; Puhka et al., 2017), most literature only discusses the issue at a qualitative level. Most of the studies did not set up appropriate blanks and may have been looking at the effects of metabolites outside the EVs. The relationship between the hydrophilic metabolite profile of cells and that in EVs is unknown.

1.3.3 Problems of the metabolomic analysis of EVs

There are three possible reasons for the lack of progress in metabolomic analysis of EVs. First, the number of EVs that can be recovered is minimal. Frequently studied nucleic acid molecules such as mRNA and miRNA can be amplified and analyzed using relatively small sample volumes. However, a certain amount of EVs is needed because the metabolites cannot be amplified. The second is the effect of metabolites outside EVs. miRNAs and mRNAs have different structures depending on their origin; therefore, it is possible to distinguish whether they originate from human cells. However, in the case of metabolites, there is no distinction between cells and EVs. Therefore, it is necessary to control the effects of large amounts of metabolites in the medium used for analysis. The third factor is the compatibility with MS. Depending on the method used to recover EVs, the composition of many reagents is unknown and some may damage the mass spectrometer. In addition, these methods require a mass spectrometer capable of measuring trace amounts of metabolites with high sensitivity.

1.4 Purpose of this study

In this study, I developed a comprehensive method for measuring metabolites in EVs released by cultured cancer cell lines (Figure 1-2). I then clarified whether metabolite profiles in EVs change depending on the microenvironment and genetic mutations and the differences in metabolite profiles in cells and EVs. In Chapter 2, I developed a method for metabolomic analysis of EVs using UC. I have also focused on hypoxia, a microenvironment involved in the malignant conditions of pancreatic cancer, and its effect on metabolite profiles in EVs (Hayasaka et al., 2021). In Chapter 3, I describe the development of a semi-automated system for fractionating EVs using size-exclusion chromatography. I have elucidated the effects on metabolites of the different methods of EV recovery, the gold standard UC and SEC (Hayasaka et al., 2023). In Chapter 4, I used the constructed method to recover EVs with and without mutations in isocitrate dehydrogenase (IDH) 1 and found that the 2-HG of oncometabolites accumulates due to IDH1 mutations (Hayasaka et al., 2023). Chapter 5 summarizes the thesis and discusses these issues.

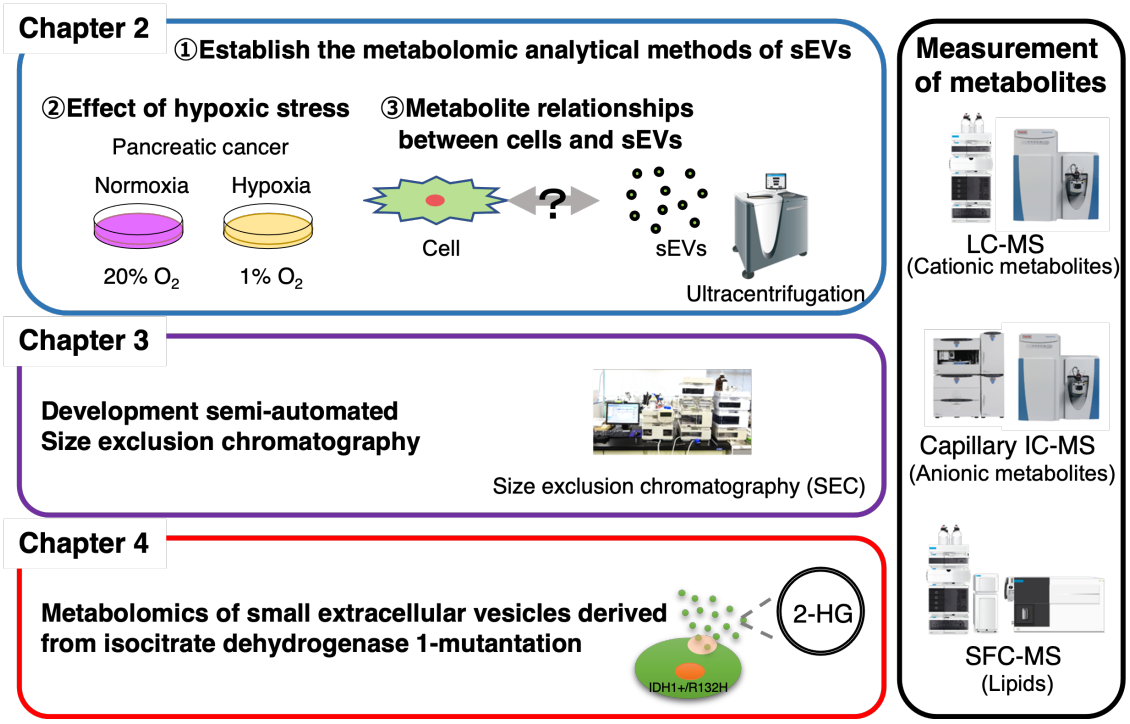

Figure 1-2. Overview of the thesis.

Chapter 2 Metabolomic analysis of small extracellular vesicles derived from pancreatic cancer cells cultured under normoxia and hypoxia

2.1 Introduction

EVs are lipid bilayer structures with a diameter less than 1 μm; they include exosomes (50–150 nm) and microvesicles (100–1000 nm) (Théry et al., 2018). EVs are contained in body fluids, such as blood, urine, and saliva, and are also present in the supernatant of cultured cells (Théry et al., 2018). In addition, they play important roles in promoting cancer progression, such as in distant metastasis, proliferation, angiogenesis, and resistance to treatment (Hoshino et al., 2015; Liu et al., 2012; McCready et al., 2010; Tadokoro et al., 2013). EVs contain DNA, mRNAs, miRNAs, proteins, and lipids, and their amounts vary depending on the type of cell and physiological conditions. Among proteins, tetraspanins, such as CD9, CD63, and CD81, as well as Syntenin-1 and Alix, are found to accumulate in EVs as compared to cells (Jeppesen et al., 2019). Moreover, in various cancer cell lines, lipids including cholesterol, SM, glycosphingolipid, and PS are enriched in EVs, whereas PC and PI are less abundant (Chapuy-Regaud et al., 2017; Laulagnier et al., 2004; Llorente et al., 2013; Trajkovic et al., 2008). Zhao *et al.* reported that EVs derived from cancer associated fibroblasts contain 34 hydrophilic metabolites, including organic acids and amino acids, some of which are metabolized by the recipient's cells (Zhao et al., 2016). Therefore, some of the hydrophilic metabolites contained in EVs are possibly involved in the malignant transformation of cancer (Zhao et al., 2016), but their details remain unclear.

Metabolomic analysis, which comprehensively analyzes metabolites in a given sample, is currently used in various fields, such as cancer metabolism and biomarker research (Hirayama et al., 2009; Satoh et al., 2017; Sugimoto et al., 2010). Because individual metabolites have a wide variety of physical and chemical properties, it is impossible to measure all the metabolites using a single method. Therefore, it is necessary to select an appropriate method for metabolite analysis. GC/MS, LC-MS, and CE-MS have been frequently employed as mass spectrometric methods for metabolomic analysis. Furthermore, in recent years, the development of novel analytical methods has made it possible to measure metabolites using different separation strategies. For example, IC-MS has been developed to analyze highly hydrophilic compounds (Cui et al., 2017; Hu et al., 2015; Petucci et al., 2016; J. Wang et al., 2014). I have also developed a capillary IC-MS method for metabolomic analysis and have reported its high selectivity and sensitivity for anionic metabolites, such as nucleotides, sugar phosphates, and organic

acids (Hirayama et al., 2020). In addition, supercritical fluid chromatography coupled with triple quadrupole mass spectrometer (SFC-QqQMS) has attracted attention as a novel lipid analysis method that can chromatographically separate individual lipid classes and quantify each lipid species without being significantly affected by ion suppression (Takeda et al., 2018).

Pancreatic cancer is the fourth leading cause of cancer-related deaths in the USA (Siegel et al., 2020) and Japan (Hori et al., 2015). The three-year survival rate of pancreatic cancer in Japan is 15.1%, and it is known to be associated with the worst prognosis among all cancers (Hori et al., 2015). Poor prognosis in patients with pancreatic cancer includes difficulty in detection at an early stage, local infiltration, and rapid metastasis. Furthermore, hypoxia is also considered a cause of poor prognosis of pancreatic cancer (Zhu et al., 2014). In various cancers, hypoxia provides a specific microenvironment. Hypoxic stress controls the expression of more than 800 genes involved in energy metabolism, cancer growth, angiogenesis, and apoptosis (Schödel et al., 2011). Metabolism-related genes are also among the genes whose levels are altered under hypoxic stress, which significantly changes the metabolism in cancer cells, aiding their survival (Eales et al., 2016).

Studies on EVs released from cells under hypoxic stress have been reported. In many cancer types, miR-210 is upregulated in both cells and EVs under hypoxic stress and is involved in angiogenesis (Jung et al., 2017). EVs released under hypoxic stress are also involved in the inhibition of natural killer cell function, induction of macrophages to the M2 type, and regulation of T cell proliferation and differentiation in a specific cancer type (Berchem et al., 2016; Chen et al., 2017; X. Wang et al., 2018; Ye et al., 2016). However, the effect of hypoxic stress on the metabolomic profile of EVs remains unclear.

In this study, I comprehensively analyzed the metabolomic profile of cells and EVs derived from the human pancreatic cancer cell line, PANC-1, using three different methods for the analysis of metabolome: capillary IC-MS, LC-MS, and SFC-QqQMS. The target EVs were sEVs with a diameter less than 200 μm, which is closer to that of exosomes. I also investigated the changes in the number of metabolites in sEVs when cells were subjected to hypoxic stress. I found that the metabolomic profiles of cells and sEVs are different, and the levels of metabolites present in sEVs fluctuate under hypoxic stress.

2.2 Materials and Methods

2.2.1 Cell culture

Human pancreatic cancer cells, PANC-1, were obtained from the American Type Culture Collection (ATCC, Manassas, VA, USA). PANC-1 cells were confirmed to be mycoplasma-free using a Mycoalert detection kit (Lonza, Basel, Switzerland). PANC-1 cells were cultured in Roswell Park memorial institute (RPMI) 1640 (FUJIFILM Wako Pure Chemical Corporation, Osaka, Japan), supplemented with 10% (*v*/*v*) FBS (Biowest, Nuaillé, France) and antibiotics (100 U/mL penicillin, 100 mg/mL streptomycin, and 0.25 mg/mL amphotericin B, Nacalai Tesque, Kyoto, Japan), at 37°C in a humidified atmosphere with 5% CO_2 and 20% O_2.

2.2.2 Isolation of sEVs

For isolation of sEVs, 6.0×10^6 PANC-1 cells were seeded in thirteen 150 mm dishes and precultured with RPMI 1640 containing FBS and antibiotics for 24 h. They were washed twice with Dulbecco's phosphate-buffered saline (D-PBS, Nacalai Tesque). Because FBS also includes large amounts of sEVs, it is necessary to change to advanced RPMI 1640 medium (Thermo Fisher Scientific, Waltham, MA, USA) containing 2 mmol/L glutamine (Thermo Fisher Scientific) and antibiotics. Thereafter, the cells were cultured for 48 h under hypoxia (1% O_2) or normal oxygen conditions (n = 3). Fresh (non-cultured) advanced RPMI 1640 medium was used as a blank (n = 3). The cell-conditioned medium was collected and centrifuged at 2000× *g* for 25 min at 4°C to pellet and remove cells, debris, and apoptotic bodies. The supernatant was filtered using a 0.22 μm pore poly ether sulfone (PES) filter (Merck Millipore, Burlington, MA, USA) to remove large sEVs. The filtrate was concentrated with a 100 kDa cut-off filter (Merck Millipore). The concentrate was ultracentrifuged at 37,000 rpm [average relative centrifugal force (RCF) is 234,700× *g*] for 70 min at 4°C (SW41Ti rotor, Beckman Coulter, Brea, CA, USA). The pellet was washed with physiological saline (Hikari Pharmaceutical, Tokyo, Japan) and was collected by ultracentrifuge. This washing procedure was repeated twice. Finally, the weight of the pellet was adjusted to 0.05 g (≈ 50 μL) by adding physiological saline.

2.2.3 Nanoparticle tracking analysis

I measured the number of particles and size distribution by nanoparticle tracking analysis (NTA) (NanoSight LM10, Malvern Analytical, Malvern, UK) (biological n = 3, technical n = 3).

2.2.4 Transmission electron microscopy

Transmission electron microscopy (TEM) analysis was performed by Tokai Electron Microscopy, Inc. The sEV samples were absorbed onto carbon-coated copper grids (400 mesh) and were stained with 2% phosphotungstic acid solution (pH 7.0) for 15 s. The grids were observed using a transmission electron microscope (JEM-1400 plus, JEOL Ltd., Tokyo, Japan) at an acceleration voltage of 100 kV. Digital images were taken with a charge coupled device (CCD) camera (EM-14830RUBY2, JEOL Ltd.).

2.2.5 Enzyme-linked immuno-sorbent assay

Protein levels of CD9 were determined by enzyme-linked immune-sorbent assay (ELISA) (biological n = 3, technical n = 4). 96-well plate were coated anti-CD9 antibodies (ANC-156-820, Ancell Corporation, Stillwater, MN, USA, 1:200) and incubated during one night at 4°C. After 150 μL per well of 5% (*w*/*v*) bovine serum albumin (BSA) was added at room temperature for 30 min, washing with D-PBS 3 times. 50-fold dilution samples after UC were added to the well and incubated for 3 h at room temperature. After washing with D-PBS 3 times, anti-human CD9 (ANC-156-030, Ancell Corporation, 1:2000) was added to the well and incubated for 1 h at room temperature. After washing with D-PBS 3 times, streptavidin (Vector Laboratories Inc., Newark, CA, USA, 1:2000) was added to the well and incubated for 45 min at room temperature. After washing with D-PBS 3 times, 1-Step Ultra TMB-ELISA (Thermo Fisher Scientific) was added to the well and incubated for 15 min at room temperature. The reaction was stopped by adding 2 N HCl, and the wavelength at 450 nm was measured by using an Infinite M200 microplate reader (Tecan, Männedorf, Switzerland).

2.2.6 miRNA analysis of sEVs

Isolation of exosomal miRNAs was performed using the miRNeasy Mini Kit (Qiagen, Venlo, Netherlands). The sEV pellets were dissolved in 100 μL of physiological saline. Five hundred microliters of QIAzol lysis reagent (Qiagen) were added to the sample. After 5-min of incubation, 5 μL of 100 pmol/L *syn-cel-miR-39* (Qiagen) was added to the tube as a spike-in control for losses in preparation. The subsequent steps were performed according to the manufacturer's instructions. For complementary deoxyribonucleic acid (cDNA) synthesis, the TaqMan MicroRNA Reverse Transcription Kit (Thermo Fisher Scientific) was used. Quantitative real-time polymerase chain reaction (PCR) was performed using the TaqMan MicroRNA Assay (Thermo Fisher Scientific) and TaqMan Universal PCR Master Mix, no AmpErase UNG (Thermo Fisher Scientific) on a StepOnePlus Real-time PCR system (Applied Biosystems) according to the manufacturer's instructions. Quantitation was performed using the ΔΔCt method, with synthetic spike control (*syn-cel-miR-39*) used as an invariant control. miRNA data were normalized by the number of particles determined by NTA.

2.2.7 Isolation of cellular RNA and mRNA analysis

PANC-1 cells (ATCC) were seeded in 6-well plates at 2.0×10^5 cells/well and precultured in RPMI 1640 containing 10% (*v*/*v*) FBS, antibiotics under normoxic conditions for 24 h. The cells were washed twice with D-PBS. Thereafter, the medium was changed to advanced RPMI 1640 medium containing 2 mmol/L glutamine and antibiotics. The cells were then cultured for 48 h under hypoxic (1% O_2) or normal oxygen conditions. After washing with D-PBS, the cells were sampled and stored at -80 °C. mRNA was extracted with TRIzol Reagent (Thermo Fisher Scientific) according to the manufacturer's protocol. For cDNA synthesis, a cDNA synthesis kit (ReverTra Ace α, Toyobo, Osaka, Japan) was used. Quantitative real-time PCR was performed using TB Green *Premix Ex Taq*™ II (Takara Bio, Shiga, Japan) on a StepOnePlus Real-time PCR system (Thermo Fisher Scientific) according to the manufacturer's instructions. Quantitation was performed using the ΔΔCt method, with the expression of ribosomal protein L27 (*RPL27*) used as an internal reference. The primers used for real-time PCR are shown in Table 2-1.

Table 2-1. Primer sequences for real-time PCR assays.

Gene Name	Forward Primer Sequence (5′-3′)	Reverse Primer Sequence (5′-3′)
GLUT1	ATCGTCGTCGGCATCCTCAT	TGTCCCGCGCAGCTTCTTTA
LDHA	TATCTTGACCTACGTGGCTT	CATTAGGTAACGGAATCGGG
VEGF	ACCATGAACTTTCTGCTGTC	TACTCCTGGAAGATGTCCAC
CA9	GGATCTACCTACTGTTGAGGCT	CATAGCGCCAATGACTCTGGT
EGLN3	CTGGGCAAATACTACGTCAAGG	GACCATCACCGTTGGGGTT
HK2	GAGCCACCACTCACCCTACT	CCAGGCATTCGGCAATGTG
PGK1	TGGACGTTAAAGGGAAGCGG	GCTCATAAGGACTACCGACTTGG
PFKFB3	TTGGCGTCCCCACAAAAGT	AGTTGTAGGAGCTGTACTGCTT
PFKFB4	TCCCCACGGGAATTGACAC	GGGCACACCAATCCAGTTCA
BNIP3	CAGGGCTCCTGGGTAGAACT	CTACTCCGTCCAGACTCATGC
RPL27	CTGTCGTCAATAAGGATGTCT	CTTGTTCTTGCCTGTCTTGT

2.2.8 Immunoblot analysis

Whole cells and sEVs were extracted using M-PER™ mammalian protein extraction reagent (Thermo Fisher Scientific) containing protease inhibitor cocktails (Roche, Basel, Switzerland). Protein concentration in cells was measured by the Bradford method (Quick Start™ Bradford 1x Dye Reagent, Bio-Rad, Hercules, CA, USA). Protein concentration in sEVs was measured by Micro BCA™ Protein Assay Kit (Thermo Fisher Scientific). Equal amounts of each of protein samples were separated on a 4%–15% Mini-PROTEAN® TGX™ precast protein gel (BioRad) and transferred to a poly vinylidene fluoride (PVDF) membrane (Bio-Rad) using the Trans-Blot® Turbo™ Transfer System (Bio-Rad). Membranes were blocked with the Blocking One reagent (Nacalai Tesque). Antibodies specific for anti-glucose transporter 1 (GLUT1) (ab14683, Abcam, Cambridge, UK), anti-β-actin (sc-47778, Santa Cruz, Dallas, TX, USA), anti-CD63 (ab8219, Abcam), anti-CD81 (ANC-302-020, Ancell Corporation), anti-Syntenin-1 (ab133267, Abcam), and anti-calnexin (Cell signaling Technology, Danvers, MA, USA) were used as primary antibodies. Horseradish peroxidase (HRP) -labeled anti-rabbit Immunoglobulin G (IgG) antibody (Cytiva Marlborough, MA, USA) and anti-mouse IgG

antibodies (Cytiva) were used as the secondary antibodies. The membranes were subjected to chemiluminescent analysis using the Clarity Western ECL Substrate (Bio-Rad) and the images were analyzed using the Image Quant LAS 4000 mini software (Cytiva).

2.2.9 Extraction of hydrophilic metabolites from cells

For metabolite extraction, 3.0×10^5 PANC-1 cells were seeded in 60 mm dishes and cultured as described above. To extract hydrophilic metabolites, cells were washed twice with 4 mL of ice-cold 5% (*w*/*v*) aqueous mannitol and 1 mL of MeOH containing 20 μmol/L internal standards (methionine sulfone and camphor 10-sulfonic acid) was added to each dish. Four hundred microliter of sample solution was transferred into a glass jacket tube. The homogenate was mixed with 100 μL of chloroform. After centrifugation (2,400× *g*, 10 min, 4°C), 200 μL of the upper layer was transferred to a new glass vial. The supernatant was dried using a centrifugal concentrator. Dried samples were dissolved in 50 μL of 50% (*v*/*v*) aqueous acetonitrile and immediately used for hydrophilic metabolome analysis.

2.2.10 Extraction of hydrophilic metabolites from sEVs

Hydrophilic metabolites were extracted from 45 μL of sEV pellet suspension. The sEV pellet suspension was mixed with 200 μL of MeOH containing 1 μmol/L internal standards (methionine sulfone and camphor 10-sulfonic acid) and 50 μL of chloroform. After centrifugation (2,400× *g*, 10 min, 4°C), 150 μL of the upper layer was transferred to a glass vial and concentrated by a centrifugal concentrator. Dried samples were dissolved in 20 μL of 50% (*v*/*v*) aqueous acetonitrile and immediately used for the analysis of the hydrophilic metabolome.

2.2.11 Extraction of lipids from cells

First, I prepared a lipid extraction solvent, supplemented with 10 μL of the mouse SPLASH® LIPIDOMIX® Mass Spec Internal Standard (Avanti Polar Lipids, Alabaster, AL, USA) containing [LPE 18:1 (d7), 2 μmol/L; phosphatidylglycerol (PG)

15:0-18:1 (d7) and alkenyl-acyl phosphatidylethanolamine (pPE) C18 (plasmalogen) - 18:1 (d9), 5 μmol/L; phosphatidylethanolamine (PE) 15:0-18:1 (d7), 7 μmol/L; phosphatidic acid (PA) 15:0-18:1 (d7), 10 μmol/L; diacylglycerol (DAG) 15:0-18:1 (d7), 15 μmol/L; PS 15:0-18:1 (d7), PI 15:0-18:1 (d7), alkenyl-acyl phosphatidylcholine (pPC) C18 (plasmalogen)-18:1 (d9), and SM d18:1-18:1 (d9), 20 μmol/L; TAG 15:0-18:1 (d7)-15:0, 35 μmol/L; lysophosphatidylcholine (LPC) 18:1 (d7), 45 μmol/L; PC 15:0-18:1 (d7), 100 μmol/L; cholesterol ester 18:1 (d7), 250 μmol/L], and 10 μL of internal standard mix [Cer d18:1–17:0, hexosylceramide (HexCer) d18:1 (d5)-18:1, and free fatty acid (FFA) 17:0, 10 μmol/L; monoacylglycerol (MAG) 17:1, 100 μmol/L; cholesterol (d7), 300 μmol/L], and made up the volume to 1 mL with MeOH.

The cells were washed twice with 4 mL of Ice-cold D-PBS and then lysed in 700 μL of the lipid extraction solvent. The supernatant (400 μL) was mixed vigorously with 160 μL of MeOH, 280 μL of chloroform, and 160 μL of Milli-Q water using a vortex mixer for 1 min followed by 5 min of sonication.

After centrifugation (16,000× *g*, 5 min, 4°C), 800 μL of supernatant was transferred to a new tube. The supernatant was mixed vigorously with 220 μL of chloroform and Milli-Q water, and centrifuged (16,000× *g*, 5 min, 4°C). The bottom layer (500 μL) was concentrated to dryness under a nitrogen stream. The dried samples were dissolved in 100 μL of 50% (*v*/*v*) chloroform/MeOH for lipid analysis. Target lipids were determined using a pooled sample prepared with an equal amount of all cells and sEV samples.

2.2.12 Extraction of lipids from sEVs

The lipid extraction solvent (560 μL) was added to 45 μL of sEV pellet suspension. The suspension was mixed vigorously with 280 μL of chloroform and 160 μL of Milli-Q water using a vortex mixer for 1 min followed by 5 min of sonication. The subsequent steps were the same as those described for cells.

2.2.13 Analysis of hydrophilic metabolites

Anionic metabolites were analyzed by capillary IC-MS as previously described

(Hirayama et al., 2020). Briefly, capillary IC-MS was performed using a Dionex ICS-5000+ system coupled with a Q Exactive Orbitrap MS system (Thermo Fisher Scientific, San Jose, CA, USA). Separation of anionic metabolites was performed using a Dionex IonPac AS11-HC-4 μm column (250 × 0.4 mm, 4 μm; Thermo Fisher Scientific). The column temperature was maintained at 35°C. The eluent flow rate was 20 μL/min and the KOH gradient was as follows: 1 mmol/L, 0–2 min; 1 mmol/L to 20 mmol/L, 2–16 min; 20 mmol/L to 100 mmol/L, 16–35 min; 100 mmol/L, 35–40 min; 100 mmol/L to 1 mmol/L, 40–40.1 min; 1 mmol/L, 40.1–45.1 min. To enhance the ionization, iso-propanol containing 0.1% acetic acid was delivered as the make-up solution at 5 μL/min. Sample injection volume was 0.4 μL. The Q Exactive mass spectrometer was operated in electrospray ionization (ESI) negative-ion mode. ESI parameters were as follows: sheath gas, 20 (arbitrary units); auxiliary gas, 10 (arbitrary units); sweep gas, 0; spray voltage, 4.0 kV; capillary temperature, 300°C; S-lens, 35 (arbitrary units). Data were acquired in full MS scan mode and the parameters were as follows: resolution, 70,000; auto gain control target, 1×10^6; maximum ion injection time, 100 ms; scan range, 70–1000 *m/z*.

Cationic metabolites were measured using LC-MS, as described previously (Tadokoro et al., 2020). Briefly, LC-MS analysis was performed using an Agilent 1290 Infinity LC system (Agilent Technologies, Santa Clara, CA, USA) equipped with a Q Exactive Orbitrap MS system. Separations were performed on a SeQuant® ZIC®-pHILIC column (150 × 2.1 mm, 5 μm; EMD Millipore, Billerica, MA, USA). The mobile phase was composed of 10 mmol/L ammonium acetate, pH 9.8 (A) and acetonitrile (B). The flow rate was 0.25 mL/min, and the following linear gradient was used: 0–15 min, 90% to 30% B; 15–18 min, 30% B; 18–19 min, 30% to 90% B, followed by equilibration with 90% B for 15 min. The injection volume was 2 μL, and the column temperature was maintained at 20°C. The Q Exactive mass spectrometer was operated in a heated electrospray ionization (HESI) positive-ion mode using the following source parameters: spray voltage = 3.0 kV, capillary temperature = 250°C, sheath gas flow rate = 40 (arbitrary units), auxiliary gas flow rate = 10 (arbitrary units), auxiliary gas temperature = 300°C, sweep gas flow rate = 0, S-lens = 35 (arbitrary units). Data were acquired in full MS scan mode and the parameters were as follows: resolution, 35,000; auto gain control target, 1×10^6; maximum ion injection time, 100 ms; scan range, 70–1000 *m/z*.

2.2.14 Lipidomic analyses

Lipids were measured by SFC-QqQMS as previously described (Takeda et al., 2018) with modifications. Briefly, SFC-QqQMS experiments were performed using an Agilent 1260 Infinity II SFC system equipped with an Agilent 6470A triple quadrupole LC/MS system with an Agilent jet stream (AJS) ESI interface. Lipids were separated on an ACQUITY UPC2 Torus diethanolamine (DEA) column (3.0 × 100 mm, 1.7 μm; Waters, Milford, MA, USA) maintained at 60°C. The mobile phase comprised supercritical carbon dioxide (A) and 0.1% (*w*/*v*) ammonium acetate in 95% (*v*/*v*) MeOH (B). The flow rate of the mobile phase was 1.0 mL/min. The gradient of solution B was as follows: 1% from 0 min to 1 min, 75% at 24 min, 75% from 24 to 26 min, and 1% at 26.4 min; this was maintained until 30 min. The back pressure regulator was operated at 90 bar and 60°C. The injection volume was 2 μL. To improve the ionization efficacy in ESI, mobile phase B was added as a make-up solution after the backpressure regulator at 0.05 mL/min.

AJS-ESI-MS/MS was operated in a positive/negative ion mode using the following source parameters: dry gas temperature = 300°C, dry gas flow rate = 10 L/min, nebulizer pressure = 30 psi, sheath gas temperature = 350°C, sheath gas flow rate = 12 L/min, capillary voltage = 3.0 kV, nozzle voltage = 0 V, fragmentor voltage = 380 V. Data were acquired using dynamic MRM mode, and the MRM transition setting was based on the in-house lipid MRM library described previously (Takeda et al., 2018).

2.2.15 Data analysis

The data acquired using capillary IC-MS and LC-MS were analyzed using the TraceFinder software (version 3.2, Thermo Fisher Scientific). The raw data obtained by SFC-QqQMS were analyzed using the MassHunter software (version 10.0, Agilent Technologies). To calculate the amounts of metabolites in sEVs and cells, the mol of individual metabolite species detected in the non-cultured medium sample and technical blank were subtracted from sEV and cell samples, respectively. The negative values were changed to zero. The amount of metabolites in sEVs was normalized to the number of particles, and that in cells was calculated with respect to the number of cells. Data of metabolites detected in 50% or more samples were used. Student's *t*-test was used for

statistical analysis. Principal component analysis (PCA) was analyzed using SIMCA (version 13.0, Sartorius Stedim Biotech, Aubagne, France). Coefficient of determination and multiple correlation coefficients were analyzed using GraphPad Prism (version 8.4.3, GraphPad Software, San Diego, CA, USA).

2.3 Results

2.3.1. Isolation of sEVs released from PANC-1 cells cultured under normoxia and hypoxia

I isolated the sEVs released from PANC-1 cells cultured under conditions of 20% (normoxia) or 1% (hypoxia) O_2 by UC (234,700 × *g* for 70 min at 4°C) of 260 mL of conditioned medium. As seen in Figure 2-1A, almost no particles were detected in the NTA of the uncultured medium, but a considerable number of particles were observed in the cell-cultured medium under normoxia and hypoxia (normoxia, 7.8×10^9 particles/mL; hypoxia, 8.6×10^9 particles/mL; $P = 0.41$). The average particle sizes of sEVs obtained under normoxia and hypoxia were 135.6 and 134.1 nm, respectively (Figure 2-1B). TEM revealed that the particles were round and had a lipid bilayer structure (Figure 2-1C). The levels of CD9, which is a marker protein for sEVs, were measured using ELISA. The level of CD9 under hypoxia was 1.2-times higher than under normoxia (Figure 2-1D). In addition, immunoblotting confirmed the presence of other sEV markers, including CD63, CD81 and Syntenin-1, and the absence of endoplasmic reticulum (non-sEVs) marker, calnexin (Figure 2-2). Furthermore, to verify the response to hypoxic stress in cells and sEVs, I examined the expression of genes and miRNAs that have been reported to be upregulated under hypoxia in cells or sEVs (Jung et al., 2017; Schödel et al., 2011). The induction of hypoxia-mediated genes in cells and of miR-210 in sEVs was confirmed (Figure 2-1E, 2-3AB).

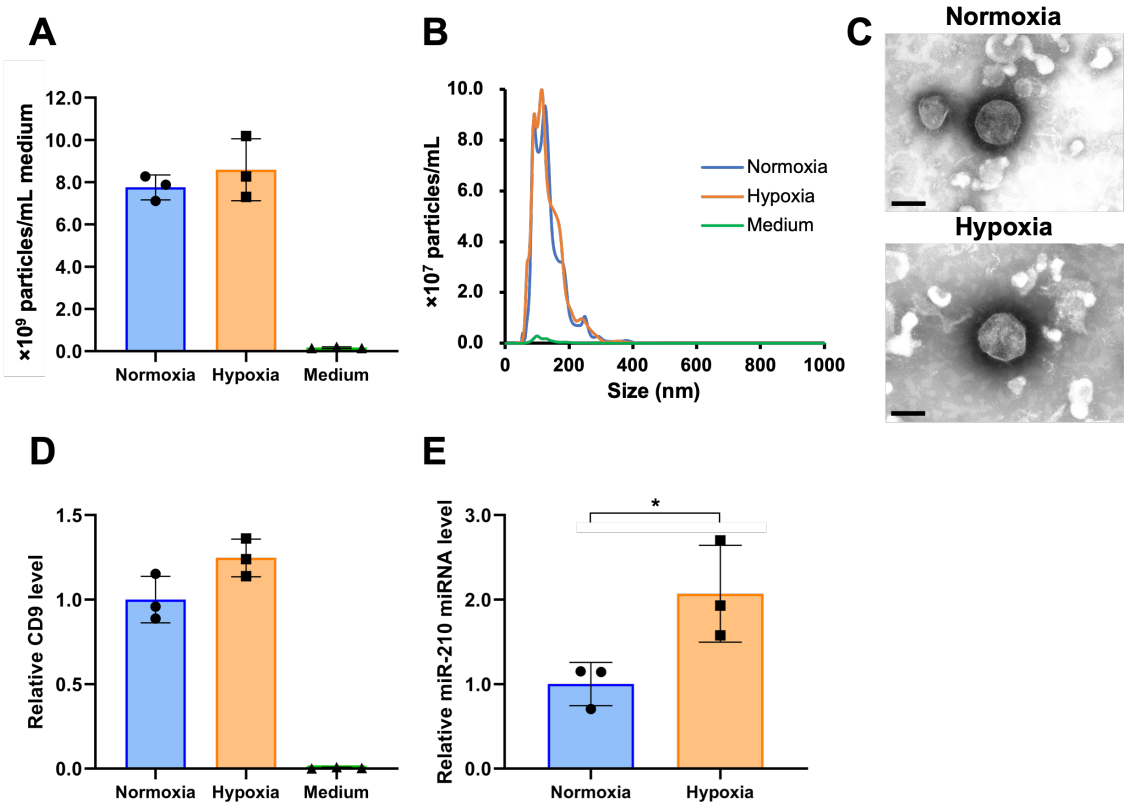

Figure 2-1. Characterization of sEVs derived from PANC-1 cells cultured under different oxygen concentrations.

(A) The number of particles in normoxia, hypoxia, and medium samples. (B) Particle size distribution in normoxia, hypoxia, and medium samples. (C) Transmission electron microscopic images of sEVs under normoxia and hypoxia. Scale bar, 100 nm. (D) The relative expression levels of CD9 in normoxia, hypoxia, and medium samples. (E) The expression level of miR-210 in normoxia and hypoxia samples. The expression data were normalized to the number of particles. Symbols indicate the result of each sample, and the bar graphs indicate the mean ± standard deviation (SD) (n = 3). The Student's *t*-test was used to determine the statistical significance. * *P* value < 0.05.

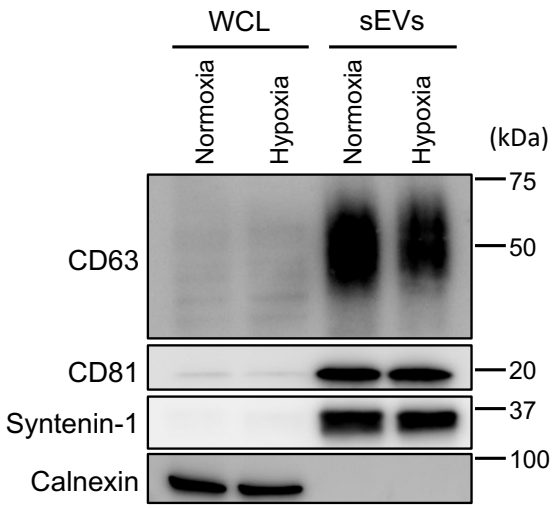

Figure 2-2. Validation of sEVs derived from PANC-1 cells cultured under normoxia and hypoxia.

Immunoblotting of CD63, CD81, Syntenin-1, and calnexin in PANC-1 cells and sEVs under normoxia and hypoxia. sEV markers, CD63, CD81, and Syntenin-1; EV negative protein marker, Calnexin. The protein content was 10 μg for the whole cell lysate (WCL) sample and 1.5 μg for the sEV sample.

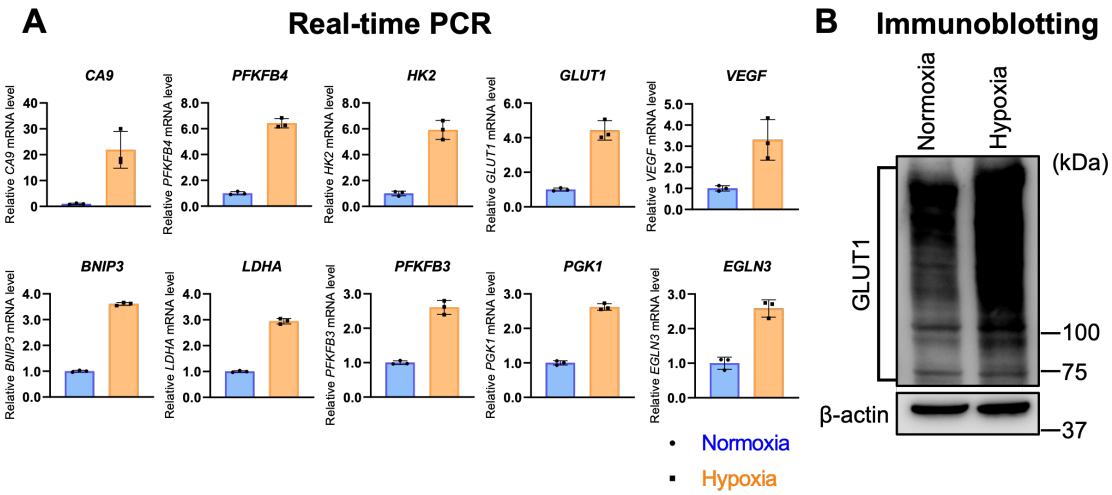

Figure 2-3. Response of PANC-1 cells to hypoxia.

(A) Expression of hypoxia-related mRNAs in PANC-1 cells under normoxia (blue) and hypoxia (orange). Gene expression was determined by real-time PCR. Values were normalized to normoxia. (B) Immunoblotting of GLUT1 in PANC-1 cells under normoxia and hypoxia. β-Actin was used as a loading control.

2.3.2 Analysis of hydrophilic metabolites

2.3.2.1 Relationship of hydrophilic metabolites in cells and sEVs

I analyzed the hydrophilic metabolome of cells and sEVs using capillary IC-MS and LC-MS. For sEVs, to remove the influence of metabolites contained in the medium, uncultured medium was similarly pretreated and analyzed, and the amount of metabolites identified in it was subtracted from those identified in sEVs. A total of 198 and 133 hydrophilic metabolites were detected in more than 50% of cell and sEV samples under normoxia, respectively (Figure 2-4A). Of these, 122 metabolites were common in both the samples. Seventy-six metabolites, including amino acids, such as tryptophan (Trp), beta-alanine (beta-Ala), and gamma-aminobutyric acid (GABA), as well as lactic acid and deoxynucleotides were detected only in cells. In contrast, 11 metabolites, including ribonucleosides, such as cytidine, uridine, and guanosine, were detected only in sEVs (Supplementary Table S2-1). A scatter plot of 122 hydrophilic metabolites that were common in cells and sEVs showed a significant correlation between the two types of samples ($R^2 = 0.5686$, P value < 0.001; Figure 2-4B).

Next, I compared the top 20 most abundant metabolites in cells and sEVs (Table 2-2, Supplementary Table S2-2). Among these top 20 metabolites, seven, viz., phosphorylcholine, glycerophosphory-lcholine, glutamic acid (Glu), ethanolamine phosphate, UDP-*N*-acetylglucosamine, glutamine (Gln), and glycine (Gly), were common to both the samples. Of the 11 metabolites detected only in sEVs, four compounds, namely inosine; *N*,*N*-dimethylglycine; cytidine; and uridine, were included among the top 20 metabolites.

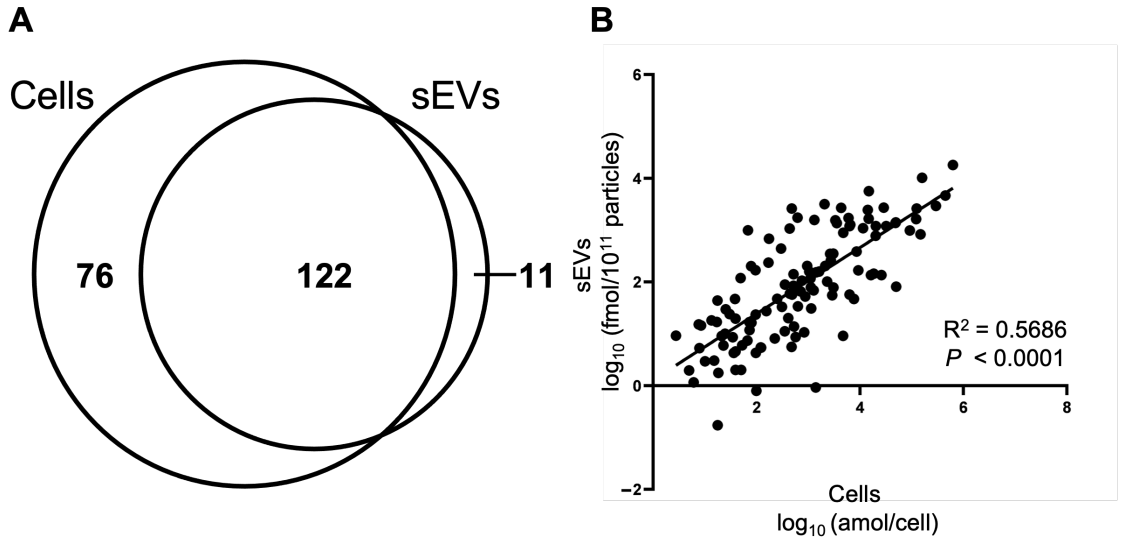

Figure 2-4. The relationship of hydrophilic metabolites presents in cells and sEVs obtained under normoxia.

(A) Venn-diagram representing the number of hydrophilic metabolites detected in cell and sEV samples. (B) Correlation of the hydrophilic metabolites present in cells and sEVs.

Table 2-2. Top 20 hydrophilic metabolites in cells and sEVs under normoxia.

	Cells		sEVs		
Rank	**Metabolite**	**Amount (fmol/cell)**	**Metabolite**	**Amount (pmol/10^{11} particles)**	**Cell Rank**
1	**Phosphorylcholine**	628	**Phosphorylcholine**	18.0	1
2	Glutathione (reduced)	617	**Glycerophosphorylcholine**	10.2	5
3	**Glu**	447	Arg	5.7	24
4	**Ethanolamine phosphate**	294	**Glu**	4.7	3
5	**Glycerophosphorylcholine**	159	Lys	3.2	56
6	Asp	148	**Ethanolamine phosphate**	2.9	4
7	**Gln**	124	Inosine	2.8	−
8	**Gly**	122	**UDP-*N*-acetylglucosamine**	2.7	15
9	Pro	92.1	ADP	2.7	40
10	Lactic acid	77.0	**Gln**	2.6	7
11	ATP	49.9	Glucose 1-phosphate	2.6	95
12	Gly-Gly	49.2	Ala	2.5	26
13	Asn	48.4	GDP	1.7	86
14	*N*-Acetylaspartate	32.2	UMP	1.7	35
15	**UDP-*N*-acetylglucosamine**	28.7	*N,N*-dimethylglycine	1.7	−
16	UTP	26.0	UDP-glucose	1.7	25
17	Citric acid	20.3	**Gly**	1.6	8
18	Creatine	20.0	Cytidine	1.6	−
19	beta-Ala	19.2	Uridine	1.6	−
20	Malic acid	18.4	UDP	1.6	63

The mean values of metabolites are shown. The names in bold font are of metabolites detected in both the samples. Cell rank indicates the rank among all the metabolites quantified in cells.

2.3.2.2 Effect of hypoxic stress on the level of hydrophilic metabolites in sEVs

To investigate the differences in the levels of hydrophilic metabolites in sEVs under normoxia and hypoxia, I performed PCA and volcano plot analysis. The normoxia and hypoxia samples were separated by principal component 1 (Figure 2-5A). The volcano plot shows that the amounts of 2-deoxyribose 1-phosphate, cysteine S-sulfate, and azelaic acid were increased (*P* value < 0.05, fold-change > 1.5), and a decrease was observed for 12 metabolites, namely valine (Val), alanine (Ala), tartaric acid, threonine (Thr), o-acetylcarnitine, adenosine triphosphate (ATP), glycylleucine (Gly-Leu), cytosine triphosphate (CTP), 2-oxoglutaric acid, cytidine, fumaric acid, and hexylamine (Figure 2-5B).

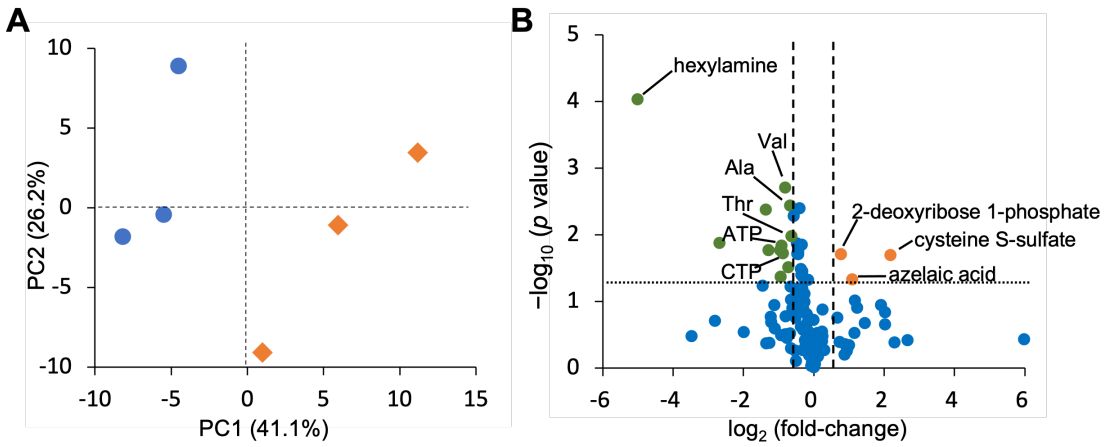

Figure 2-5. Effect of hypoxic stress on hydrophilic metabolite profiles in sEVs.

(A) Principal component analysis (PCA) score plots for normoxia (blue circle) and hypoxia (orange diamond) samples based on hydrophilic metabolome data. The contribution ratios were 41.1% and 26.2% for first principal component (PC1) and second principal component (PC2), respectively. (B) Volcano plot showing the differential accumulation of metabolites under normoxia and hypoxia. The Student's *t*-test was used to determine the *P* value. The plots marked in orange and green are for metabolites that were increased and decreased under hypoxia, respectively. Metabolites that were detected in over 50% samples were included for the analysis. Data were normalized by the number of particles, as quantified by NanoSight. Because hexylamine was detected only under normoxia, its $\log_2$ (fold-change) value is displayed as -5, n = 3.

2.3.3. Lipid analysis

Analysis of lipids in cells and sEVs was performed using SFC-QqQMS. Similar to the measurement of hydrophilic metabolites, the amount of lipids in sEVs was calculated by subtracting the result obtained for the blank sample collected from the uncultured medium. A total of 596 and 485 lipids belonging to 18 lipid classes were identified in cells and sEVs, respectively, and 465 of these were common in both the samples (Figure 2-6A). Table 2-3 shows the number of lipids in each lipid class in the cell and sEV samples. The lipids detected only in cells were PC, PE, PI, and LPC, and of the 20 lipids detected only in sEVs, 12 were DAG.

Next, the relationship between the content of each of the lipid classes in cells and sEVs was examined. In cells, the content of PC (46.6%), cholesterol (18.5%), PE (10.9%), and pPE (9.4%) was relatively higher, whereas that of cholesterol (44.9%), pPE (15.4%), PC (14.7%), and PS (8.3%) was higher in sEVs (Figure 2-6B). A comparison of the ratio of each lipid class to the total lipid content showed that the levels of cholesterol ester (2.9 times), LPE (2.9 times), cholesterol (2.4 times), HexCer (2.4 times), FFA (2.1 times), and PS (2.0 times) increased more than two times in sEVs compared with their respective levels in cells. In contrast, the levels of TAG (0.05 times), PG (0.09 times), PI (0.2 times), PC (0.31 times), PE (0.37 times), LPC (0.44 times), and Cer (0.48 times) in sEVs decreased to less than half of their levels in the cells (Figure 2-6C). Furthermore, the relationship between individual lipids in cells and sEVs was also investigated. Figure 2-6D shows the differences in the levels of 465 lipids that were common in cells and sEVs. Overall, these profiles were adequately correlated ($R^2 = 0.6785$, P value < 0.001).

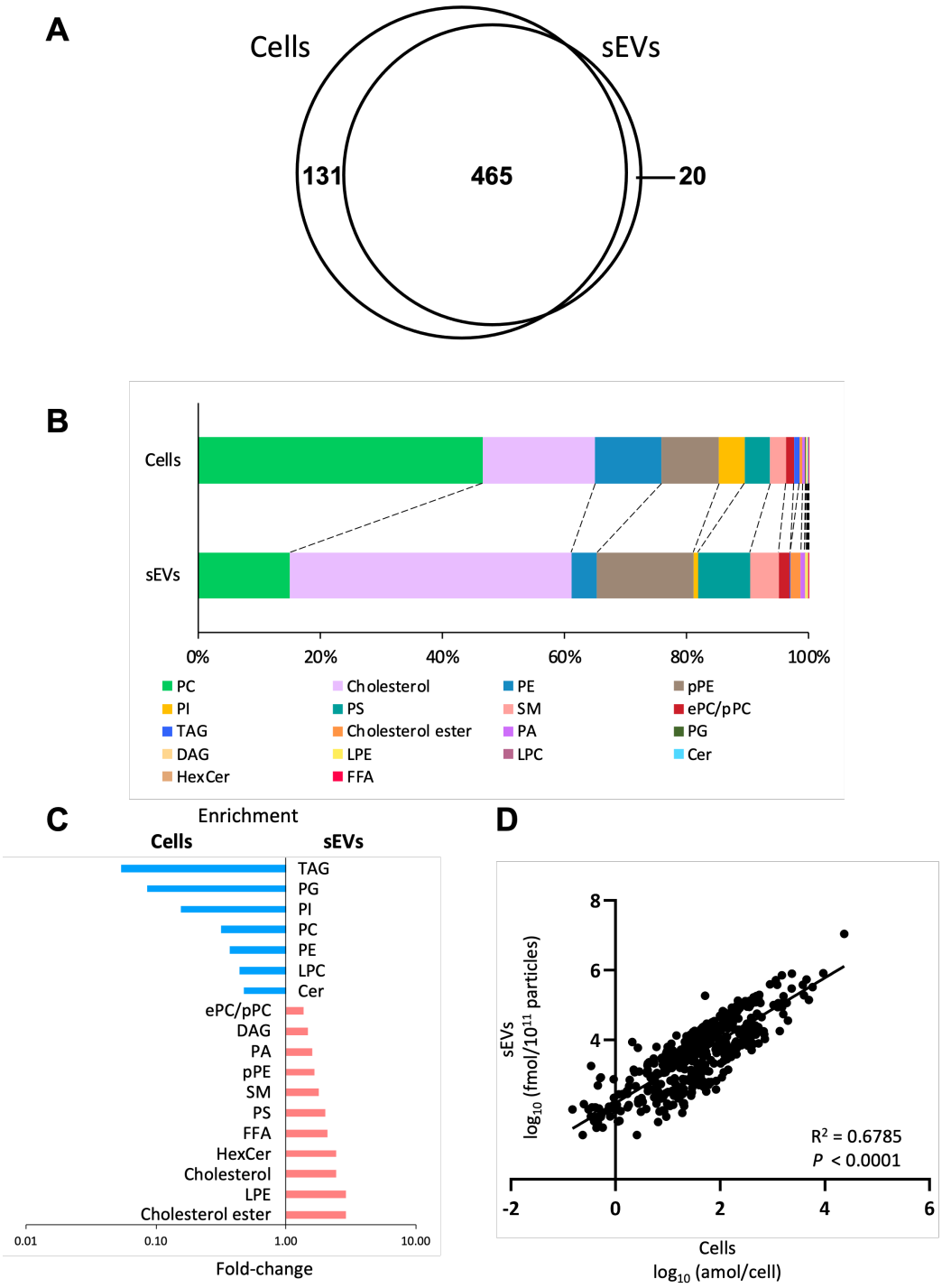

Figure 2-6. Lipidomic profiles of cells and sEVs under normoxia.

(A) Venn-diagram representing the number of lipids detected in cell and sEV samples. (B) Pie plots showing the mol-based percentile of each lipid class in cells and sEVs. (C) Enrichment of lipid classes in cells or sEVs. The data are shown as fold-changes of the ratio of lipid contents in sEVs per those of cells. (D) Correlation of the lipids in cells and sEVs.

Table 2-3. Number of lipids of each class identified in cells and sEVs.

Lipid class	Abbreviation	Number of Lipids Detected				
		Cells	sEVs	Common	Only Cells	Only sEVs
Free Fatty Acid	FFA	3	3	1	2	2
Lysophosphatidylcholine	LPC	19	9	9	10	0
Lysophosphatidylethanolamine	LPE	14	15	14	0	1
Phosphatidylcholine	PC	80	50	48	32	2
Alkyl-acyl phosphatidylcholine/ Alkenyl-acyl phosphatidylcholine	ePC/ pPC	27	27	26	1	1
Phosphatidylethanolamine	PE	90	60	60	30	0
Alkenyl-acyl phosphatidylethanolamine	pPE	79	73	72	7	1
Phosphatidylglycerol	PG	16	9	9	7	0
Phosphatidic acid	PA	17	15	15	2	0
Phosphatidylinositol	PI	82	53	53	29	0
Phosphatidylserine	PS	51	51	51	0	0
Sphingomyelin	SM	15	13	13	2	0
Ceramide	Cer	13	12	12	1	0
Hexosylceramides	HexCer	8	8	8	0	0
Cholesterol	Cholesterol	1	1	1	0	0
Cholesterol ester	Cholesterol ester	5	6	5	0	1
Diacylglycerol	DAG	43	51	39	4	12
Triacylglycerol	TAG	33	29	29	4	0
	Total	596	485	465	131	20

Finally, the difference in the amount of each lipid class in cells and sEVs between normoxia and hypoxia was investigated (Table 2-4). In cells, an increase (P value < 0.05) was observed under hypoxic stress in 16 of the 19 lipid classes. However, no obvious effect of hypoxic stress on lipid classes was observed in sEVs.

Table 2-4. Lipid content in cells and sEVs under different oxygen conditions.

Lipid class	Cells							sEVs						
	amol/cell							pmol/10^{11} particles						
	Normoxia			Hypoxia			*P* value	Normoxia			Hypoxia			*P* value
	Mean	±	SD	Mean	±	SD		Mean	±	SD	Mean	±	SD	
Free Fatty Acid (FFA)	18.2	±	6.7	9.4	±	12.9	0.3538	7.8	±	6.5	3.6	±	3.2	0.3631
Lysophosphatidylcholine (LPC)	83.2	±	10.4	151	±	20.9	0.0074	6.6	±	3.4	5.7	±	2.1	0.7302
Lysophosphatidylethanolamine (LPE)	104	±	17.9	193	±	25.9	0.0082	56.8	±	23.8	42.5	±	16.7	0.4420
Phosphatidylcholine (PC)	59338	±	8356	93637	±	11729	0.0146	3608	±	715	3388	±	860	0.7506
Alkyl-acyl phosphatidylcholine (ePC)/ Alkenyl-acyl phosphatidylcholine (pPC)	1689	±	213	2870	±	247	0.0033	452	±	105	379	±	91.5	0.4192
Phosphatidylethanolamine (PE)	13766	±	706	21431	±	279	0.0001	999	±	230	899	±	214	0.6105
Alkenyl-acyl phosphatidylethanolamine (pPE)	11795	±	1200	22803	±	5034	0.0211	3792	±	910	2927	±	472	0.2172
Phosphatidylglycerol (PG)	243	±	20.7	397	±	39.5	0.0040	4.1	±	1.1	2.8	±	0.7	0.1570
Phosphatidic Acid (PA)	524	±	28.1	953	±	125	0.0043	161	±	30.8	153	±	37.1	0.8030
Phosphatidylinositol (PI)	5381	±	464	8851	±	468	0.0008	162	±	36.7	139	±	32.8	0.4580
Phosphatidylserine (PS)	5257	±	377	8850	±	491	0.0006	2038	±	352	1970	±	444	0.8456
Sphingomyelin (SM)	3279	±	220	5346	±	274	0.0005	1134	±	250	938	±	202	0.3501
Ceramide (Cer)	77.3	±	8.1	98.6	±	4.1	0.0152	7.2	±	2.1	5.2	±	1.2	0.2197
Hexosylceramides (Hexcer)	68.9	±	4.3	125	±	7.0	0.0003	32.3	±	5.9	31.6	±	6.5	0.8995
Cholesterol	23504	±	2817	36016	±	3118	0.0067	11080	±	2242	9346	±	2925	0.4608
Cholesterol ester	704	±	172	739	±	152	0.8063	388	±	16.1	492	±	147	0.2923
Diacylglycerol (DAG)	174	±	22.1	275	±	38.7	0.0172	49.9	±	14.5	42.1	±	10.1	0.4855
Triacylglycerol (TAG)	1104	±	308	1755	±	457	0.1102	10.7	±	5.9	7.6	±	5.1	0.5210

The Student's *t*-test was used to determine the *P* value.

2.4. Discussion

In this study, I performed metabolomic analysis of PANC-1 cells cultured under normoxia and hypoxia and sEVs obtained from the culture supernatant of these cells by UC. Hypoxic stress has been reported to increase the release of sEVs from cells (Shao et al., 2018; X. Wang et al., 2018). However, no apparent difference in the number of particles, particle size distribution, or the content of marker protein was observed in the presence and absence of hypoxic stress in this study. In a previous study using another pancreatic cancer cell line, AsPc-1, no difference was observed relative to the number of particles under hypoxic stress (1% O_2) and 20% O_2 conditions, but a significant increase was observed at 0.1% O_2 (Patton et al., 2020). Furthermore, in an experiment in which chronic myelogenous leukemia cells were subjected to hypoxic stress (1% O_2) for 24 h, no increase was observed in the number of sEVs (Tadokoro et al., 2013). On the contrary, miR-210, a hypoxia marker gene, whose expression increases in various cancers (Jung et al., 2017; King et al., 2012; Tadokoro et al., 2013), was also found to increase in this study. Therefore, I conclude that the sEVs analyzed in this study can be collected under sufficient hypoxic stress.

I could quantify 140 hydrophilic metabolites from sEVs by hydrophilic metabolome analysis using capillary IC-MS and LC-MS, and 485 lipids by lipidome analysis using SFC-QqQMS. There have been several reports on hydrophilic metabolites since it was first shown in 2015 that sEVs derived from bone marrow mesenchymal stem/stromal cells contain lactic acid and glutamic acid (Luo et al., 2020; Puhka et al., 2017; Vallabhaneni et al., 2015; Zhao et al., 2016). In the present study, I have succeeded in quantifying 140 hydrophilic metabolites, including amino acids and their derivatives, organic acids, sugar phosphates, and nucleotides, and this number is the largest compared to previous reports.

Of the 11 hydrophilic metabolites detected only in sEVs, inosine, guanosine, hypoxanthine, and xanthine are involved in purine metabolism, and cytidine and uridine are involved in pyrimidine metabolism. Furthermore, inosine, cytidine, and uridine were among the top 20 metabolites with the highest amounts in sEVs. The existence of intermediate metabolites of purine and pyrimidine metabolism in sEVs has already been reported. For example, sEVs derived from a breast cancer cell line were reported to have

high concentrations of uridine and guanosine (Tadokoro et al., 2020). In addition, it has been reported that sEVs derived from head and neck squamous cell carcinoma cell lines and plasma from patients also contain intermediates for purine metabolism, which exhibit an immunosuppressive effect (Beccard et al., 2020; Ludwig et al., 2020). Taking these results into account, even in the sEVs derived from PANC-1, intermediate metabolites of purine and pyrimidine metabolism are actively incorporated into sEVs and might create a favorable environment for cancer metastasis and growth through immunosuppression.

I found a significant correlation for 122 hydrophilic metabolites that were commonly between cells and sEVs. However, when comparing the top 20 hydrophilic metabolites with high amounts in cells and sEVs, only seven metabolites were common. This suggests that the concentration of hydrophilic metabolites in sEVs is not largely affected by their concentration in the cells from which they originate. There are several possible causes for this—for example, a specific metabolite is selectively taken up by the sEVs when it is produced into the cell, or it is metabolized or decomposed internally after the generation of sEVs. However, a detailed mechanism for the uptake of metabolites by sEVs is unknown and needs further investigation in the future.

When PCA was performed using the quantitative values of hydrophilic metabolites in sEVs recovered under normoxia and hypoxia, it was found that both the samples were separated for principal component 1. In addition, volcano plots revealed changes in 15 metabolites (P value < 0.05, fold-change < 0.67 or > 1.5). Among these, 2-deoxyribose 1-phosphate, cysteine S-sulfate, and azelaic acid were increased in sEVs under hypoxic stress. In this study, 2-deoxyribose 1-phosphate was not detected in cells but was only detected in sEVs. Thymidine phosphorylase (TP), uridine phosphorylase, and purine nucleoside phosphorylase are major enzymes involved in the production of 2-deoxyribose 1-phosphate (Pugmire & Ealick, 2002). TP promotes tumor cell proliferation in hypoxia and resists hypoxic stress-induced apoptosis (Kitazono et al., 1998). In addition, 2-deoxyribose 1-phosphate promotes angiogenesis by attracting vascular epithelial cells in an nuclear factor-kappa B (NF-κB)-dependent manner (Vara et al., 2018). It has already been reported that the expression of many molecules, such as urothelial cancer associated 1 (UCA1), carbonic anhydrase 9 (CA9), tissue factor (TF), miR-135b, miR-23a, and miR-494, increases with hypoxia, and they are involved in

angiogenesis (Guo et al., 2020; Shao et al., 2018). Therefore, in addition to these molecules, 2-deoxyribose 1-phosphate may also be involved in the progression of cancer through the promotion of angiogenesis.

Cysteine S-sulfate is a precursor of the antioxidant cysteine (Cys). The concentrations of Cys and cysteine S-sulfate decrease in the serum of glioma patients (Huang et al., 2017). Azelaic acid is the final product of linoleic acid decomposed into peroxides (Raghavamenon et al., 2009) and is detected in the blood, feces, and saliva of patients with gastric cancer (Brown et al., 2016; Yu et al., 2011). However, the relationship between these metabolites and pancreatic cancer and hypoxic stress is unclear. In contrast, hypoxic stress resulted in a decrease in valine, alanine, tartaric acid, threonine, o-acetylcarnitine, ATP, Gly-Leu, CTP, 2-oxoglutaric acid, cytidine, fumaric acid, and hexylamine. Cell metabolism shifts from aerobic phosphorylation to glycolysis under hypoxic stress—a phenomenon that has long been known as the Warburg effect (O Warburg & Minami, 1924). Moreover, in some cancers, hypoxic stress significantly changes amino acid metabolism and expression of some amino acid transporters (Biancur et al., 2017; Qin et al., 2020; Yoo et al., 2020). These intracellular metabolic changes induced by hypoxic stress might have affected the metabolite content of sEVs.

Since the study conducted by Vidal et al. (Vidal et al., 1989), a lot of research has been performed on lipid analysis in sEVs (Lydic et al., 2015; Nishida-Aoki et al., 2020; Skotland et al., 2020; Trajkovic et al., 2008). The commonly observed phenomena in these studies were an increase in cholesterol, SM, and PS, and a decrease in PC and PI in sEVs compared to cells. Because similar trends were observed in our study, I consider that lipid analysis of sEVs performed by us was successful.

A comparison of the content of each lipid class in cells and sEVs revealed a decrease in TAG and a substantial increase in DAG in sEVs. Additionally, the FFA content increased by 2.1-times in sEVs, and several DAGs, which were not detected in cells, were detected in sEVs. It may be possible that some kind of decomposition occurred in sEVs. In fact, it has been reported that sEVs derived from pancreatic cancer carry a bioactive peptide called adrenomedullin, which is involved in the breakdown of lipids in adipose tissue, and may contribute to the decomposition of lipids in sEVs (Sagar et al., 2016).

As only a single pancreatic cancer cell line was used in this study, it is not possible

to determine whether the metabolomic profile in sEVs observed here are common to pancreatic cancer. In addition, because the recovery rate of sEVs by UC was low, a large amount of culture supernatant (260 mL) was required. Owing to the limitations of the equipment used for the culture and processing, I could analyze only three biological replicates. In the future, if a method that can recover sEVs more efficiently is developed, it may be possible to perform a more detailed analysis by increasing the number of replicates.

In conclusion, I detected 140 hydrophilic metabolites and 485 lipids in sEVs derived from the pancreatic cancer cell line PANC-1, using a comprehensive metabolomic analysis method involving capillary IC-MS, LC-MS, and SFC-QqQMS. The profiles of hydrophilic metabolites and lipids in sEVs were found to be different from those in cells. The intermediates of purine and pyrimidine metabolism were found to be specifically accumulated in sEVs. Furthermore, it is suggested that the metabolomic profile of sEVs may be altered by hypoxic stress. These metabolites, which fluctuate in sEVs due to external stress, may have some involvement in cancer growth and metastasis.

Chapter 3 Development of semi-automated size exclusion chromatography and effects of different recovery methods on metabolites

3.1 Introduction

EVs are lipid bilayer structures released by various cells (Théry et al., 2018). EVs are observed in body fluids, such as urine, blood, saliva, and culture supernatants from cultured cells (Raposo & Stoorvogel, 2013). It is not possible to distinguish between exosomes (50−150 nm), microvesicles (100−1000 nm), and apoptotic vesicles (100−1000 nm), which all have a lipid bilayer structure. Therefore, the ISEV recommends that these vesicles should be called EVs (Théry et al., 2018). sEVs contain functional molecules, such as DNA, mRNA, miRNA, proteins, lipids, and metabolites (Kreimer et al., 2015; Momen-Heravi et al., 2018; Skotland et al., 2020; Williams et al., 2019). Because the components in sEVs are altered by cancer and other diseases, they have been extensively studied (Shah et al., 2018; Steinbichler et al., 2017). In many cell types, tetraspanins, such as CD9, CD63, and CD81, as well as Alix and Syntenin-1, which are involved in late endosomes, are more enriched in sEVs than in cells (Van Niel et al., 2018) and therefore, have been used as sEV markers (Jeppesen et al., 2019). In recent years, several studies have been conducted on the hydrophilic metabolites in sEVs (Hayasaka et al., 2021; Ludwig et al., 2020; Tadokoro et al., 2020; Zhao et al., 2016). However, it is unclear which metabolites are contained in sEVs and whether an increase in a given metabolite in the cell is reflected in its hydrophilic metabolite content in the sEVs.

UC is the gold standard for sEV recovery; however, it is often compromised by the co-precipitation and aggregation of proteins with sEVs (Nordin et al., 2015) and rupture of sEVs (Guan et al., 2020). In addition, the sample volume must be appropriate for the ultracentrifuge rotor used (e.g., 3.5 mL for an SW41Ti rotor). When the volume of the liquid is small, dilution with D-PBS is necessary, leading to a lower recovery rate. To overcome the limitations of current methods, the development of an easy method of recovery that does not require expensive equipment and inability to recover sEVs from multiple samples would greatly improve the study of sEVs.

In addition to UC, other recovery methods for sEVs include density gradient centrifugation, the down pellet approach, and affinity purification utilizing antibodies (Taylor & Shah, 2015). Some current obstacles include variation in the purification and recovery rates among collection methods (Brennan et al., 2020; Patel et al., 2019) and undisclosed constituents of the recovery buffers used in commercial kits. The latter is

particularly challenging to sEV isolation for metabolomic and proteomic analyses because ion suppression and column failure occur when samples are prepared in buffers with a high salt content or surfactants. In the worst case, the mass spectrometer is damaged, making stable measurements impossible. Therefore, it was necessary to use a solution with a known buffer composition.

Recently, the recovery of sEVs using SEC has attracted much attention (Sidhom et al., 2020). SEC is a method of isolation that is based on the difference between the time required for the migration of molecules based on their size, which can efficiently recover fractions containing sEVs that are highly pure (Baranyai et al., 2015). sEVs collection kits using SEC, such as qEV (Izon Science), EV Second (GL Sciences Inc.), and PURE-EV (HansaBioMed), have been used in previous studies (Alameldin et al., 2021; Du et al., 2021; Kitamura et al., 2018), but are limited in their versatility, automation, and multi-specimen processing. Although some studies have used SEC to collect sEVs for metabolomic analysis, the effect of different EV collection methods on metabolites is unknown.

In this study, I established a semi-automated method to selectively collect sEVs derived from cultured cells using SEC while monitoring the amount collected.

3.2 Materials and methods

3.2.1 Cell culture

The human colon cancer cell line HT29 ectopically expressing CD63-Nanoluc (HT29-CD63-Nluc) cell was generated at the Aichi Cancer Center Research Institute. This cell line was labeled with the exosome marker CD63 with high-intensity luciferase Nanoluc (Hikita et al., 2018). HT29-CD63-Nluc cells were grown in RPMI1640 medium containing 10% (*v*/*v*) FBS and antibiotics. The cells were cultured at 37°C in a humidified atmosphere containing 5% CO_2. All cells were confirmed to be mycoplasma-free using the Mycoalert detection kit whenever sEVs were collected.

3.2.2 Collection of cell-cultured medium

HT29-CD63-Nluc cells (3.0×10^6) were seeded into 150-mm dishes and pre-cultured with RPMI1640 containing 10% FBS and antibiotics for 24 h. The cells were washed twice with D-PBS. Next, the culture medium was exchanged for advanced RPMI1640 medium containing 2 mmol/L glutamine and antibiotics and cultured for 2 days.

The cell-culture medium was centrifuged at 2,000 × *g* for 25 min and 15,000 × *g* for 50 min at 4°C to pellet and remove cells, debris, and apoptotic bodies. The supernatants were filtered using a 220-nm PES filter to remove the large EVs. The filtrates were concentrated using a 100 kDa cut-off filter. This suspension was used to prepare the samples.

3.2.3 sEVs collection using SEC

High-performance liquid chromatography (HPLC) was performed using an Agilent infinity 1200 series (Agilent Technologies). The samples were injected with 50- or 100-fold enrichment medium. For the separation of sEVs, size-controlled hydrophilic porous silica gel was packed in a 4.6 × 250 mm column [the average particle semidiameter (d50) : 7.25 μm, the average pore diameter : 71.8 nm, the pore volume : 1.85 mL/g, and the surface area : 98 m^2/g, AGC Inc., Yokohama, Japan] (Yoshitake et al., 2022). The column temperature was maintained at 20°C. The diode array detector (DAD) was

monitored at 190–600 nm and fractionated using a wavelength of 204 nm. The mobile phase was composed of D-PBS (A) and MeOH (B; LC-MS grade, FUJIFILM Wako Pure Chemical Corporation). The flow rate of the mobile phase was 0.00–15.01 at 0.25 mL/min and 15.01–25.0 at 0.50 mL/min. The gradient used was 0.00–10.00 min 0% B; 10.00–10.10 min 0 to 70% B; 10.10–15.00 min 70% B; and 15.00–15.01 min 70 to 0% B, which was maintained until 25.00 min. The collected fractions were adjusted to 0.05 g (≈ 50 μL) using a 100 kDa cut-off filter.

3.2.4 sEVs collection using UC

The concentrate of the cell culture medium was ultracentrifuged at 37,000 rpm (average RCF of 234,700 × *g*) for 70 min at 4°C (SW41Ti rotor and Optima XE-90 Ultracentrifuge). The pellet was washed with D-PBS and collected via UC. This washing procedure was repeated twice. The weight of the pellet was adjusted to 0.05 g (≈ 50 μL) by adding D-PBS.

3.2.5 Nanoluc assay

Samples collected and weighed were diluted to 50 μL with D-PBS and transferred to white-walled 96-well plates. 50 μL of Nano-Glo substrate diluted 1:50 provided buffer (Nano-Glo Luciferase Assay System, Promega, Madison, WI, USA) were added. Nanoluc luciferase intensity were measured by infinite M200 ABS-FL.

3.2.6 Protein quantification of sEVs

The collection sample were diluted using D-PBS, 10 μL of m-PER buffer added. The sample were reacted with micro BCA™ Protein Assay Kit for 2 h at 37°C. The wavelengths of 562 nm were measured using infinite M200 ABS-FL. The protein content was measured by constructing a calibration curve with 8 points ranging from 0 to 40 μg/mL.

3.2.7 Extraction of hydrophilic metabolites and lipids from cells

For the measurement of hydrophilic metabolites and lipids, I prepared the extraction solvent, supplemented in 10 μL internal standards mix for lipids [Cer d18:1–

17:0, and HexCer d18:1 (d5)-18:1 10 μmol/L; cholesterol (d7), 300 μmol/L; FFA 17:0, 500 μmol/L], 10 μL mouse SPLASH® LIPIDOMIX® Mass Spec Standard, and 10 μL internal standards mix for hydrophilic metabolites (10-camphorsulfonic acid, L-tryptophan-$^{13}C_{11}$-$^{15}N_2$, and L-methionine sulfone 100 μmol/L) per 1 mL MeOH. The cells were washed twice with pre-warmed (37°C) D-PBS and dissolved in 700 μL extraction solvent. The homogenate was then sonicated for 5 min. Then, 400 μL supernatant was mixed with 160 μL MeOH, 500 μL chloroform, and 200 μL Milli-Q water using a vortex mixer for 1 min, followed by 5 min of sonication. After centrifugation at 16,000 × *g*, 4°C for 5 min, 800 μL supernatant was transferred to a clean tube. Finally, 220 μL chloroform and 220 μL Milli-Q water was added to the supernatant before it was vortexed and centrifuged at 16,000× *g*, 4°C for 5 min.

For hydrophilic analysis, 400 μL supernatant was transferred to clean tubes and lyophilized. Samples were dissolved in 100 μL 50% (*v*/*v*) aqueous acetonitrile and immediately used for hydrophilic metabolome analysis.

For lipidomic analysis, 400 μL of the bottom layer was concentrated to dryness under a nitrogen stream and dissolved in 100 μL 50% (*v*/*v*) chloroform/MeOH.

3.2.8 Extraction of hydrophilic metabolites and lipids from sEVs

Hydrophilic metabolites and lipids were extracted from 45 μL sEVs samples. The extraction solvent (560 μL) was then added to the sEVs. Chloroform (280 μL) and Milli-Q water (160 μL) were added to the samples and mixed vigorously by vortexing, followed by sonication. The subsequent steps were the same as those described for cell preparations. Samples were centrifugated at 16,000 × *g*, 4°C, 5 min and 800 μL supernatant was transferred to a clean tube. This supernatant sample was vortexed and centrifuged at 16,000 × *g*, 4°C for 5 min after adding 220 μL chloroform and 220 μL Milli-Q water.

For hydrophilic analysis, 600 μL supernatant was transferred to clean tubes and lyophilized. Samples were dissolved in 50 μL 50% (*v*/*v*) aqueous acetonitrile and immediately used for hydrophilic metabolome analysis.

For lipidomic analysis, 400 μL of the bottom layer was concentrated to dryness

under a nitrogen stream and dissolved in 100 μL of 50% (*v*/*v*) chloroform/MeOH.

3.2.9 Analysis of hydrophilic metabolites and lipids

Anionic metabolites were measured using capillary IC-MS as previously described (2.2.2).

Cationic metabolites were analyzed using LC-MS as previously described (Suzuki et al., 2022). Briefly, the LC-MS system is composed of Agilent 1290 Infinity LC system equipped with a Q Exactive Orbitrap MS system (Agilent Technologies). Cationic metabolites were separated on a HILIC-Z column (150 × 2.1 mm, 2.7 μm; Agilent Technologies) maintained at 40°C. The injection volume was 1 μL. The mobile phase consisted of 20 mmol/L ammonium formic acid + 0.25% (*v*/*v*) formic acid as solution A and 20 mmol/L ammonium formic acid + 0.25% formic acid in 90% (*v*/*v*) acetonitrile as solution B. The flow rate was 0.25 mL/min, and the gradient of solution B was as follows: 0–15 min, 100% to 70%; 15–20 min, 70% to 10%; 20–23 min, 10%; and 23–30 min, 100%. The Q Exactive mass spectrometer was operated in a HESI positive ion mode. Data were acquired in the full MS scan and parallel reaction monitoring (PRM) modes. The parameters in full MS scan were as follows: resolution, 35,000; auto gain control target, 3.0×10^6; maximum ion injection time, 200 ms; and scan range, 50–750 *m/z*. Additionally, the parameters in PRM mode were as follows: resolution, 17,500; auto gain control target, 2×10^5; maximum ion injection time, 100 ms; inclusion *m/z* list: 104.0706 (GABA), 118.0863 (Val), 132.1019 [leucine (Leu), isoleucine (Ile)], 166.0863 [phenylalanine (Phe)], and 182.0482 (methionine sulfone).

Lipids were measured using SFC-QqQMS as previously described, but with major modifications (Hayasaka et al., 2021; Takeda et al., 2018) . SFC-QqQMS analysis was performed using an Agilent 1260 Infinity II SFC system equipped with an Agilent 6470A triple quadrupole LC/MS system with AJS ESI interface (Agilent Technologies, Santa Clara, CA, USA). The injection volume was 2.0 μL, and the column temperature at 60°C. The mobile phase consisted of supercritical carbon dioxide (A) and MeOH/water (95/5, *v*/*v*) with 0.1% (*w*/*v*) ammonium acetate (B). Analysis of FFA, DAG, TAG, Cer, HexCer, PE, and pPE were separated on a Viridis HSS C18 SB column (3.0 × 100 mm, 1.8 μm; Waters). The flow rate of the mobile phase was 1.0 mL/min, and the gradient of

solution B was as follows: 1% at 0 min, 50% at 25.0 min, 50% from 25.0 to 28.0 min, and 0% at 28.1 min; this was maintained until 30 min. Analysis of cholesterol, PC, ePC/pPC, SM, LPC, LPE, PG, PI, PS, and PA were separated on a Torus DEA column (3.0 × 100 mm, 1.7 μm). The flow rate of the mobile phase was 1.0 mL/min, and the following linear gradient was used: 0–1.0 min, 1% B; 1.0–24.0 min, 1 to 75% B; 24.0–26.0 min, 75% B; 26.0–26.4 min, 70 to 1% B; this was maintained until 30 min.

AJS-ESI-MS/MS analysis was performed in a positive and negative ion mode, and the conditions were as follows: dry gas temperature = 300°C, dry gas flow rate = 10 L/min, nebulizer pressure = 30 psi, sheath gas temperature = 350°C, sheath gas flow rate = 12 L/min, capillary voltage = 3.0 kV, nozzle voltage = 0 V, fragmentor voltage = 380 V. Data were acquired using dynamic MRM mode, and the MRM transition setting was based on the in-house lipid MRM library described previously (Takeda et al., 2018). NTA, TEM, and immunoblot analysis were conducted as previously described (section 2.2.3, 2.2.4, 2.2.8).

3.2.10 Data analysis

The data acquired with preparative HPLC were analyzed using ChemStation (version B.04.02, Agilent Technologies). The raw data obtained by capillary IC-MS and LC-MS were analyzed using the TraceFinder software (version 5.0, Thermo Fisher Scientific). The multiple reaction monitoring data acquired using SFC-QqQMS were analyzed using MassHunter software (version 10.0, Agilent Technologies). The metabolite data for the cells and sEVs were subtracted from the value of each blank sample in which no cells were cultured. If the value was negative, it was set to 0. Statistical significance was determined using the Student's *t*-test. The Student's *t*-test and the coefficient of determination were analyzed using GraphPad Prism (version 8.4.3). PCA and heatmaps were analyzed using JMP (version 16.2.0, JMP Statistical Discovery, Cary, NC, USA) and MeV (version 10.2, Dana-Farber Cancer Institute, Boston, MA, USA).

3.3 Results

3.3.1 Development of the sEVs recovery method using semi-automated SEC

I developed a method in which a column for SEC was attached to an HPLC system and monitored using a DAD to perform automated preparative separation of sEVs (Figure 3-1). The column consisted of size-controlled hydrophilic porous silica gel packed into columns for HPLC. First, I investigated which fractions contained sEVs after recovery from culture supernatants using SEC. For sEVs recovery experiments, I used the human colon cancer cell line, HT29-CD63-Nluc, which ectopically expresses Nanoluc, a highly sensitive luciferase fused with CD63, as an sEV marker (Hikita et al., 2018). In these cells, the expression of CD63 was detectable as Nanoluc luciferase intensity. The 100 μL sample of HT29-CD63-Nluc cell culture supernatant as a 50-fold concentration with a 100 kDa filter, was injected and allowed to swim for 30 min, and the peptide binding wavelength, 204 nm, was measured continuously with DAD. While protein absorbance is often measured at 280 nm, in this study I used 204 nm, which is the wavelength at which peptides bind and thus, it is more sensitive. The results showed a peak intensity of approximately 500 milli arbitrary unit (mAU) after 6.5 min and a significant peak of approximately 1,500 mAU from 12.5 to 16.0 min (Figure 3-2A, Figure S3-1). To determine which peak corresponded to sEVs, fractions were sampled every 2.5 min such that 10 fractions were collected. Nanoluc luciferase intensity was observed in the third fraction (5.0−7.5 min), and a large amount of protein was observed in the sixth fraction (12.5−15.0 min) (Figure 3-2A). The uncultured medium was measured to confirm that the peak observed in the third fraction was not solvent-derived (Figure 3-2B). The third fraction, a peak at 6.5 min, is attributed to sEVs. Also, these results suggested the sixth fraction represents the elution of free protein due to change from 100% D-PBS to 70% MeOH. In subsequent analyses, I established a method to recover the peak portion when a peak was observed between 4.0 and 7.4 min.

Next, I examined whether the number of sEVs correlated with the injection volume. The number of sEVs recovered was compared by injecting 25, 50, 75, and 100 μL culture supernatant concentrates of HT29-CD63-Nluc cells. A strong correlation with the injection volume was observed when the peak area obtained by DAD was calculated (Figure 3-2C). Corresponding to the peak area, the collection volume, the number of

particles calculated by NTA, and Nanoluc intensity also showed an injection volume-dependent recovery of sEVs (Figure 3-2D–F).

The durability of the column was examined by injecting 200 samples of culture supernatant. No considerable differences were observed in either the time or peak areas (Figure 3-3A, B). This confirmed that sEVs could be stably recovered, even after multiple injections.

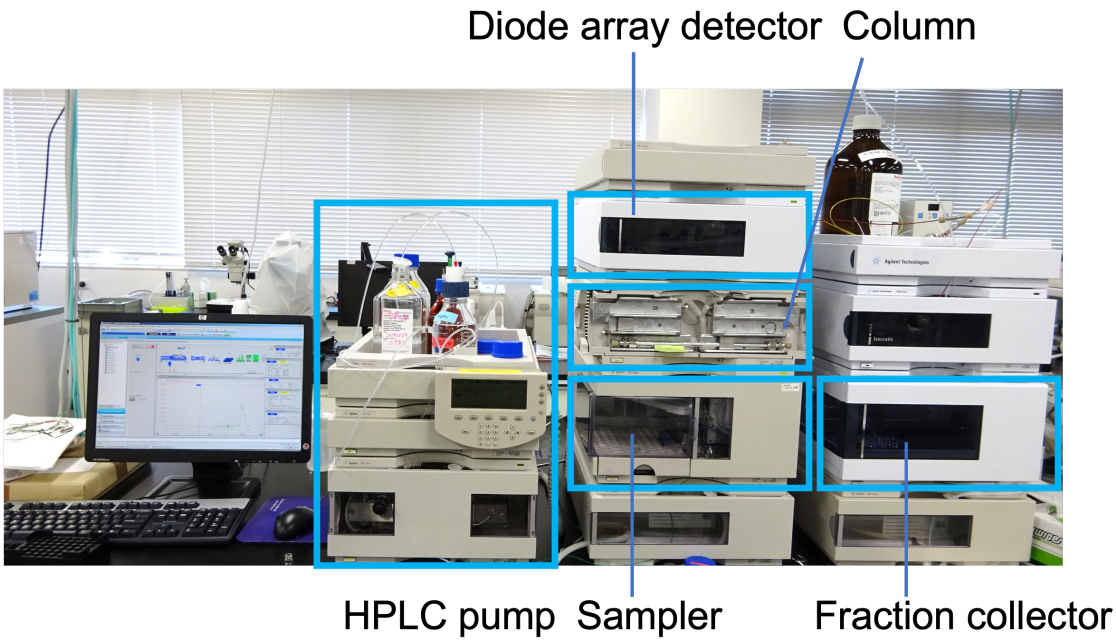

Figure 3-1. Recovery system for sEVs by combining HPLC and SEC.

Samples injected by the sampler were passed through a column using a solution adjusted by the HPLC pump. The wavelength of 204 nm was measured by a diode array detector (DAD), and the determined fraction was collected using a fraction collector.

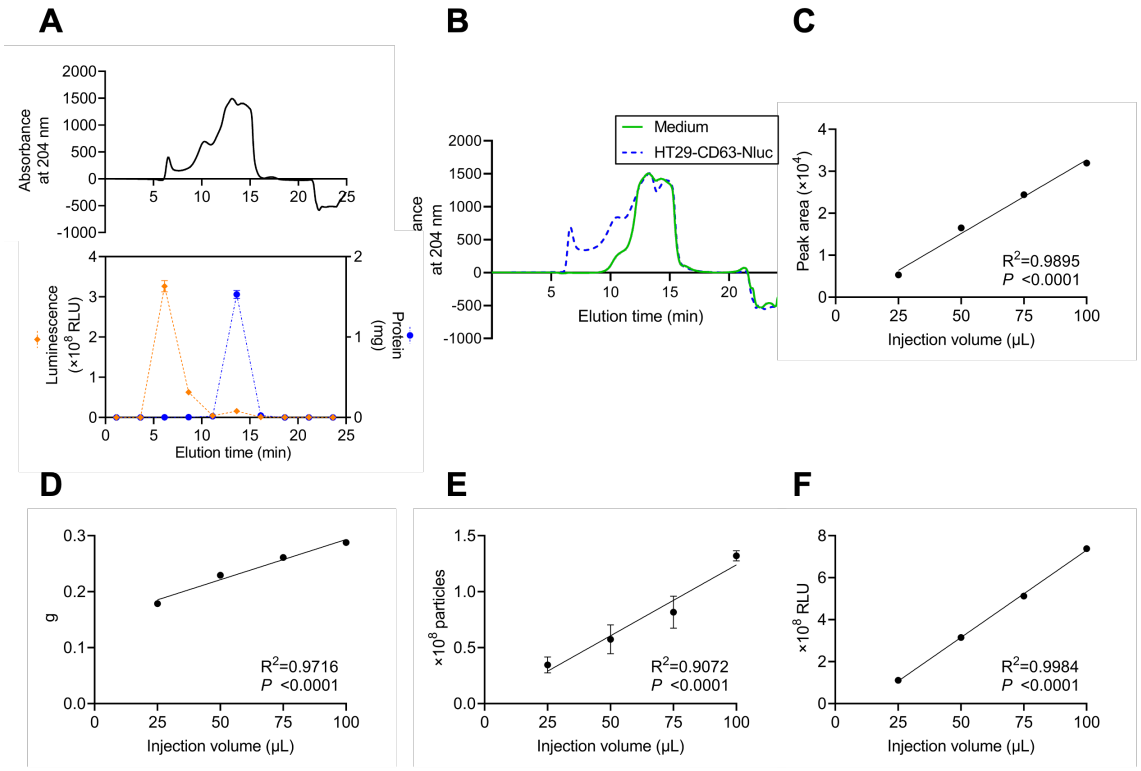

Figure 3-2. Determination of recovered fractions and injectable dose-dependent recovery of sEVs from cultured cells.

(A) Isolation of sEVs from cell-cultured medium using the SEC system. Upper panel: the absorption of peptides binds at 204 nm. Lower panel: the Nanoluc luciferase intensity [relative light unit (RLU)] and the protein content (mg) of each fraction are represented by orange diamonds (left axis) and blue circles (right axis), respectively. (B) Isolation of sEVs from the non-cultured medium (green solid line) and HT29-CD63-Nluc cell-cultured medium (blue dashed line) using the SEC system. (C) Correlation between the injection volume and the peak area of HT29-CD63-Nluc. The peak area was calculated from DAD measurements. (D) Correlation between the injection volume and the collection volume. (E) Correlation between the injection volume and the number of particles measured. The number of particles was measured by NanoSight. (F) Correlation between the injection volume and Nanoluc luciferase intensity. The luminescence was measured with a luminometer. Data are presented as the means ± SD from triplicate samples.

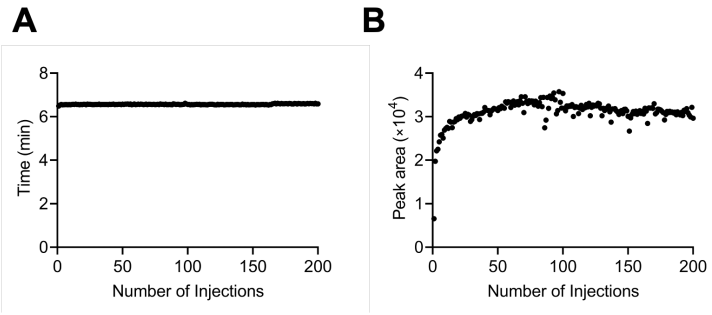

Figure 3-3. Stable recovery of sEVs derived from cultured cells using SEC.

(A) The time of the peaks from 200 injections. (B) The peak area for 200 injections.

3.3.2 The characteristics of sEVs collected using different recovery methods

From 200 mL culture supernatant collected from HT29-CD63-Nluc cells, sEVs were isolated by UC and SEC and the quantity and quality were compared. The NTA showed that the average particle size of sEVs recovered by UC and SEC were 135.6 nm and 120.4 nm, respectively, with a smaller particle size recovered by SEC (Figure 3-4A, B). TEM revealed particles corresponding to sEVs with a lipid bilayer structure (Figure 3-4C). The sEVs markers Syntenin-1, Alix, CD63, and CD81 were enriched in sEVs, and the endoplasmic reticulum (ER) marker calnexin and mitochondrial marker Tomm20 were absent (Figure 3-4D). The amount of CD63 present was confirmed by the Nanoluc intensity, which was significantly increased (P value < 0.05) in SEC (Figure 3-4E). When I calculated the recovery rate with the concentrate as 100%, it was confirmed that significantly (P value < 0.05) more sEVs were recovered with SEC than with UC (Figure 3-4F).

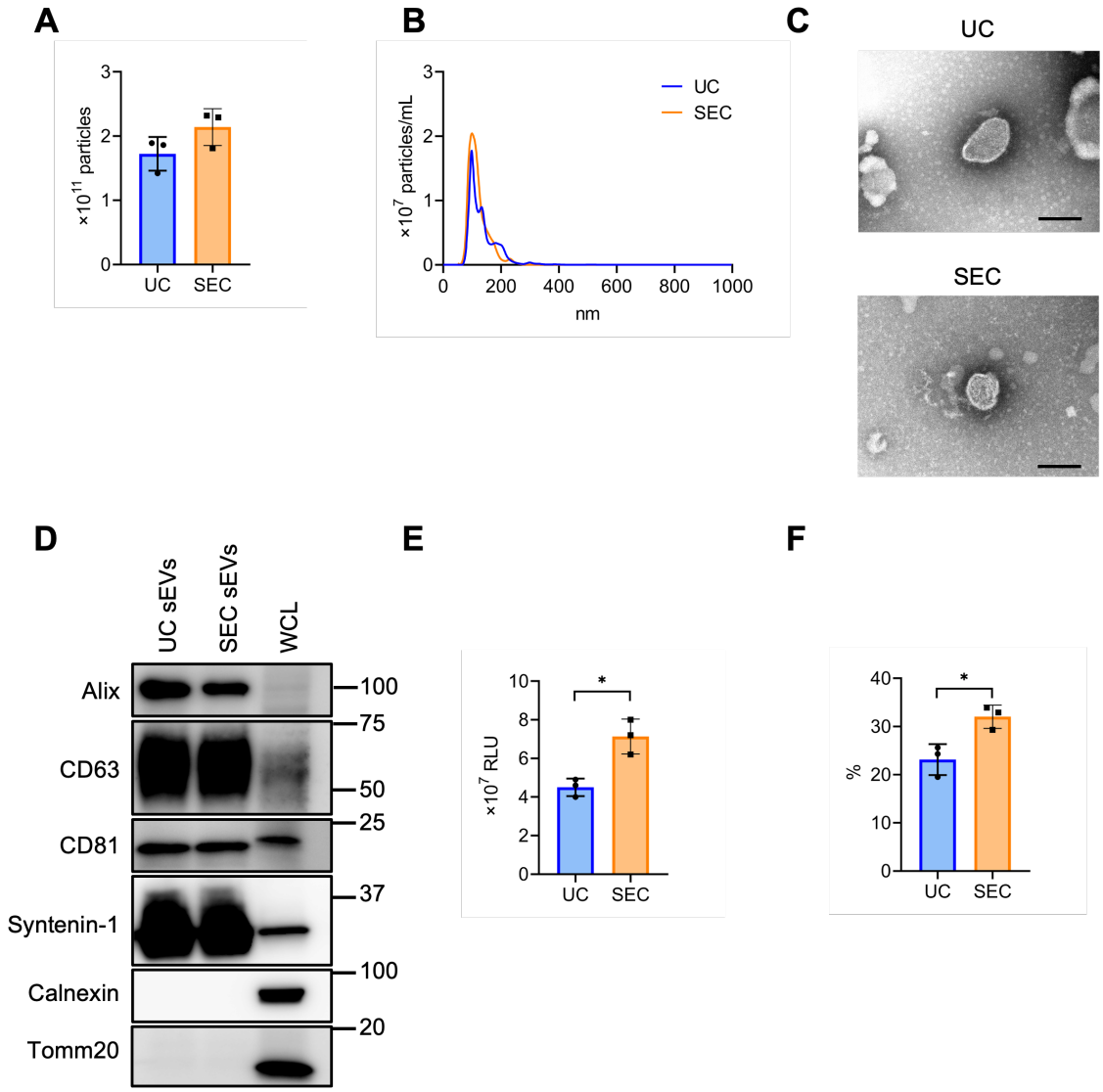

Figure 3-4. The comparison of sEV collection between UC and SEC.

(A) The number of particles in UC and SEC samples. (B) Size distribution of the particles in UC and SEC samples. (C) TEM images of sEVs using UC and SEC. Scale bar, 100 nm. (D) Immunoblotting analysis of Alix, CD63, CD81, syntenin-1, calnexin, and tomm20 expression in HT29-CD63-Nluc cells and sEVs using UC and SEC recovery systems. The sEV markers, Alix, CD63, CD81, and Syntenin-1; sEV negative protein markers, Calnexin and Tomm20. The protein content was 1.0 μg for the sEV samples and 10 μg for the WCL samples. (E) The Nanoluc luciferase intensity of UC and SEC samples. (F) The recovery rate of the EVs collected using UC and SEC. The sample after concentration was calculated as 100%. *P value < 0.05 by Student's t-test.

Table 3-1. Comparison of UC and SEC sEVs in the purification process.

	UC				SEC			
	CD63 (RLU)	Weight (g)	Specific CD63 (RLU/g)	Purification (-fold)	CD63 (RLU)	Weight (g)	Specific CD63 (RLU/g)	Purification (-fold)
Cell cultured supernatant	5.65.E+08	203.65	2.77.E+06	1.00	5.82.E+08	204.94	2.84.E+06	1.00
2,000×*g* supernatant	4.28.E+08	196.91	2.18.E+06	0.78	4.42.E+08	199.15	2.22.E+06	0.78
15,000×*g* supernatant	3.00.E+08	189.94	1.58.E+06	0.57	3.23.E+08	190.23	1.70.E+06	0.60
0.22 μm filtration	2.77.E+08	181.76	1.52.E+06	0.55	2.98.E+08	184.06	1.62.E+06	0.57
Ultrafiltration	1.95.E+08	9.00	2.16.E+07	7.80	2.22.E+08	2.00	1.11.E+08	38.99
After collection of sEVs	4.48.E+07	0.05	8.96.E+08	323.06	7.11.E+07	0.05	1.42.E+09	500.26

CD63 was detected as luminescent using Nanoluc.

I measured hydrophilic metabolites using capillary IC-MS and LC-MS, and lipids using SFC-QqQMS, from both sEVs and cell samples. When analyzing metabolites in sEVs, it is necessary to control the effects of the large amounts of metabolites present in uncultured media. Therefore, I prepared blank sEV samples for this study. Uncultured medium was incubated in a CO_2 incubator and processed with UC or SEC to prepare sEVs blank samples. A total of 586 metabolites (109 hydrophilic metabolites and 477 lipids) and 595 metabolites (115 hydrophilic metabolites and 480 lipids) were identified in sEVs from culture supernatants derived from HT29-CD63-Nluc cells recovered with UC and SEC, respectively. The common metabolites in the samples retrieved with UC and SEC were 540 (81 hydrophilic metabolites and 459 lipids). A relationship between the lipid profiles of sEVs and cells common to many cells has been reported (Llorente et al., 2013; Nishida-Aoki et al., 2020; Skotland et al., 2020). In the present study, I examined whether a similar relationship between cell and sEV lipid compositions could be measured (Figure 3-5A–C). Cholesterol, PS, and SM were enriched, whereas PC and PI were not. Compared to cells, cholesterol (UC 2.8 times, SEC 3.2 times), PS (UC 2.0 times, SEC 2.2 times), and SM (UC 2.2 times, SEC 2.2 times) were enriched in sEVs, while PC (UC 0.3 times, SEC 0.3 times) and PI (UC 0.2 times, SEC 0.2 times) were not (Figure 3-5D). Similar changes were observed, as in a previous study (Llorente et al., 2013; Nishida-Aoki et al., 2020; Skotland et al., 2020), suggesting that both UC and SEC could measure sEV-specific lipids. When analyzed by lipid class, FFA were detected only in UC; otherwise, there was no difference in the classes detected between the UC and SEC methods. For metabolites overall, the PCA showed a separation of plots between UC and SEC, suggesting metabolite profiles in sEVs differ depending on the recovery method used (Figure 3-6A). When I focused on hydrophilic metabolites that varied significantly between UC and SEC, those involved in purine-pyrimidine metabolism, such as guanosine triphosphate (GTP), ATP, uridine triphosphate (UTP), CTP, inosine, adenosine, and guanosine diphosphate (GDP), were abundant in SEC; while in contrast, amino acids such as proline (Pro), Glu, and Phe were abundant in UC (Figure 3-6B). I found that 20 lipids were significantly increased in UC when compared to SEC, including three types of TAG, three types of PE, three types of LPE, and four types of HexCer. In comparison, a total of 42 lipids were significantly increased in SEC, including 11 TAG, 12 PC, 12 LPC, and six SM (Table 3-2).

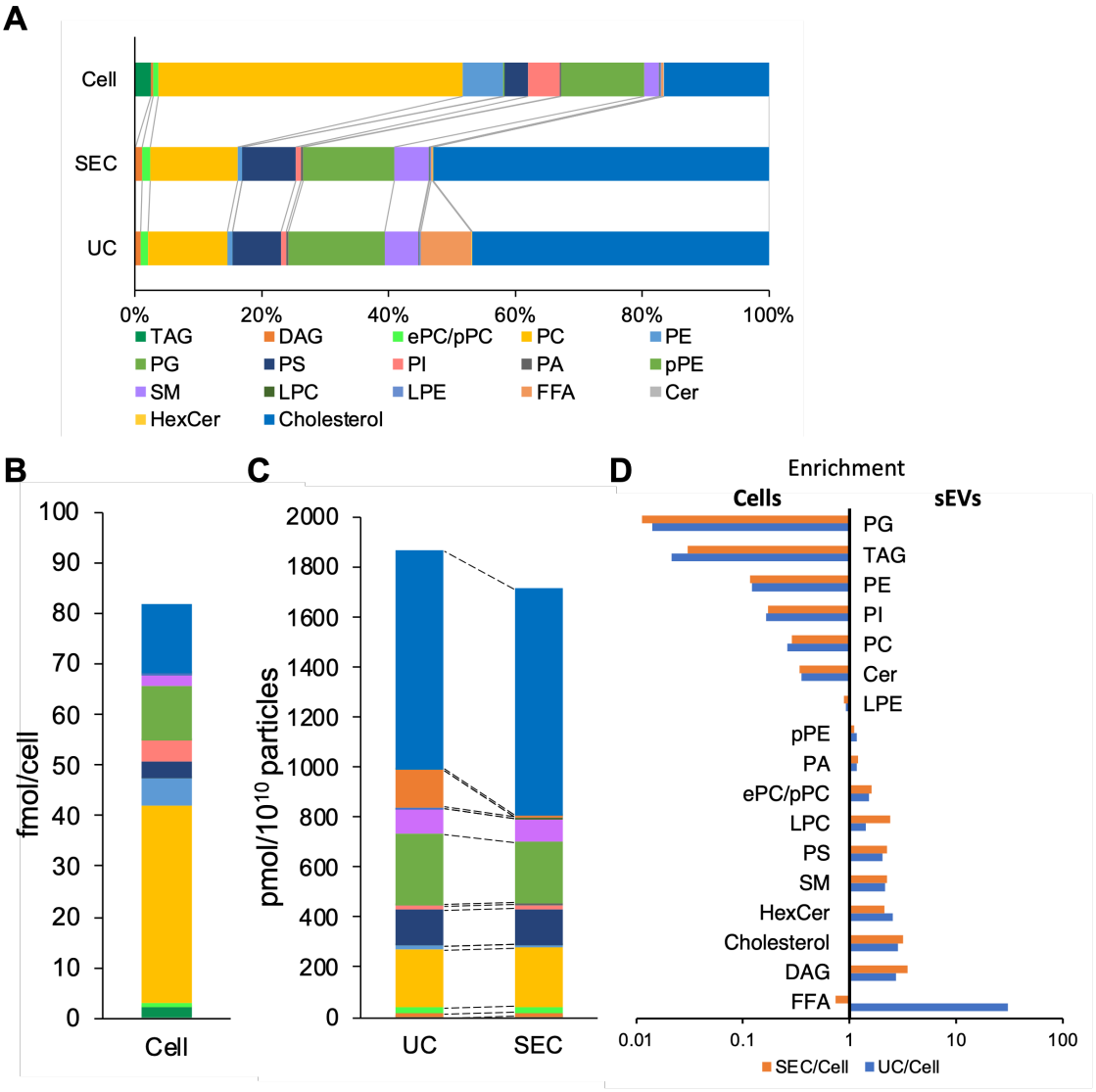

Figure 3-5. Effect of the collection method on the hydrophobic metabolite profiles in sEVs.

(A) Pie plots showing the mol-based percentile of each lipid class in cells and sEVs collected by SEC and UC. n = 3. (B) Stacked bar graph showing the abundance of each lipid class in cells. (C) Stacked bar graph showing the abundance of each lipid class in sEVs collected by SEC and UC. The correspondence between color and lipid is the same as in A. (D) Enrichment of lipid classes in cells or sEVs collected by SEC and UC. The data are shown as fold-changes of the ratio of lipid contents in sEVs per those of cells. Blue shows UC, orange shows SEC.

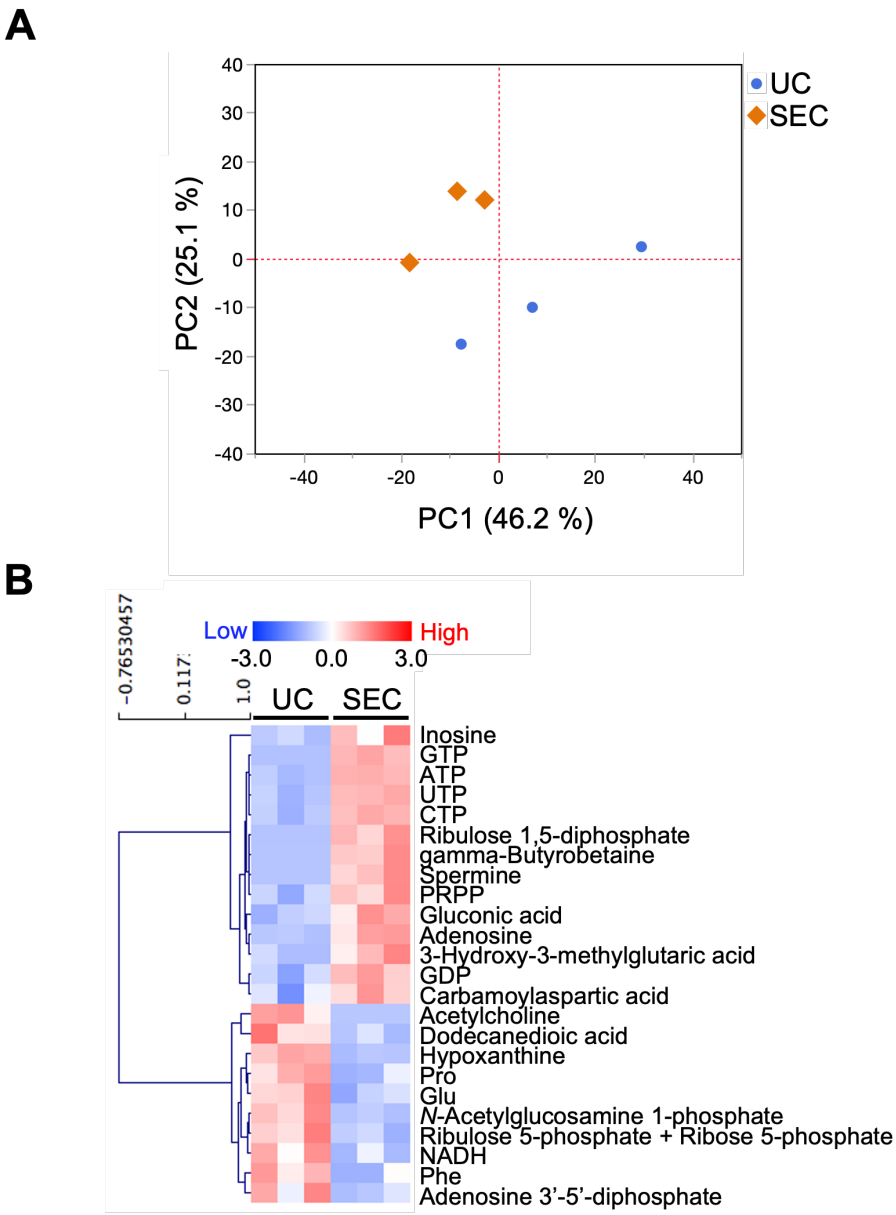

Figure 3-6. Effect of the collection method on the hydrophilic metabolite profiles in sEVs.

(A) PCA score plot of hydrophilic metabolites and lipids from UC (blue circles) and SEC (orange diamonds) samples. The contribution ratios were 46.2% and 25.1% for PC1 and PC2, respectively. Metabolites that were detected in over 50% of the samples were included in the analysis. Metabolite data from the non-cultured medium were subtracted and then normalized by particles measured by NanoSight. (B) Heatmap showing the metabolite profiles of sEVs that significantly changed metabolites between UC and SEC recovery systems. The *P* value was calculated using the Student's *t*-test, and *P* value < 0.05 was considered a significant change. n = 3.

Table 3-2. Number of lipids that significantly varied between UC and SEC recovery methods.

Lipid	UC	SEC
Triacylglycerol (TAG)	3	11
Diacylglycerol (DAG)	0	1
Phosphatidylcholine (PC)	1	12
Phosphatidylethanolamine (PE)	3	0
Phosphatidylglycerol (PG)	2	0
Alkenyl-acyl phosphatidylethanolamine (pPE)	1	0
Lysophosphatidylcholine (LPC)	2	12
Lysophosphatidylethanolamine (LPE)	3	0
Sphingomyelin (SM)	0	6
Ceramide (Cer)	1	0
Hexosylceramides (HexCer)	4	0
Free fatty acid (FFA)	0	0
Total	20	42

P value < 0.05 by Student's *t*-test.

3.4 Discussion

sEVs are involved in intercellular communication and cancer progression, and have attracted much attention (Raposo & Stoorvogel, 2013). One of the bottlenecks in sEVs research is the available collection methods for sEVs. For the further development of sEVs, a method must be efficient in recovering sEVs, suppressing foreign substances outside the sEVs, and cost- and time-efficient (Veerman et al., 2021). In addition, a method must be able to recover sEVs with minimal damage to the MS equipment for metabolomic and proteomic analyses. To solve these problems, I developed a method to fractionate and automatically collect sEVs using size-exclusion chromatography and examined their effects on metabolites.

SEC has been used to recover sEVs from urine, blood, and cultured cell supernatants (Sidhom et al., 2020). Most of the SEC protocols are kit-based, such as qEV and EV Second, and manual recovery of sEVs or kit-specific equipment are limited in their versatility (L. Sun & Meckes, 2018). In this experiment, sEVs derived from the culture supernatant were automatically collected within 30 min per injection using an HPLC column packed with size-controlled hydrophilic porous silica gel. Injection volume-dependent changes in the area, particle count, and CD63-Nanoluc of the concentrated cell culture supernatant were observed, indicating that I successfully achieved injection volume-dependent collection of sEVs. Calculating the area at 204 nm using DAD may be a used as a rough indicator for monitoring the recovery of sEVs. The time deviations were minimal, except for the first injection; however, the sEVs were stably recovered 200 times. Perhaps the solution is to perform a trial run before the first collection of sEVs and mask the adsorption with the column. UC and various kits have been problematic because of the reported effects on sEVs recovery (Brennan et al., 2020). Because the present method can set the sample and collect the sEVs, it may be possible to collect the sample with less user-dependent variation.

A comparison of sEVs recovery by SEC and UC revealed that both methods enriched the sEVs markers Alix, CD63, CD81, and Syntenin-1. Neither the ER marker calnexin nor the mitochondrial marker tomm20 were detected. Additionally, sEVs with intact lipid bilayer structures were recovered. Compared to the UC method, particles with smaller diameters were recovered to the same extent by SEC, and significantly more

particles were recovered that expressed the CD63-Nluc marker for sEVs. In addition, some of the products may have been denatured and not detected because MeOH was used for cleaning. This phenomenon has been reported in similar studies using SEC (Takov et al., 2017, 2019; Veerman et al., 2021). In this case, I prioritized purity and narrowed the recovery time. Nevertheless, I may be able to expect further improvement in the recovery rate by delaying the end time of recovery slightly longer. However, in studies using SEC on urine to recover fractions slower than the sEV fractions, I observed different protein profiles as the particles became smaller and slower (Guan et al., 2019). Because they may not be the target sEVs, careful consideration is necessary to determine whether they should be included in the recovery fraction.

Previous studies have used SEC to recover sEVs for metabolomic analyses (Du et al., 2021; Ludwig et al., 2020). Although different methods of sEVs recovery can result in different sEVs protein and RNA profiles, their effect on metabolites is unknown. Therefore, I compared the metabolomic analysis of sEVs recovered using UC as the gold standard to evaluate SEC. First, the non-cultured medium was subjected to the same process as those used for the recovery of sEVs, and metabolomic analysis identified 324 metabolites (100 hydrophilic metabolites and 224 lipids) by UC, and 250 metabolites (107 hydrophilic metabolites and 143 lipids) by SEC, indicating that the UC method is likely to detect more noise. Known contaminants during pretreatment and measurement include plasticizers, solvent impurities, reagents used during sample cleanup, and carryover contamination (Broadhurst et al., 2018). Martínez-Sena's paper reported that the blank sample detected 2843 ultra performance LC-MS signals (76% of the total) as noise (Martínez-Sena et al., 2019). In this study, these metabolites may have also originated from the culture medium, process of sEVs collection, pretreatment, or measurement. Since these metabolites were derived from sources other than sEVs, the response was to subtract them as blanks from the sample. When performing metabolite analysis of sEVs, it may be necessary to include an appropriate blank sample to determine the extent to which foreign substances affect the analysis.

In a study comparing the effects of different sEV collection methods on RNA in plasma, SEC was optimal because the miRNA-binding protein Argonaute-2 (AGO2) was the lowest, EV-specific miRNA and long non-coding RNA were observed most frequently,

and non-specific miRNA was the lowest (Y. Yang et al., 2021). In a study comparing the effect of different methods of sEV recovery on protein in urine, SEC reported better recovery of sEVs and purification in terms of protein (Guan et al., 2020). I also detected metabolite contamination of non-EVs using the UC method. Noise was present in the actual sample, as well as in the non-cultured medium, suggesting that the SEC method can recover the sample with a better degree of purification. Therefore, in this study, quantitative values were obtained by subtracting each of the metabolites detected in the non-cultured medium using the corresponding method from the actual samples. However, only advanced RPMI 1640 medium was used as the uncultured medium sample in this study, and a different medium may produce different results.

Lipid analysis of sEVs from cultured cells has shown that PS, cholesterol, and SM are enriched, and PC and PI are lower in sEVs than in cells (Llorente et al., 2013; Nishida-Aoki et al., 2020; Skotland et al., 2020). Similar changes were observed in this study when comparing the sEVs recovered by UC and SEC with the lipid class on the releasing cells. It is believed that the sEVs were successfully recovered at the lipid class level, with FFA the only lipid that showed significant variation between UC and SEC. In the non-cultured medium that was subtracted as a blank, the FFA content was higher in SEC than in UC, suggesting this lipid was not observed in SEC because of the non-cultured medium was subtracted as background in the analysis. The sEVs recovered by SEC and UC had different metabolite profiles. Specifically, the hydrophilic metabolites that varied significantly included those involved in purine-pyrimidine metabolism increased dramatically in SEC. Several metabolites involved in purine-pyrimidine metabolism, including uridine, uracil, and adenosine, have been reported in the breast cancer cell line derived sEVs (Tadokoro et al., 2020). Ludwig et al. identified many metabolites, including purines (Ludwig et al., 2020). Furthermore, in our previous study, the metabolites involved in purine-pyrimidine metabolism were more likely to be found in sEVs (Hayasaka et al., 2021). In many studies, hydrophilic metabolites involved in purine-pyrimidine metabolism have been frequently observed in sEVs (Hayasaka et al., 2021; Ludwig et al., 2020; Tadokoro et al., 2020), and many could be detected when recovered by SEC. In contrast, the UC method detected significantly more amino acids such as Pro, Glu, and Phe than SEC. These amino acids are also present in large amounts in the medium and may have accumulated under the medium influence. Focusing on the

lipids that were significantly altered, a significant increase in PC, LPC, and TAG was observed in SEC and SM, suggesting they are enriched in sEVs. PCs and LPCs are known to be limited in sEVs, but many reports indicate that they are present (Nishida-Aoki et al., 2020; Skotland et al., 2019). TAG is a lipid that, along with cholesterol ester, is abundant in high density lipoprotein (HDL), low density lipoprotein (LDL), and very low density lipoprotein (VLDL) (Y. Sun, Saito, Iiji, et al., 2019). In a study by Nishida et al. using the same medium as in this study, the authors suggested that TAG and cholesterol ester may be residues from the medium and affect sample processing (Nishida-Aoki et al., 2020), which is a potential interpretation of the results observed in this study. There may be some identically sized contamination, but this is unlikely since the mitochondrial marker Tomm20 and the ER marker calnexin were not observed. No lipid class-specific changes were observed using the UC method.

This study had several limitations. Although SEC was used to recover sEVs in this study, only the sEVs derived from cultured cells were used and results may be different from sEVs recovered from blood or urine samples. Because of the limitations of the HPLC system, only a total volume of 100 μL could be injected; therefore, multiple injections had to be performed. I believe that the SEC collection system can further shorten the sEVs collection time by improving the injection syringe and adjusting the column thickness and length to accommodate larger sample volumes. Owing to limitations of the experimental facilities, each of the experiments including in this study involved one cancer cell line, and the results may differ for other cell lines.

Chapter 4 Metabolomics of small extracellular vesicles derived from isocitrate dehydrogenase 1-mutant HCT116 cells collected by semi-automated size exclusion chromatography

4.1 Introduction

Cancer cells metabolize differently from normal cells, including the Warburg effect, in which glycolysis is used to make ATP in an oxygen-rich environment (Otto Warburg, 1956). Some metabolites, called oncometabolites, contribute to carcinogenesis and cancer progression (Khatami et al., 2019; M. Yang et al., 2013). Among these, 2-HG is the most well-known oncometabolite and 2-HG function has been linked to cancer (Xu et al., 2011). IDH1 and IDH2 are enzymes that mediate the synthesis of α-ketoglutaric acid (α-KG) from isocitrate, whereas a specific mutation in IDH1/2 results in the production of large amounts of 2-HG from α-KG (Dang et al., 2009). IDH1/2 mutations have been found in glioma, acute myelogenous leukemia (AML), chondrosarcoma, cholangiocarcinoma, and T-cell angioimmunoblastic lymphoma, as well as in colorectal and prostate cancers, with IDH1 R132H and IDH2 R140Q the frequently observed mutations (Ward et al., 2013). High concentrations of 2-HG inhibit α-KG-dependent dioxygenases, including prolyl hydroxylases (PHDs), DNA demethylases [ten-eleven translocations (TETs)], and histone lysine demethylases (KDMs), which may be involved in cancer progression by causing metabolic reprogramming via hypoxia inducible factor (HIF) stabilization and the inactivation of tumor suppressor genes via DNA and histone methylation (M. Yang et al., 2013). However, it is unclear whether 2-HG is present in sEVs released from cells.

In this study, I recovered sEVs released by IDH1 mutant colon cancer cells using the developed SEC method. I performed metabolomic analysis, which revealed a characteristic metabolomic profile with high concentrations of 2-HG.

4.2 Materials and Methods

4.2.1 Cell culture

The human colon cancer cell line HCT116 was obtained from the ATCC, and HCT116 IDH1 (R132H/+) cells were obtained from Horizon Discovery Ltd. (Cambridge, United Kingdom).

HCT116 cell and HCT116 IDH1 (R132H/+) cells were maintained in Dulbecco's modified eagle medium (DMEM) high glucose medium (FUJIFILM Wako Pure Chemical Corporation) with 10% (*v*/*v*) FBS, antibiotics, and 110 mg/mL sodium pyruvate. All the cells were cultured at 37°C in a humidified atmosphere containing 5% CO_2. All cells were confirmed to be mycoplasma-free using the Mycoalert detection kit whenever sEVs were collected.

4.2.2 Collection of cell-cultured medium

Equal numbers of cells (4.0×10^6) of HCT116 wild type (WT) cell and HCT116 IDH1 (R132H/+) cell were seeded into 150-mm dishes and pre-cultured with DMEM high glucose containing 10% FBS, antibiotics, and sodium pyruvate for 24 h. The cells were then washed twice with D-PBS. Next, the culture medium was exchanged for DMEM high glucose medium with 2% (*v*/*v*) exosome-depleted FBS (Thermo Fisher Scientific) and antibiotics and cultured for 2 days before the cell-conditioned medium was collected. Nanoparticle tracking analysis, immunoblotting, transmission electron microscopy, sEVs collection using SEC, extraction and analysis of hydrophilic metabolites and lipids from cells and sEVs, and data analysis were conducted as previously described (section 2.2.3, 2.2.4, 2.2.8, 3.2.3, 3.2.7-3.2.10).

4.3 Results

4.3.1 Isolation of sEVs released from HCT116 WT cell and HCT116 isocitrate dehydrogenase mutation cell using SEC

In this study, I attempted to recover sEVs using U87MG cells, a glioblastoma cell line transfected with a plasmid of the IDH1 (R132H/+) mutation. However, the U87MG cell line was prone to cell detachment and detached during medium exchange to medium containing exosome-depleted FBS. When exosome-depleted FBS was used, it was viscous and agglutinated, and sufficient exosomes could not be recovered. Therefore, in this study, I conducted experiments on HCT116, a colon cancer cell line frequently used in IDH1 (R132H/+) *in vitro* experiments.

To confirm that IDH1 (R132H/+) mutation alter cellular metabolism, hydrophilic metabolomic analysis using capillary IC-MS, LC-MS, and lipid analysis using SFC-MS were performed on cell samples. When metabolites were measured in IDH1-mutated HCT116 cells, 900 compounds were identified in more than 50% of the samples, including 185 hydrophilic metabolites (102 by capillary IC-MS and 83 by LC-MS) and 715 lipids. PCA revealed segregation in principal component 1, indicating that IDH1 mutations altered the cellular metabolite profile from that of the wild type (Figure 4-1A). IDH1 mutations in cancer cells result in the production of large amounts of 2-HG (Xu et al., 2011), and the volcano plot shows that 31 metabolites, including 2-HG, were increased (P value < 0.05, fold-change > 2), and a significant decrease was observed only for 2,3-bisphosphoglyceric acid when compared with that in the WT cells (Figure 4-1BC). As in the previous study (Dang et al., 2009), the IDH1 mutation cell line resulted in a high production of 2-HG in this experiment.

Next, Using the developed SEC method, sEVs were collected from 200 mL culture supernatants from the wild-type and IDH1 mutant strains of the colon cancer cell line HCT116. Significantly more sEVs were recovered from the IDH1 mutant cells than WT cells (Figure 4-2A). The mean particle size was the same for the IDH1 mutant cells and WT cells at about 135 nm (Figure 4-2B). Immunoblotting analysis detected the sEVs marker proteins Syntenin-1, Alix, CD63, and CD81, respectively, and the non-marker proteins calnexin and Tomm20, respectively, in the collected particle samples (Figure 4-2C). TEM analysis revealed particles with a diameter of approximately 100 nm in

vesicular structures in both wild-type and mutant cells (Figure 4-2D).

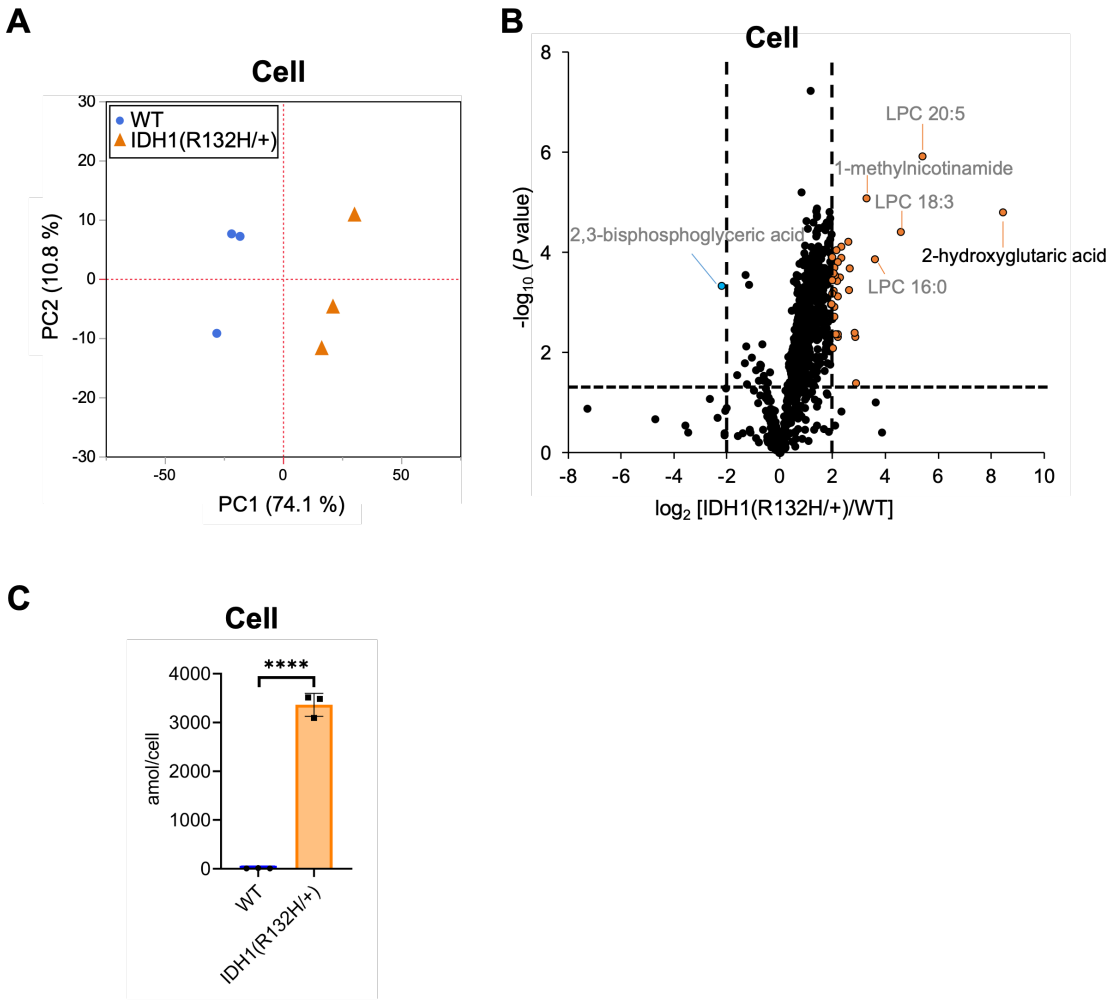

Figure 4-1. Effects of IDH1 (R132H/+) mutations on metabolites in cells.

(A) PCA score plots between wild type (WT, blue circles) and IDH1(R132H/+) (orange triangles) cells. (B) The result of a Student's *t*-test for WT cells vs. IDH1(R132H/+) is displayed as a volcano plot. The orange and blue plots are for the metabolites that increased and decreased between WT and IDH1(R132H/+), respectively. *P* value < 0.05, fold-change > 4. (C) Levels of 2-HG in sEVs. Data are represented as mean ± SD. ****P value < 0.0001.

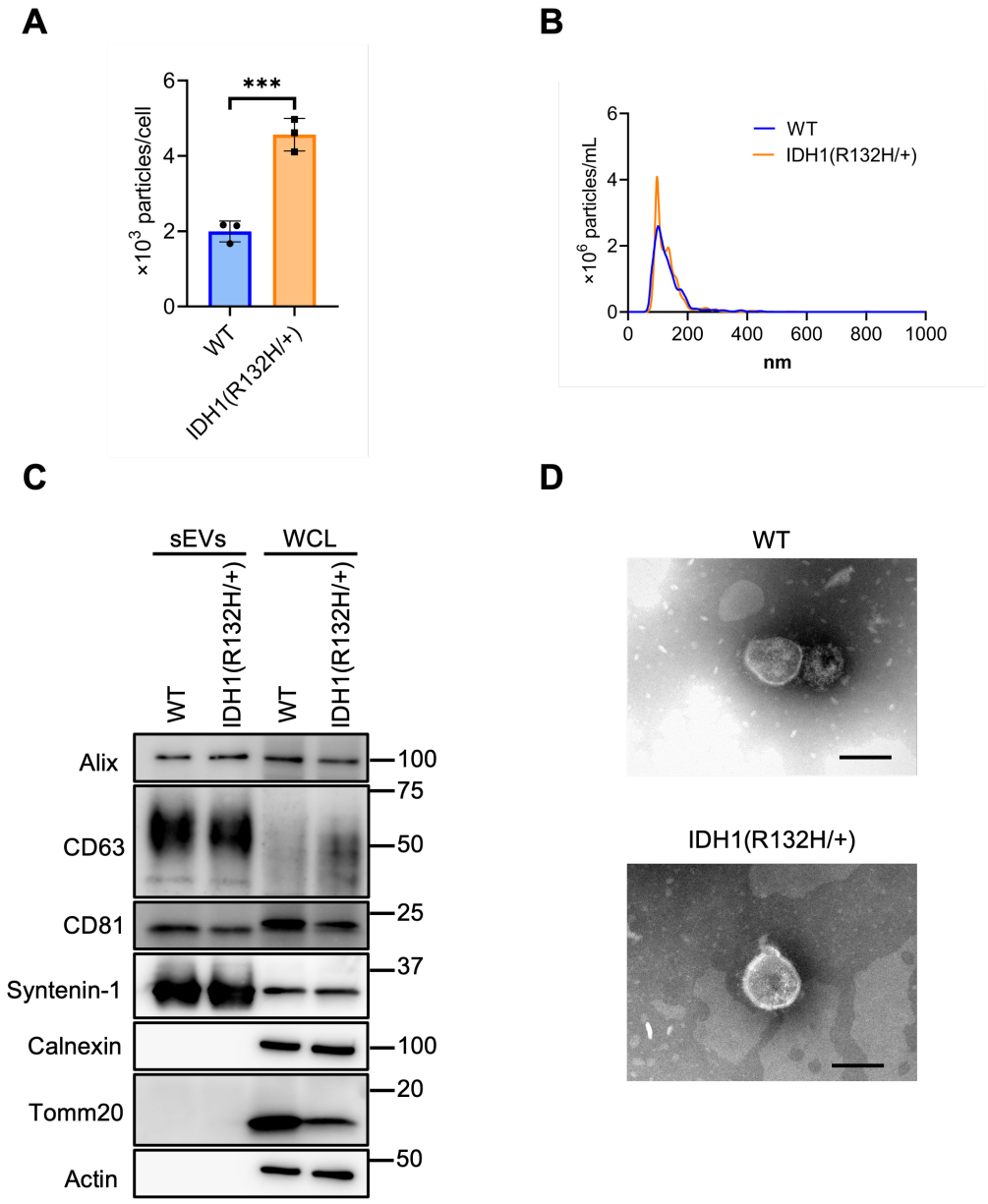

Figure 4-2. Characterization of sEVs derived from HCT116 wild-type and HCT116 IDH1 (R132H/+) cell lines.

(A) The number of particles from sEVs derived from HCT116 wild-type (WT) and IDH1 (R132H/+) cell lines. ***P value < 0.001 by Student's t-test. (B) Particles distribution of sEVs from HCT116 WT and IDH1(R132H/+) cells. (C) Immunoblotting analysis of Alix, CD63, CD81, Syntenin-1, Calnexin, Tomm20, and Actin, which was used as a loading control. The injection amount was 1.0 μg for the sEV sample and 10 μg for the WCL sample. (D) Transmission electron microscopic images of sEVs derived from HCT116 WT and IDH1(R132H/+) cells. Scale bar, 100 nm.

4.3.2 Metabolome analysis of sEVs isolated from IDH1-mutated HCT116 cells using the SEC method

Metabolite profiles in sEVs with and without mutations in the IDH1 mutation were measured. The metabolite values obtained from the non-cultured medium were subtracted from those of the sEVs samples and showed a total of 660 metabolites of which 85 were hydrophilic (64 by capillary IC-MS and 21 by LC-MS) and 575 were lipids in sEVs in more than 50% of samples. PCA was performed on metabolites that comprised more than 50% of the total metabolites, which showed a separation of the second principal component and different metabolite profiles (Figure 4-3A). As for metabolites in sEVs, in addition to 2-HG, 2-isopropylmalic acid, 3-phosphoglyceric acid (3-PG) +2-phosphoglyceric acid (2-PG), sedoheptulose 7-phosphate (S7P), creatine, and O-phosphoserine were increased in sEVs derived from the IDH1 mutation cell line, and PE 16:0p-22:2 and PE 18:1p-22:2 decreased (P value < 0.05, and less than one-fourth, Figure 4-3B). Therefore, I analyzed whether the cellular 2-HG content affected the sEV 2-HG content. The results showed that 2-HG levels were significantly increased in the mutant sEVs isolated from the IDH1 mutation cell line when compared with those of WT cell line (Figure 4-3C). Finally, I examined the extent to which the variation between WT and IDH1 mutant cell lines observed in cells was reflected in sEVs (Figure 4-4). In sEVs, only 274 of the 660 metabolites showed the same variation as that in cells, whereas the remaining 352 metabolites showed different variations. The metabolites commonly increased in cells and sEVs included 2-HG and other metabolites in the tricarboxylic acid (TCA) cycle, such as citric acid, cis-aconitic acid, isocitric acid, succinic acid, fumaric acid, malic acid; as well as metabolites involved in the glycolytic system, such as glucose 6-phosphate (G6P) and fructose 6-phosphate (F6P). Together, these results showed that the metabolite profile of the sEVs do not fully reflect the change in the cells' metabolomic profile due to IDH1 mutant. Nevertheless, sEVs derived from IDH1 mutant included 2-HG.

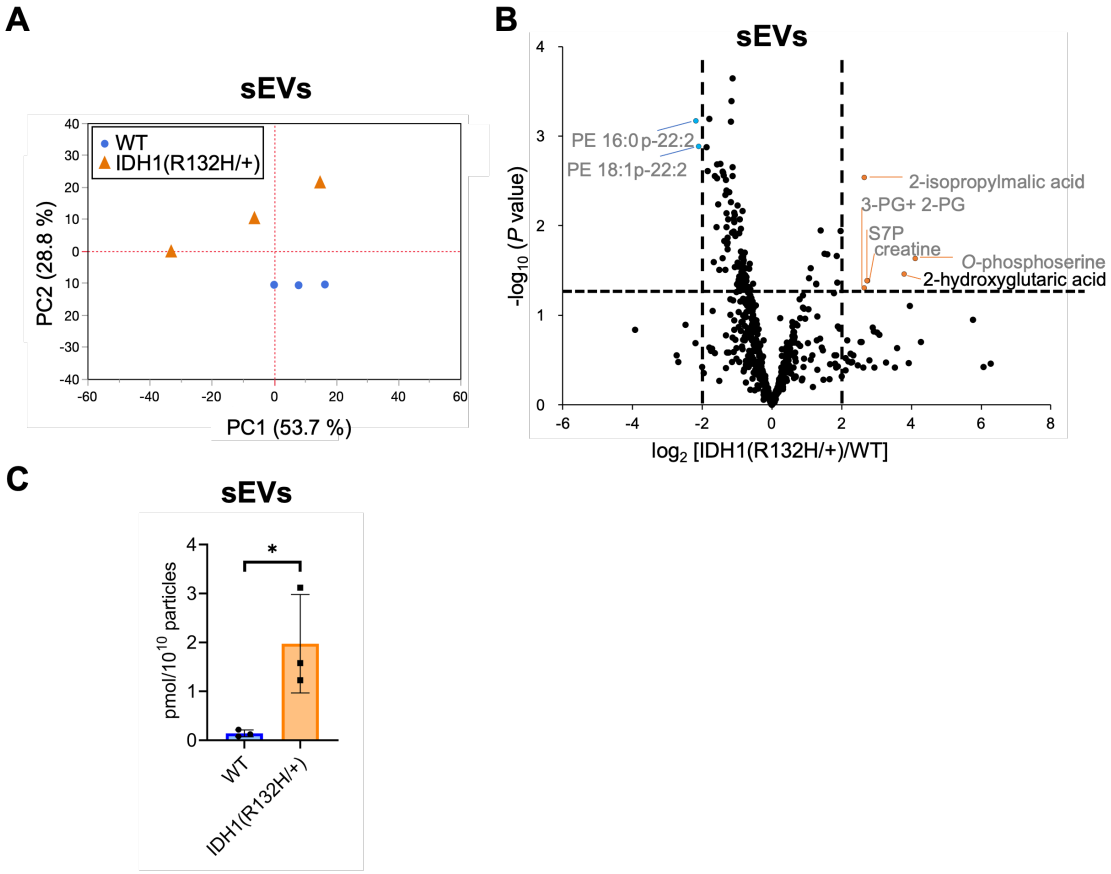

Figure 4-3. Effects of IDH1(R132H/+) mutations on metabolites in sEVs.

(A) PCA score plots between WT (blue circles) and IDH1 (R132H/+) (orange triangles) in sEVs. (B) The volcano plots illustrate the quantitative differences in metabolites in the sEV fraction. The plots marked orange and blue are same as Figure 4-1B. (C) Levels of 2-HG in sEVs. Data are represented as mean ± SD. **P* value < 0.05 by Student's *t*-test.

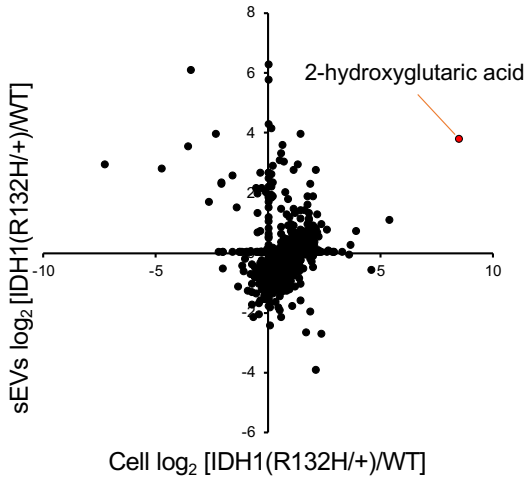

Figure 4-4. The relationship of IDH1 (R132H/+) mutations on metabolites between cells and sEVs.

The relationship between cellular and sEVs variability. The x- and y-axes indicate the variation in cell and sEVs, respectively. Variation was calculated as the ratio of IDH1 (R132H/+) to WT.

4.4 Discussion

Previous studies have reported that in cells, mutations in IDH1 produce large amounts of 2-HG, which has oncogenic functions (Ward et al., 2013). In this study, sEVs were also recovered within the marker and particle size distribution, and the IDH1 mutation cells released significantly more sEVs than the WT cells. Similar results have been reported in studies of mutant strains using glioma cells (Ludwig et al., 2022). In intrahepatic cholangiocarcinoma, a mutation in IDH1 (R132C) suggested that the downregulation of Purinergic receptor P2X 7 (*P2RX7*) was associated with the release of sEVs (X. Zhang et al., 2019), further supports that mutations in IDH1 promote the release of sEVs. I also found that the IDH1 mutation altered the metabolic profile of sEVs and significantly increased 2-HG levels in sEVs and cells. The IDH1 mutation cell line released a large number of sEVs and although the amount of 2-HG per sEVs was limited, they may carry more 2-HG to recipient cells.

Yang *et al*. reported that 5-fluorouracil (5-FU) -resistant cell lines secrete sEVs containing high levels of the IDH1 protein, which enhances 5-FU resistance (H. Yang et al., 2021). Indeed, 2-HG is involved in suppressing antitumor T-cell immunity (Bunse et al., 2018) and IDH1 mutation cell line-derived sEVs may also be involved in immunosuppression. It has also been reported that 2-HG is not readily taken up by cells and that 2-HG added to the culture medium is not intracellularly metabolized in colon cancer cell lines (Gelman et al., 2015). Therefore, additional analyses are needed to clarify if 2-HG is present in sEVs and transported to other cells.

Using the pancreatic cancer cell line PANC-1, I previously reported that the metabolite profiles of sEVs were distinct from the cells (Hayasaka et al., 2021). The present study observed similar intracellular metabolic variations in sEVs isolated from IDH1 mutation cells for only 41.5% of the metabolites identified, indicating that the intracellular metabolite fluctuations were not directly reflected in the metabolite profiles of sEVs. Among the metabolites with the same variation in cells and sEVs was 2-HG, which may be encapsulated in sEVs.

2-HG includes D-enantiomers (D-2-HG) and L-enantiomers (L-2-HG). L-2-HG levels can increase in response to changes in the tumor microenvironment, such as hypoxia and low pH (Intlekofer et al., 2017; Oldham et al., 2015), and are associated with

amino acid metabolism and other factors (Tabata et al., 2023). In this study, D-2-HG and L-2-HG were quantified together as 2-HG to measure the changes in a broader range of metabolites. Since we used a mutant strain of IDH1, it is expected that most of the analysis pertains to D-2-HG generated by the IDH1 mutation. This analysis will clarify the specific involvement of D-2-HG or L-2-HG by conducting inhibitor studies or segregation assays.

Chapter 5 Final remarks

sEVs released by cancer cells are associated with the progression of many cancers, as they facilitate angiogenesis and immunosuppression. mRNAs, miRNAs, and proteins are the main constituents of sEVs that are involved in cancer development. Limited information is available regarding the metabolites in sEVs. The lack of progress in metabolomic analysis is attributed to the low amount of recoverable sEVs, the need for a certain amount of sEVs because metabolites cannot be amplified, and the need for sensitive measurements that suppress the effects of metabolites in the culture medium. In this study, I constructed a comprehensive metabolomic system for the sEVs released by cancer cells and analyzed whether the metabolites in sEVs changed depending on the cancer microenvironment and genetic mutations.

Chapter 2 describes the establishment of a metabolomic analysis system for sEVs derived from the human pancreatic cancer cell line PANC-1 using the gold-standard UC method. sEVs were collected from 260 mL of culture supernatant per sample. The sEVs derived from PANC-1 cells contained 625 metabolites (140 hydrophilic metabolites and 485 lipids). A comparison of cells and sEVs revealed different metabolite profiles, mainly during purine-pyrimidine metabolism. Moreover, hypoxic stress, characteristic of the cancer microenvironment, induces the release of large amounts of sEVs with different metabolites, including 2-deoxyribose 1-phosphate, which is involved in angiogenesis. This is the first study to analyze a wide range of hydrophilic metabolites and lipids in sEVs using targeted metabolomic analysis.

Chapter 3 explores the effects of different methods of sEVs collection methods on metabolites. Although SEC has attracted attention as a useful sEVs collection method in recent years, it is rather complicated, and thus is more suitable for processing multiple samples. Therefore, a semi-automated sEVs recovery system was constructed by combining size-exclusion chromatography and preparative HPLC. A comparison of sEVs recovered via UC and SEC revealed different metabolite profiles, with sEVs recovered via SEC showing significantly changed metabolites in purine-pyrimidine metabolism. Semi-automated SEC may be a valuable tool for sEV recovery.

Chapter 4 describes the use of semi-automated size-exclusion chromatography to explore the effects of genetic mutations on the metabolite profiles of sEVs. The IDH1 mutation, which is involved in the production of the oncometabolite, releases large

amounts of sEVs. Similar to cells, sEVs also contain large amounts of 2-HG. To the best of my knowledge, this is the first study to demonstrate that sEVs contain 2-HG. Metabolites released by sEVs may be involved in the malignant transformation of tumors by cancer cells.

5.1 Key point of this doctoral dissertation

The following is a discussion of the key points I focused on in this doctoral dissertation:

5.1.1 Comprehensive and quantitative analysis of metabolites in sEVs is now possible

Hydrophilic metabolites were analyzed using capillary IC-MS and LC-MS, and lipids using SFC-MS, and the results showed that sEVs from the pancreatic cancer cell line PANC-1 contained 140 hydrophilic metabolites and 494 lipids. As less than 40 hydrophilic metabolites have been reported to date, these findings indicate that the method developed in this study enables the analysis of a much larger number of metabolites than was previously possible.

Most previous studies analyzed the effects of metabolites produced in a medium containing large amounts of metabolites or in the pretreatment process without considering the effects of the metabolites. Samples from uncultured media analyzed using the same method showed many metabolites, including lactic acid and MAG, which are used as plasticizers in plastics. These metabolites may have previously been classified as contaminants outside sEVs. The method developed in this study eliminated the effects of contamination outside the sEVs, including in the culture medium, resulting in data with less noise than in other studies. When performing microanalysis, including of sEVs, I propose establishing appropriate blanks, particularly to control the effects of pretreatment and other contaminants. However, in the case of body fluids such as blood and urine, it is impossible to set up a blank as for non-cultured media; therefore, an appropriate blank would need to be considered separately.

This is the first study to quantitatively analyze hydrophilic metabolites and lipids from a single sEV sample. The method developed here is an efficient approach for

analyzing hydrophilic metabolites and lipids, mainly because the number of sEVs that can be recovered is limited.

5.1.2 Efficient recovery of sEVs by preparative HPLC combined with SEC

To adapt the SEC method, which has been frequently used for sEV recovery in recent years, to recover sEVs from multiple samples, a semi-automated sEV recovery system combining preparative HPLC and SEC was constructed. The SEC method developed here was superior to UC in terms of sEV recovery. The sEVs recovered by SEC reflected the hydrophilic metabolite and lipid profiles of sEVs and were sufficiently recovered.

I focused on sEVs derived from cultured cells; however, sEVs are also present in body fluids such as blood, urine, and saliva. SEC is a useful method for analyzing sEVs from body fluids, where the amount of available fluid is limited, as it enables efficient multi-sample processing while monitoring the presence of sEVs without the need for sample dilution. Moreover, the SEC method enables the analysis of sEVs more efficiently and with a shorter handling time than conventional methods.

This method can be used for the analysis of metabolites, nucleic acids, and proteins and is expected to be an effective method for biomarker search in body fluids. It is important to analyze the sEVs analysis while considering the effects of components that co-elute with sEVs, such as lipoproteins in blood and uromodulin in urine.

5.1.3. Cells and sEVs have different metabolite profiles, with sEVs containing characteristic metabolites

The relationship between cells and sEVs is known for proteins and lipids, but not for hydrophilic metabolites. Metabolites, such as those involved in purine-pyrimidine metabolism, were observed in the sEVs in pancreatic and colorectal cancer cell lines. Therefore, the metabolite profiles of the cells are not always reflected in sEVs.

Marker lipids of sEVs, such as cholesterol, SM, and PS, and marker proteins of sEVs, such as CD9, CD63, and CD81, are involved in sEV release. Indeed, proteins involved in purine-pyrimidine metabolism, such as GTPases and ATP-induced P2X7

receptor, support release sEVs. Metabolites of purine-pyrimidine metabolism, the characteristic metabolites of sEVs observed in this study, may also be involved in the release process.

The localization of metabolites within the cell may be related to the metabolites in sEVs. Although imaging analyses of intracellular metabolites are currently underway, additional information on the subcellular localization of these metabolites is necessary. This information will be obtained as future studies further explore metabolite localization.

Cancer cells are heterogeneous and comprise a variety of cell types. A single cell also releases sEVs with different markers during multiple release processes. Currently, sEV analysis is performed in bulk to obtain an average metabolite profile. Analyzing sEVs in a more controlled environment would provide valuable information on sEV metabolites.

5.1.4 Metabolites in sEVs fluctuate according to genetic mutations and the cancer microenvironment and include metabolites involved in cancer progression

I investigated how the metabolism of sEVs is altered in an environment that significantly alters cancer cell metabolism. Hypoxic stress, a characteristic of the cancer microenvironment in pancreatic cancer, and mutations in the IDH1 gene in colorectal cancer alter intracellular metabolism as well as the metabolite profile of sEVs. During hypoxic stress in pancreatic cancer, 2-deoxyribose 1-phosphate, a metabolite involved in angiogenesis that is released extracellularly as soon as it is synthesized in the cell, was found to be significantly increased in sEVs. It may be selectively released by sEVs upon their release from the cell.

This study shows that 2-HG, an oncometabolite involved in cancer progression, is increased in sEVs in IDH1 mutation in colorectal cancer. To the best of my knowledge, this is the first study to demonstrate the presence of oncometabolites in sEVs. Owing to its absence on the cell surface, the 2-HG transporter may contribute to cancer malignancy by facilitating metabolite uptake into recipient cells for the first time through sEVs. This is the first study to suggest that hydrophilic metabolites may also play a role in cancer progression, although miRNAs, proteins, and lipids are thought to be involved in the malignant transformation of cancer cells via sEVs.

Finally, in this doctoral dissertation, a metabolomic method suitable for sEVs was developed that facilitated the quantitative analysis of many metabolites in sEVs. The technology developed in this study enabled the analysis of numerous metabolites in sEVs and, for the first time, elucidated the characteristics of sEVs released by cancer cells and the inclusion of metabolites involved in cancer progression. Although this doctoral dissertation focuses on sEVs released by cancer cells into culture supernatants, sEVs are also present in body fluids such as blood, urine, and saliva. The therapeutic effects of sEVs released by mesenchymal stem cells have also been reported. In addition to vertebrates, sEVs released by microorganisms and plants have attracted attention for their application as drug delivery systems. These cells release sEVs that are involved in intercellular communication. The techniques developed in this doctoral dissertation can be used to elucidate the functions and roles of metabolites in sEVs. This study can lead to a better understanding of communications via sEVs.

Acknowledgements

I would first like to thank Professor Masaru Tomita. After listening to Professor Tomita's dreamy lecture on biology in the fall of my first year of high school, I was inspired to study biology. As a special research student, I studied at the Institute for Advanced Biosciences (IAB), Keio University, beginning in my second year of high school. If I had not met Prof. Tomita, and the lab had not been in Tsuruoka, I would not have been able to advance my research to this point. In addition, thank you, Professor Tomita, for taking on the role of chief executive for so long.

I would next like to thank Associate Professor Akiyoshi Hirayama for serving as primary advisor for my doctoral dissertation. I am very grateful for your support from the first year of my master's program until I graduated with my doctorate. I learned about metabolome analysis technology and how to live as a researcher. I have enjoyed and grown from a variety of experiences, and without Associate Professor Hirayama, I would not have been able to write my doctoral dissertation. I cannot thank you enough.

I would like to thank Professor Tomoyoshi Soga for accepting me as a sub-examiner. I was fortunate to have been able to conduct my research using the metabolomics analysis facilities. I would like to thank Professor Akio Kanai for graciously accepting to be my sub-examiner. Professor Kanai regularly shared information on exosomes with me and provided me with sound advice.

My first advisor, Professor Akira Oikawa, taught me fascinating aspects of biological metabolism as a high school student. I also appreciated the opportunity to present my work at an international conference during my second year of undergraduate studies. I am grateful to my second advisor, Kaori Tanaka, for teaching me the basics of research and for guiding me in many other aspects of life. I learned from Dr. Masataka Wakayama the importance of focusing on various specific aspects of this research subject. I am grateful to Dr. Sho Tabata for teaching me about molecular biology in cultured cells. Even after leaving Keio University, I had many discussions with him despite his busy schedule.

I would like to thank Prof. Masahiro Sugimoto, Prof. Atsuo T. Sasaki, Assoc. prof. Yasuhiro Saito, Dr. Junko Murai, Dr. Shojiro Kitajima, Dr. Masaru Mori, and

Takamasa Ishikawa for their insightful discussions on various occasions and for giving me much advice. I would like to thank Masako Hasebe, Satsuki Ikeda, Ryuhei Kudo, and other members of the Metabolome Group, and Sumiko Onuma for their technical support in various fields, including metabolomic and proteomic analyses.

I am grateful to Prof. Kazuharu Arakawa, director of the IAB, for providing me with a favorable research environment.

I would also like to thank Satomi Yokoi, Chisa Namba, Junko Hamada, Mayumi Ochiai, Kazumi Saita, Yoko Ogiso, Reiko Kato, Miho Sato, Tomomi Yamashina, Akiko Shiozawa, Komatsu Katsunori, and all lab administrative staff for maintaining a pleasant research environment. I am grateful to all my advisees, Megumi Tsurumaki, Yoshiro Kita, Kaoruko Uchimura, Nodoka Fukumitsu, Yixiao Ma, Mayako Kureyasu, Yukako Suzuki, Momo Sato, Eri Takagi, Shota Suzuki, and Haruna Aiba, from whom I learned much.

I am grateful to Dr. Hitoshi Ozawa, Dr. Hitoshi Iuchi, Arisa Matsuura, Dr. Megumi Uetaki, Jing Guo, Shota Hida, Yuki Yamazaki, Hitomi Okazaki, and Mayuko Takato, senior members of the Metabolome Group, for their meaningful advice at group meetings. I am very grateful to Dr. Satoshi Tamaki, Dr. Doshun Ito, Gakuto Makino, Dr. Yuki Yoshida, Dr. Hideto Mori, Dr. Fumie Nakasuka, Airi Hosoya, Rira Matsuta, Takahiro Masuda, Atsuki Kawai, Dr. Shiori Hikichi, Maiko Wakita, Dr. Tomoki Oyama, and Dr. Hironori Iwai for the wonderful times I have shared during my research life.

I would like to thank Dr. Hiroko Tadokoro and Prof. Takahiro Ochiya from Tokyo Medical University, Dr. Koji Ueda from the Japanese Foundation for Cancer Research, Prof. Chitose Oneyama and Dr. Tomoya Hikita from Aichi Cancer Center Research Institute, and Prof. Takeshi Bamba, Dr. Yoshihiro Izumi and Dr. Masatomo Takahashi from Kyushu University for their support in conducting these studies.

Finally, I thank my family for their support, especially in my daily life.

References

Alameldin, S., Costina, V., Abdel-Baset, H. A., Nitschke, K., Nuhn, P., Neumaier, M., & Hedtke, M. (2021). Coupling size exclusion chromatography to ultracentrifugation improves detection of exosomal proteins from human plasma by LC-MS. *Practical Laboratory Medicine*, *26*(June), e00241. https://doi.org/10.1016/j.plabm.2021.e00241

Altadill, T., Campoy, I., Lanau, L., Gill, K., Rigau, M., Gil-Moreno, A., Reventos, J., Byers, S., Colas, E., & Cheema, A. K. (2016). Enabling Metabolomics Based Biomarker Discovery Studies Using Molecular Phenotyping of Exosome-Like Vesicles. *PLOS ONE*, *11*(3), e0151339. https://doi.org/10.1371/journal.pone.0151339

Baietti, M. F., Zhang, Z., Mortier, E., Melchior, A., Degeest, G., Geeraerts, A., Ivarsson, Y., Depoortere, F., Coomans, C., Vermeiren, E., Zimmermann, P., & David, G. (2012). Syndecan-syntenin-ALIX regulates the biogenesis of exosomes. *Nature Cell Biology*, *14*(7), 677–685. https://doi.org/10.1038/ncb2502

Baranyai, T., Herczeg, K., Onódi, Z., Voszka, I., Módos, K., Marton, N., Nagy, G., Mäger, I., Wood, M. J., El Andaloussi, S., Pálinkás, Z., Kumar, V., Nagy, P., Kittel, Á., Buzás, E. I., Ferdinandy, P., & Giricz, Z. (2015). Isolation of Exosomes from Blood Plasma: Qualitative and Quantitative Comparison of Ultracentrifugation and Size Exclusion Chromatography Methods. *PloS One*, *10*(12), e0145686. https://doi.org/10.1371/journal.pone.0145686

Barrès, C., Blanc, L., Bette-Bobillo, P., André, S., Mamoun, R., Gabius, H. J., & Vidal, M. (2010). Galectin-5 is bound onto the surface of rat reticulocyte exosomes and modulates vesicle uptake by macrophages. *Blood*, *115*(3), 696–705. https://doi.org/10.1182/blood-2009-07-231449

Beccard, I. J., Hofmann, L., Schroeder, J. C., Ludwig, S., Laban, S., Brunner, C., Lotfi, R., Hoffmann, T. K., Jackson, E. K., Schuler, P. J., & Theodoraki, M.-N. (2020). Immune Suppressive Effects of Plasma-Derived Exosome Populations in Head and Neck Cancer. *Cancers*, *12*(7), 1997. https://doi.org/10.3390/cancers12071997

Bellio, M. A., Young, K. C., Milberg, J., Santos, I., Abdullah, Z., Stewart, D., Arango, A., Chen, P., Huang, J., Williams, K., Kelly, K., Sterling, S., Khan, A., Xu, X., Shapiro, G. C., & Mitrani, M. I. (2021). Amniotic fluid-derived extracellular vesicles: characterization and therapeutic efficacy in an experimental model of bronchopulmonary dysplasia. *Cytotherapy*, *23*(12), 1097–1107. https://doi.org/10.1016/j.jcyt.2021.07.011

Berchem, G., Noman, M. Z., Bosseler, M., Paggetti, J., Baconnais, S., Le cam, E., Nanbakhsh, A., Moussay, E., Mami-Chouaib, F., Janji, B., & Chouaib, S. (2016). Hypoxic tumor-derived microvesicles negatively regulate NK cell function by a mechanism involving TGF-β and miR23a transfer.

OncoImmunology, *5*(4), 1–13. https://doi.org/10.1080/2162402X.2015.1062968

Bergsmedh, A., Szeles, A., Henriksson, M., Bratt, A., Folkman, M. J., Spetz, A. L., & Holmgren, L. (2001). Horizontal transfer of oncogenes by uptake of apoptotic bodies. *Proceedings of the National Academy of Sciences of the United States of America*, *98*(11), 6407–6411. https://doi.org/10.1073/pnas.101129998

Biancur, D. E., Paulo, J. A., Małachowska, B., Quiles Del Rey, M., Sousa, C. M., Wang, X., Sohn, A. S. W., Chu, G. C., Gygi, S. P., Harper, J. W., Fendler, W., Mancias, J. D., & Kimmelman, A. C. (2017). Compensatory metabolic networks in pancreatic cancers upon perturbation of glutamine metabolism. *Nature Communications*, *8*(1), 15965. https://doi.org/10.1038/ncomms15965

Brennan, K., Martin, K., FitzGerald, S. P., O'Sullivan, J., Wu, Y., Blanco, A., Richardson, C., & Mc Gee, M. M. (2020). A comparison of methods for the isolation and separation of extracellular vesicles from protein and lipid particles in human serum. *Scientific Reports*, *10*(1), 1039. https://doi.org/10.1038/s41598-020-57497-7

Broadhurst, D., Goodacre, R., Reinke, S. N., Kuligowski, J., Wilson, I. D., Lewis, M. R., & Dunn, W. B. (2018). Guidelines and considerations for the use of system suitability and quality control samples in mass spectrometry assays applied in untargeted clinical metabolomic studies. *Metabolomics*, *14*(6), 72. https://doi.org/10.1007/s11306-018-1367-3

Brown, D. G., Rao, S., Weir, T. L., O'Malia, J., Bazan, M., Brown, R. J., & Ryan, E. P. (2016). Metabolomics and metabolic pathway networks from human colorectal cancers, adjacent mucosa, and stool. *Cancer & Metabolism*, *4*(1), 11. https://doi.org/10.1186/s40170-016-0151-y

Bunse, L., Pusch, S., Bunse, T., Sahm, F., Sanghvi, K., Friedrich, M., Alansary, D., Sonner, J. K., Green, E., Deumelandt, K., Kilian, M., Neftel, C., Uhlig, S., Kessler, T., von Landenberg, A., Berghoff, A. S., Marsh, K., Steadman, M., Zhu, D., … Platten, M. (2018). Suppression of antitumor T cell immunity by the oncometabolite (R)-2-hydroxyglutarate. *Nature Medicine*, *24*(8), 1192–1203. https://doi.org/10.1038/s41591-018-0095-6

Chapuy-Regaud, S., Dubois, M., Plisson-Chastang, C., Bonnefois, T., Lhomme, S., Bertrand-Michel, J., You, B., Simoneau, S., Gleizes, P. E., Flan, B., Abravanel, F., & Izopet, J. (2017). Characterization of the lipid envelope of exosome encapsulated HEV particles protected from the immune response. *Biochimie*, *141*, 70–79. https://doi.org/10.1016/j.biochi.2017.05.003

Chen, X., Ying, X., Wang, X., Wu, X., Zhu, Q., & Wang, X. (2017). Exosomes derived from hypoxic epithelial ovarian cancer deliver microRNA-940 to induce macrophage M2 polarization. *Oncology Reports*, *38*(1), 522–528. https://doi.org/10.3892/or.2017.5697

Cui, L., Liu, J., Yan, X., & Hu, S. (2017). Identification of Metabolite Biomarkers for Gout Using Capillary Ion Chromatography with Mass Spectrometry. *Analytical Chemistry*, *89*(21), 11737–11743.

https://doi.org/10.1021/acs.analchem.7b03232

Dang, L., White, D. W., Gross, S., Bennett, B. D., Bittinger, M. A., Driggers, E. M., Fantin, V. R., Jang, H. G., Jin, S., Keenan, M. C., Marks, K. M., Prins, R. M., Ward, P. S., Yen, K. E., Liau, L. M., Rabinowitz, J. D., Cantley, L. C., Thompson, C. B., Vander Heiden, M. G., & Su, S. M. (2009). Cancer-associated IDH1 mutations produce 2-hydroxyglutarate. *Nature*, *462*(7274), 739–744. https://doi.org/10.1038/nature08617

de Gassart, A., Géminard, C., Février, B., Raposo, G., & Vidal, M. (2003). Lipid raft-associated protein sorting in exosomes. *Blood*, *102*(13), 4336–4344. https://doi.org/10.1182/blood-2003-03-0871

Du, Y., Chen, L., Li, X.-S., Li, X., Xu, X., Tai, S., Yang, G., Tang, Q., Liu, H., Liu, S.-H., Zhang, S.-Y., & Cheng, Y. (2021). Metabolomic Identification of Exosome-Derived Biomarkers for Schizophrenia: A Large Multicenter Study. *Schizophrenia Bulletin*, *47*(3), 615–623. https://doi.org/10.1093/schbul/sbaa166

Eales, K. L., Hollinshead, K. E. R., & Tennant, D. A. (2016). Hypoxia and metabolic adaptation of cancer cells. *Oncogenesis*, *5*(1), e190. https://doi.org/10.1038/oncsis.2015.50

Erdbrügger, U., Blijdorp, C. J., Bijnsdorp, I. V., Borràs, F. E., Burger, D., Bussolati, B., Byrd, J. B., Clayton, A., Dear, J. W., Falcón-Pérez, J. M., Grange, C., Hill, A. F., Holthöfer, H., Hoorn, E. J., Jenster, G., Jimenez, C. R., Junker, K., Klein, J., Knepper, M. A., … Martens-Uzunova, E. S. (2021). Urinary extracellular vesicles: A position paper by the Urine Task Force of the International Society for Extracellular Vesicles. *Journal of Extracellular Vesicles*, *10*(7), e12093. https://doi.org/10.1002/jev2.12093

Escrevente, C., Keller, S., Altevogt, P., & Costa, J. (2011). Interaction and uptake of exosomes by ovarian cancer cells. *BMC Cancer*, *11*(1), 108. https://doi.org/10.1186/1471-2407-11-108

Feingold, K. R. (2000). Introduction to Lipids and Lipoproteins. In *Endotext*. http://www.ncbi.nlm.nih.gov/pubmed/23075464

Février, B., & Raposo, G. (2004). Exosomes: Endosomal-derived vesicles shipping extracellular messages. *Current Opinion in Cell Biology*, *16*(4), 415–421. https://doi.org/10.1016/j.ceb.2004.06.003

Gelman, S. J., Mahieu, N. G., Cho, K., Llufrio, E. M., Wencewicz, T. A., & Patti, G. J. (2015). Evidence that 2-hydroxyglutarate is not readily metabolized in colorectal carcinoma cells. *Cancer & Metabolism*, *3*(1), 13. https://doi.org/10.1186/s40170-015-0139-z

Guan, S., Guan, S., Yu, H., Yu, H., Yan, G., Gao, M., Sun, W., & Zhang, X. (2020). Characterization of Urinary Exosomes Purified with Size Exclusion Chromatography and Ultracentrifugation. *Journal of Proteome Research*, *19*(6), 2217–2225. https://doi.org/10.1021/acs.jproteome.9b00693

Guan, S., Yu, H., Yan, G., Gao, M., Sun, W., & Zhang, X. (2019). Size-dependent sub-proteome analysis

of urinary exosomes. *Analytical and Bioanalytical Chemistry*, *411*(18), 4141–4149. https://doi.org/10.1007/s00216-019-01616-5

Guo, Z., Wang, X., Yang, Y., Chen, W., Zhang, K., Teng, B., Huang, C., Zhao, Q., & Qiu, Z. (2020). Hypoxic Tumor-Derived Exosomal Long Noncoding RNA UCA1 Promotes Angiogenesis via miR-96-5p/AMOTL2 in Pancreatic Cancer. *Molecular Therapy. Nucleic Acids*, *22*(December), 179–195. https://doi.org/10.1016/j.omtn.2020.08.021

Hayasaka, R., Tabata, S., Hasebe, M., Ikeda, S., Hikita, T., Oneyama, C., Yoshitake, J., Onoshima, D., Takahashi, K., Shibata, T., Uchida, K., Baba, Y., Soga, T., Tomita, M., & Hirayama, A. (2023). Metabolomics of small extracellular vesicles derived from isocitrate dehydrogenase 1-mutant HCT116 cells collected by semi-automated size exclusion chromatography. *Frontiers in Molecular Biosciences*, *9*(January), 1049402. https://doi.org/10.3389/fmolb.2022.1049402

Hayasaka, R., Tabata, S., Hasebe, M., Ikeda, S., Ohnuma, S., Mori, M., Soga, T., Tomita, M., & Hirayama, A. (2021). Metabolomic Analysis of Small Extracellular Vesicles Derived from Pancreatic Cancer Cells Cultured under Normoxia and Hypoxia. *Metabolites*, *11*(4), 215. https://doi.org/10.3390/metabo11040215

Hefley, B. S., Deighan, C., Vasini, B., Khan, A., Hjortdal, J., Riaz, K. M., Liu, Y., & Karamichos, D. (2022). Revealing the presence of tear extracellular vesicles in Keratoconus. *Experimental Eye Research*, *224*(June), 109242. https://doi.org/10.1016/j.exer.2022.109242

Hikita, T., Kuwahara, A., Watanabe, R., Miyata, M., & Oneyama, C. (2019). Src in endosomal membranes promotes exosome secretion and tumor progression. *Scientific Reports*, *9*(1), 3265. https://doi.org/10.1038/s41598-019-39882-z

Hikita, T., Miyata, M., Watanabe, R., & Oneyama, C. (2018). Sensitive and rapid quantification of exosomes by fusing luciferase to exosome marker proteins. *Scientific Reports*, *8*(1), 14035. https://doi.org/10.1038/s41598-018-32535-7

Hirayama, A., Kami, K., Sugimoto, M., Sugawara, M., Toki, N., Onozuka, H., Kinoshita, T., Saito, N., Ochiai, A., Tomita, M., Esumi, H., & Soga, T. (2009). Quantitative metabolome profiling of colon and stomach cancer microenvironment by capillary electrophoresis time-of-flight mass spectrometry. *Cancer Research*, *69*(11), 4918–4925. https://doi.org/10.1158/0008-5472.CAN-08-4806

Hirayama, A., Tabata, S., Kudo, R., Hasebe, M., Suzuki, K., Tomita, M., & Soga, T. (2020). The use of a double coaxial electrospray ionization sprayer improves the peak resolutions of anionic metabolites in capillary ion chromatography-mass spectrometry. *Journal of Chromatography A*, *1619*, 460914. https://doi.org/10.1016/j.chroma.2020.460914

Hirayama, A., Tomita, M., & Soga, T. (2012). Sheathless capillary electrophoresis-mass spectrometry with a high-sensitivity porous sprayer for cationic metabolome analysis. *Analyst*, *137*(21), 5026–5033.

https://doi.org/10.1039/c2an35492f

Hori, M., Matsuda, T., Shibata, A., Katanoda, K., Sobue, T., & Nishimoto, H. (2015). Cancer incidence and incidence rates in Japan in 2009: A study of 32 population-based cancer registries for the Monitoring of Cancer Incidence in Japan (MCIJ) project. *Japanese Journal of Clinical Oncology*, *45*(9), 884–891. https://doi.org/10.1093/jjco/hyv088

Hoshino, A., Costa-Silva, B., Shen, T.-L., Rodrigues, G., Hashimoto, A., Tesic Mark, M., Molina, H., Kohsaka, S., Di Giannatale, A., Ceder, S., Singh, S., Williams, C., Soplop, N., Uryu, K., Pharmer, L., King, T., Bojmar, L., Davies, A. E., Ararso, Y., … Lyden, D. (2015). Tumour exosome integrins determine organotropic metastasis. *Nature*, *527*(7578), 329–335. https://doi.org/10.1038/nature15756

Hu, S., Wang, J., Ji, E. H., Christison, T., Lopez, L., & Huang, Y. (2015). Targeted Metabolomic Analysis of Head and Neck Cancer Cells Using High Performance Ion Chromatography Coupled with a Q Exactive HF Mass Spectrometer. *Analytical Chemistry*, *87*(12), 6371–6379. https://doi.org/10.1021/acs.analchem.5b01350

Huang, J., Weinstein, S. J., Kitahara, C. M., Karoly, E. D., Sampson, J. N., & Albanes, D. (2017). A prospective study of serum metabolites and glioma risk. *Oncotarget*, *8*(41), 70366–70377. https://doi.org/10.18632/oncotarget.19705

Ikeda, C., Haga, H., Makino, N., Inuzuka, T., Kurimoto, A., Ueda, T., Matsuda, A., Kakizaki, Y., Ishizawa, T., Kobayashi, T., Sugahara, S., Tsunoda, M., Suda, K., & Ueno, Y. (2021). Utility of Claudin-3 in extracellular vesicles from human bile as biomarkers of cholangiocarcinoma. *Scientific Reports*, *11*(1), 1195. https://doi.org/10.1038/s41598-021-81023-y

Intlekofer, A. M., Wang, B., Liu, H., Shah, H., Carmona-Fontaine, C., Rustenburg, A. S., Salah, S., Gunner, M. R., Chodera, J. D., Cross, J. R., & Thompson, C. B. (2017). L-2-Hydroxyglutarate production arises from noncanonical enzyme function at acidic pH. *Nature Chemical Biology*, *13*(5), 494–500. https://doi.org/10.1038/nchembio.2307

Iwai, K., Minamisawa, T., Suga, K., Yajima, Y., & Shiba, K. (2016). Isolation of human salivary extracellular vesicles by iodixanol density gradient ultracentrifugation and their characterizations. *Journal of Extracellular Vesicles*, *5*(1), 30829. https://doi.org/10.3402/jev.v5.30829

Jeppesen, D. K., Fenix, A. M., Franklin, J. L., Higginbotham, J. N., Zhang, Q., Zimmerman, L. J., Liebler, D. C., Ping, J., Liu, Q., Evans, R., Fissell, W. H., Patton, J. G., Rome, L. H., Burnette, D. T., & Coffey, R. J. (2019). Reassessment of Exosome Composition. *Cell*, *177*(2), 428-445.e18. https://doi.org/10.1016/j.cell.2019.02.029

Johnstone, R. M., Adam, M., Hammond, J. R., Orr, L., & Turbide, C. (1987). Vesicle formation during reticulocyte maturation. Association of plasma membrane activities with released vesicles

(exosomes). *Journal of Biological Chemistry*, *262*(19), 9412–9420. https://doi.org/10.1016/s0021-9258(18)48095-7

Jung, K. O., Youn, H., Lee, C. H., Kang, K. W., & Chung, J. K. (2017). Visualization of exosome-mediated miR-210 transfer from hypoxic tumor cells. *Oncotarget*, *8*(6), 9899–9910. https://doi.org/10.18632/oncotarget.14247

Kalra, H., Simpson, R. J., Ji, H., Aikawa, E., Altevogt, P., Askenase, P., Bond, V. C., Borràs, F. E., Breakefield, X., Budnik, V., Buzas, E., Camussi, G., Clayton, A., Cocucci, E., Falcon-Perez, J. M., Gabrielsson, S., Gho, Y. S., Gupta, D., Harsha, H. C., … Mathivanan, S. (2012). Vesiclepedia: A Compendium for Extracellular Vesicles with Continuous Community Annotation. *PLoS Biology*, *10*(12), 8–12. https://doi.org/10.1371/journal.pbio.1001450

Kawai, T., Ota, N., Okada, K., Imasato, A., Owa, Y., Morita, M., Tada, M., & Tanaka, Y. (2019). Ultrasensitive Single Cell Metabolomics by Capillary Electrophoresis–Mass Spectrometry with a Thin-Walled Tapered Emitter and Large-Volume Dual Sample Preconcentration. *Analytical Chemistry*, *91*(16), 10564–10572. https://doi.org/10.1021/acs.analchem.9b01578

Keerthikumar, S., Chisanga, D., Ariyaratne, D., Al Saffar, H., Anand, S., Zhao, K., Samuel, M., Pathan, M., Jois, M., Chilamkurti, N., Gangoda, L., & Mathivanan, S. (2016). ExoCarta: A Web-Based Compendium of Exosomal Cargo. *Journal of Molecular Biology*, *428*(4), 688–692. https://doi.org/10.1016/j.jmb.2015.09.019

Khatami, F., Aghamir, S. M. K., & Tavangar, S. M. (2019). Oncometabolites: A new insight for oncology. *Molecular Genetics and Genomic Medicine*, *7*(9), 7–9. https://doi.org/10.1002/mgg3.873

Kilinc, S., Paisner, R., Camarda, R., Gupta, S., Momcilovic, O., Kohnz, R. A., Avsaroglu, B., L'Etoile, N. D., Perera, R. M., Nomura, D. K., & Goga, A. (2021). Oncogene-regulated release of extracellular vesicles. *Developmental Cell*, *56*(13), 1989-2006.e6. https://doi.org/10.1016/j.devcel.2021.05.014

Kim, D. K., Lee, J., Kim, S. R., Choi, D. S., Yoon, Y. J., Kim, J. H., Go, G., Nhung, D., Hong, K., Jang, S. C., Kim, S. H., Park, K. S., Kim, O. Y., Park, H. T., Seo, J. H., Aikawa, E., Baj-Krzyworzeka, M., Van Balkom, B. W. M., Belting, M., … Gho, Y. S. (2015). EVpedia: A community web portal for extracellular vesicles research. *Bioinformatics*, *31*(6), 933–939. https://doi.org/10.1093/bioinformatics/btu741

King, H. W., Michael, M. Z., & Gleadle, J. M. (2012). Hypoxic enhancement of exosome release by breast cancer cells. *BMC Cancer*, *12*(1), 421. https://doi.org/10.1186/1471-2407-12-421

Kitamura, Y., Kojima, M., Kurosawa, T., Sasaki, R., Ichihara, S., Hiraku, Y., Tomimoto, H., Murata, M., & Oikawa, S. (2018). Proteomic Profiling of Exosomal Proteins for Blood-based Biomarkers in Parkinson's Disease. *Neuroscience*, *392*, 121–128. https://doi.org/10.1016/j.neuroscience.2018.09.017

Kitazono, M., Takebayashi, Y., Ishitsuka, K., Takao, S., Tani, A., Furukawa, T., Miyadera, K., Yamada, Y., Aikou, T., & Akiyama, S. I. (1998). Prevention of hypoxia-induced apoptosis by the angiogenic factor thymidine phosphorylase. *Biochemical and Biophysical Research Communications*, *253*(3), 797–803. https://doi.org/10.1006/bbrc.1998.9852

Kosaka, N., Iguchi, H., Yoshioka, Y., Takeshita, F., Matsuki, Y., & Ochiya, T. (2010). Secretory mechanisms and intercellular transfer of microRNAs in living cells. *Journal of Biological Chemistry*, *285*(23), 17442–17452. https://doi.org/10.1074/jbc.M110.107821

Kreimer, S., Belov, A. M., Ghiran, I., Murthy, S. K., Frank, D. A., & Ivanov, A. R. (2015). Mass-spectrometry-based molecular characterization of extracellular vesicles: Lipidomics and proteomics. *Journal of Proteome Research*, *14*(6), 2367–2384. https://doi.org/10.1021/pr501279t

Laulagnier, K., Motta, C., Hamdi, S., Roy, S., Fauvelle, F., Pageaux, J. F., Kobayashi, T., Salles, J. P., Perret, B., Bonnerot, C., & Record, M. (2004). Mast cell- and dendritic cell-derived display a specific lipid composition and an unusual membrane organization. *Biochemical Journal*, *380*(1), 161–171. https://doi.org/10.1042/BJ20031594

Liu, W., Glunde, K., Bhujwalla, Z. M., Raman, V., Sharma, A., & Phang, J. M. (2012). Proline oxidase promotes tumor cell survival in hypoxic tumor microenvironments. *Cancer Research*, *72*(14), 3677–3686. https://doi.org/10.1158/0008-5472.CAN-12-0080

Llorente, A., Skotland, T., Sylvänne, T., Kauhanen, D., Róg, T., Orłowski, A., Vattulainen, I., Ekroos, K., & Sandvig, K. (2013). Molecular lipidomics of exosomes released by PC-3 prostate cancer cells. *Biochimica et Biophysica Acta - Molecular and Cell Biology of Lipids*, *1831*(7), 1302–1309. https://doi.org/10.1016/j.bbalip.2013.04.011

Lötvall, J., Hill, A. F., Hochberg, F., Buzás, E. I., Di Vizio, D., Gardiner, C., Gho, Y. S., Kurochkin, I. V., Mathivanan, S., Quesenberry, P., Sahoo, S., Tahara, H., Wauben, M. H., Witwer, K. W., & Théry, C. (2014). Minimal experimental requirements for definition of extracellular vesicles and their functions: a position statement from the International Society for Extracellular Vesicles. *Journal of Extracellular Vesicles*, *3*(1), 26913. https://doi.org/10.3402/jev.v3.26913

Ludwig, N., Gillespie, D. G., Reichert, T. E., Jackson, E. K., & Whiteside, T. L. (2020). Purine Metabolites in Tumor-Derived Exosomes May Facilitate Immune Escape of Head and Neck Squamous Cell Carcinoma. *Cancers*, *12*(6), 1602. https://doi.org/10.3390/cancers12061602

Ludwig, N., Rao, A., Sandlesh, P., Yerneni, S. S., Swain, A. D., Bullock, K. M., Hansen, K. M., Zhang, X., Jaman, E., Allen, J., Krueger, K., Hong, C.-S., Banks, W. A., Whiteside, T. L., & Amankulor, N. M. (2022). Characterization of systemic immunosuppression by IDH mutant glioma small extracellular vesicles. *Neuro-Oncology*, *24*(2), 197–209. https://doi.org/10.1093/neuonc/noab153

Luo, P., Mao, K., Xu, J., Wu, F., Wang, X., Wang, S., Zhou, M., Duan, L., Tan, Q., Ma, G., Yang, G., Du,

R., Huang, H., Huang, Q., Li, Y., Guo, M., & Jin, Y. (2020). Metabolic characteristics of large and small extracellular vesicles from pleural effusion reveal biomarker candidates for the diagnosis of tuberculosis and malignancy. *Journal of Extracellular Vesicles*, *9*(1), 1790158. https://doi.org/10.1080/20013078.2020.1790158

Lydic, T. A., Townsend, S., Adda, C. G., Collins, C., Mathivanan, S., & Reid, G. E. (2015). Rapid and comprehensive "shotgun" lipidome profiling of colorectal cancer cell derived exosomes. *Methods*, *87*, 83–95. https://doi.org/10.1016/j.ymeth.2015.04.014

Martínez-Sena, T., Luongo, G., Sanjuan-Herráez, D., Castell, J. V., Vento, M., Quintás, G., & Kuligowski, J. (2019). Monitoring of system conditioning after blank injections in untargeted UPLC-MS metabolomic analysis. *Scientific Reports*, *9*(1), 9822. https://doi.org/10.1038/s41598-019-46371-w

McCready, J., Sims, J. D., Chan, D., & Jay, D. G. (2010). Secretion of extracellular hsp90α via exosomes increases cancer cell motility: a role for plasminogen activation. *BMC Cancer*, *10*(1), 294. https://doi.org/10.1186/1471-2407-10-294

Mitani, F., Hayasaka, R., Hirayama, A., & Oneyama, C. (2022). SNAP23-Mediated Perturbation of Cholesterol-Enriched Membrane Microdomain Promotes Extracellular Vesicle Production in Src-Activated Cancer Cells. *Biological & Pharmaceutical Bulletin*, *45*(10), 1572–1580. https://doi.org/10.1248/bpb.b22-00560

Momen-Heravi, F., Getting, S. J., & Moschos, S. A. (2018). Extracellular vesicles and their nucleic acids for biomarker discovery. *Pharmacology and Therapeutics*, *192*, 170–187. https://doi.org/10.1016/j.pharmthera.2018.08.002

Morelli, A. E., Larregina, A. T., Shufesky, W. J., Sullivan, M. L. G., Stolz, D. B., Papworth, G. D., Zahorchak, A. F., Logar, A. J., Wang, Z., Watkins, S. C., Falo, L. D., & Thomson, A. W. (2004). Endocytosis, intracellular sorting, and processing of exosomes by dendritic cells. *Blood*, *104*(10), 3257–3266. https://doi.org/10.1182/blood-2004-03-0824

Muraoka, S., Hirano, M., Isoyama, J., Nagayama, S., Tomonaga, T., & Adachi, J. (2022). Comprehensive proteomic profiling of plasma and serum phosphatidylserine-positive extracellular vesicles reveals tissue-specific proteins. *IScience*, *25*(4), 104012. https://doi.org/10.1016/j.isci.2022.104012

Nakai, W., Yoshida, T., Diez, D., Miyatake, Y., Nishibu, T., Imawaka, N., Naruse, K., Sadamura, Y., & Hanayama, R. (2016). A novel affinity-based method for the isolation of highly purified extracellular vesicles. *Scientific Reports*, *6*(June), 1–11. https://doi.org/10.1038/srep33935

Nazarenko, I., Rana, S., Baumann, A., McAlear, J., Hellwig, A., Trendelenburg, M., Lochnit, G., Preissner, K. T., & Zöller, M. (2010). Cell surface tetraspanin Tspan8 contributes to molecular pathways of exosome-induced endothelial cell activation. *Cancer Research*, *70*(4), 1668–1678. https://doi.org/10.1158/0008-5472.CAN-09-2470

Nishida-Aoki, N., Izumi, Y., Takeda, H., Takahashi, M., Ochiya, T., & Bamba, T. (2020). Lipidomic Analysis of Cells and Extracellular Vesicles from High- and Low-Metastatic Triple-Negative Breast Cancer. *Metabolites*, *10*(2), 67. https://doi.org/10.3390/metabo10020067

Nordin, J. Z., Lee, Y., Vader, P., Mäger, I., Johansson, H. J., Heusermann, W., Wiklander, O. P. B., Hällbrink, M., Seow, Y., Bultema, J. J., Gilthorpe, J., Davies, T., Fairchild, P. J., Gabrielsson, S., Meisner-Kober, N. C., Lehtiö, J., Smith, C. I. E., Wood, M. J. A., & Andaloussi, S. E. L. (2015). Ultrafiltration with size-exclusion liquid chromatography for high yield isolation of extracellular vesicles preserving intact biophysical and functional properties. *Nanomedicine: Nanotechnology, Biology, and Medicine*, *11*(4), 879–883. https://doi.org/10.1016/j.nano.2015.01.003

Oldham, W. M., Clish, C. B., Yang, Y., & Loscalzo, J. (2015). Hypoxia-Mediated Increases in l-2-hydroxyglutarate Coordinate the Metabolic Response to Reductive Stress. *Cell Metabolism*, *22*(2), 291–303. https://doi.org/10.1016/j.cmet.2015.06.021

Paget, S. (1889). The Distribution of Secondary Growths in Cancer of the Breast. *The Lancet*, *133*(3421), 571–573. https://doi.org/10.1017/CBO9781107415324.004

Pan, B. T., & Johnstone, R. M. (1983). Fate of the transferrin receptor during maturation of sheep reticulocytes in vitro: Selective externalization of the receptor. *Cell*, *33*(3), 967–978. https://doi.org/10.1016/0092-8674(83)90040-5

Patel, G. K., Khan, M. A., Zubair, H., Srivastava, S. K., Khushman, M., Singh, S., & Singh, A. P. (2019). Comparative analysis of exosome isolation methods using culture supernatant for optimum yield, purity and downstream applications. *Scientific Reports*, *9*(1), 5335. https://doi.org/10.1038/s41598-019-41800-2

Patton, M. C., Zubair, H., Khan, M. A., Singh, S., & Singh, A. P. (2020). Hypoxia alters the release and size distribution of extracellular vesicles in pancreatic cancer cells to support their adaptive survival. *Journal of Cellular Biochemistry*, *121*(1), 828–839. https://doi.org/10.1002/jcb.29328

Pegtel, D. M., Cosmopoulos, K., Thorley-Lawson, D. A., Van Eijndhoven, M. A. J., Hopmans, E. S., Lindenberg, J. L., De Gruijl, T. D., Würdinger, T., & Middeldorp, J. M. (2010). Functional delivery of viral miRNAs via exosomes. *Proceedings of the National Academy of Sciences of the United States of America*, *107*(14), 6328–6333. https://doi.org/10.1073/pnas.0914843107

Petucci, C., Zelenin, A., Culver, J. A., Gabriel, M., Kirkbride, K., Christison, T. T., & Gardell, S. J. (2016). Use of ion chromatography/mass spectrometry for targeted metabolite profiling of polar organic acids. *Analytical Chemistry*, *88*(23), 11799–11803. https://doi.org/10.1021/acs.analchem.6b03435

Phuyal, S., Skotland, T., Hessvik, N. P., Simolin, H., Øverbye, A., Brech, A., Parton, R. G., Ekroos, K., Sandvig, K., & Llorente, A. (2015). The ether lipid precursor hexadecylglycerol stimulates the release and changes the composition of exosomes derived from PC-3 cells. *Journal of Biological Chemistry*,

290(7), 4225–4237. https://doi.org/10.1074/jbc.M114.593962

Pugmire, M. J., & Ealick, S. E. (2002). Structural analyses reveal two distinct families of nucleoside phosphorylases. *The Biochemical Journal*, *361*(Pt 1), 1–25. https://doi.org/10.1042/0264-6021:3610001

Puhka, M., Takatalo, M., Nordberg, M. E., Valkonen, S., Nandania, J., Aatonen, M., Yliperttula, M., Laitinen, S., Velagapudi, V., Mirtti, T., Kallioniemi, O., Rannikko, A., Siljander, P. R. M., & Af Hällström, T. M. (2017). Metabolomic profiling of extracellular vesicles and alternative normalization methods reveal enriched metabolites and strategies to study prostate cancer-related changes. *Theranostics*, *7*(16), 3824–3841. https://doi.org/10.7150/thno.19890

Qin, C., Yang, G., Yang, J., Ren, B., Wang, H., Chen, G., Zhao, F., You, L., Wang, W., & Zhao, Y. (2020). Metabolism of pancreatic cancer: paving the way to better anticancer strategies. *Molecular Cancer*, *19*(1), 50. https://doi.org/10.1186/s12943-020-01169-7

Raghavamenon, A., Garelnabi, M., Babu, S., Aldrich, A., Litvinov, D., & Parthasarathy, S. (2009). αtocopherol is ineffective in preventing the decomposition of preformed lipid peroxides and may promote the accumulation of toxic aldehydes: A potential explanation for the failure of antioxidants to affect human atherosclerosis. *Antioxidants and Redox Signaling*, *11*(6), 1237–1248. https://doi.org/10.1089/ars.2008.2248

Rana, S., Yue, S., Stadel, D., & Zöller, M. (2012). Toward tailored exosomes: The exosomal tetraspanin web contributes to target cell selection. *International Journal of Biochemistry and Cell Biology*, *44*(9), 1574–1584. https://doi.org/10.1016/j.biocel.2012.06.018

Raposo, G., & Stoorvogel, W. (2013). Extracellular vesicles: Exosomes, microvesicles, and friends. *Journal of Cell Biology*, *200*(4), 373–383. https://doi.org/10.1083/jcb.201211138

Ronquist, G., & Hedström, M. (1977). Restoration of detergent-inactivated adenosine triphosphatase activity of human prostatic fluid with concanavalin A. *BBA - Enzymology*, *483*(2), 483–486. https://doi.org/10.1016/0005-2744(77)90078-X

Sagar, G., Sah, R. P., Javeed, N., Dutta, S. K., Smyrk, T. C., Lau, J. S., Giorgadze, N., Tchkonia, T., Kirkland, J. L., Chari, S. T., & Mukhopadhyay, D. (2016). Pathogenesis of pancreatic cancer exosome-induced lipolysis in adipose tissue. *Gut*, *65*(7), 1165–1174. https://doi.org/10.1136/gutjnl-2014-308350

Satoh, K., Yachida, S., Sugimoto, M., Oshima, M., Nakagawa, T., Akamoto, S., Tabata, S., Saitoh, K., Kato, K., Sato, S., Igarashi, K., Aizawa, Y., Kajino-Sakamoto, R., Kojima, Y., Fujishita, T., Enomoto, A., Hirayama, A., Ishikawa, T., Taketo, M. M., … Soga, T. (2017). Global metabolic reprogramming of colorectal cancer occurs at adenoma stage and is induced by MYC. *Proceedings of the National Academy of Sciences of the United States of America*, *114*(37), E7697–E7706.

https://doi.org/10.1073/pnas.1710366114

Schödel, J., Oikonomopoulos, S., Ragoussis, J., Pugh, C. W., Ratcliffe, P. J., & Mole, D. R. (2011). High-resolution genome-wide mapping of HIF-binding sites by ChIP-seq. *Blood*, *117*(23), 207–217. https://doi.org/10.1182/blood-2010-10-314427

Shah, R., Patel, T., & Freedman, J. E. (2018). Circulating Extracellular Vesicles in Human Disease. *New England Journal of Medicine*, *379*(10), 958–966. https://doi.org/10.1056/nejmra1704286

Shao, C., Yang, F., Miao, S., Liu, W., Wang, C., Shu, Y., & Shen, H. (2018). Role of hypoxia-induced exosomes in tumor biology. *Molecular Cancer*, *17*(1), 120. https://doi.org/10.1186/s12943-018-0869-y

Si-Hung, L., & Bamba, T. (2022). Current state and future perspectives of supercritical fluid chromatography. *TrAC Trends in Analytical Chemistry*, *149*, 116550. https://doi.org/10.1016/j.trac.2022.116550

Sidhom, K., Obi, P. O., & Saleem, A. (2020). A Review of Exosomal Isolation Methods: Is Size Exclusion Chromatography the Best Option? *International Journal of Molecular Sciences*, *21*(18), 6466. https://doi.org/10.3390/ijms21186466

Siegel, R. L., Miller, K. D., & Jemal, A. (2020). Cancer statistics, 2020. *CA: A Cancer Journal for Clinicians*, *70*(1), 7–30. https://doi.org/10.3322/caac.21590

Simons, K., & Sampaio, J. L. (2011). Membrane organization and lipid rafts. *Cold Spring Harbor Perspectives in Biology*, *3*(10), a004697. https://doi.org/10.1101/cshperspect.a004697

Skotland, T., Hessvik, N. P., Sandvig, K., & Llorente, A. (2019). Exosomal lipid composition and the role of ether lipids and phosphoinositides in exosome biology. *Journal of Lipid Research*, *60*(1), 9–18. https://doi.org/10.1194/jlr.R084343

Skotland, T., Sagini, K., Sandvig, K., & Llorente, A. (2020). An emerging focus on lipids in extracellular vesicles. *Advanced Drug Delivery Reviews*, *159*, 308–321. https://doi.org/10.1016/j.addr.2020.03.002

Soga, T., & Heiger, D. N. (2000). Amino Acid Analysis by Capillary Electrophoresis Electrospray Ionization Mass Spectrometry. *Anal. Chem*, *72*(6), 1236–1241. https://doi.org/10.1021/ac990976y

Soga, T., Igarashi, K., Ito, C., Mizobuchi, K., Zimmermann, H.-P., & Tomita, M. (2009). Metabolomic Profiling of Anionic Metabolites by Capillary Electrophoresis Mass Spectrometry. *Analytical Chemistry*, *81*(15), 6165–6174. https://doi.org/10.1021/ac900675k

Stein, J. M., & Luzio, J. P. (1991). Ectocytosis caused by sublytic autologous complement attack on human neutrophils. The sorting of endogenous plasma-membrane proteins and lipids into shed vesicles. *Biochemical Journal*, *274*(2), 381–386. https://doi.org/10.1042/bj2740381

Steinbichler, T. B., Dudás, J., Riechelmann, H., & Skvortsova, I.-I. (2017). The role of exosomes in cancer metastasis. *Seminars in Cancer Biology*, *44*, 170–181. https://doi.org/10.1016/j.semcancer.2017.02.006

Sugimoto, M., Wong, D. T., Hirayama, A., Soga, T., & Tomita, M. (2010). Capillary electrophoresis mass spectrometry-based saliva metabolomics identified oral, breast and pancreatic cancer-specific profiles. *Metabolomics*, *6*(1), 78–95. https://doi.org/10.1007/s11306-009-0178-y

Sun, L., & Meckes, D. (2018). Methodological Approaches to Study Extracellular Vesicle miRNAs in Epstein–Barr Virus-Associated Cancers. *International Journal of Molecular Sciences*, *19*(9), 2810. https://doi.org/10.3390/ijms19092810

Sun, Y., Saito, K., Iiji, R., & Saito, Y. (2019). Application of Ion Chromatography Coupled with Mass Spectrometry for Human Serum and Urine Metabolomics. *SLAS Discovery*, *24*(7), 778–786. https://doi.org/10.1177/2472555219850082

Sun, Y., Saito, K., & Saito, Y. (2019). Lipid profile characterization and lipoprotein comparison of extracellular vesicles from human plasma and serum. *Metabolites*, *9*(11), 10–14. https://doi.org/10.3390/metabo9110259

Suzuki, Y., Hayasaka, R., Hasebe, M., Ikeda, S., Soga, T., Tomita, M., Hirayama, A., & Kuroda, H. (2022). Comparative Metabolomics of Small Molecules Specifically Expressed in the Dorsal or Ventral Marginal Zones in Vertebrate Gastrula. *Metabolites*, *12*(6), 566. https://doi.org/10.3390/metabo12060566

Tabata, S., Kojima, Y., Sakamoto, T., Igarashi, K., Umetsu, K., Ishikawa, T., Hirayama, A., Kajino-Sakamoto, R., Sakamoto, N., Yasumoto, K.-I., Okano, K., Suzuki, Y., Yachida, S., Aoki, M., & Soga, T. (2023). L-2hydroxyglutaric acid rewires amino acid metabolism in colorectal cancer via the mTOR-ATF4 axis. *Oncogene*, *42*(16), 1294–1307. https://doi.org/10.1038/s41388-023-02632-7

Tadokoro, H., Hirayama, A., Kudo, R., Hasebe, M., Yoshioka, Y., Matsuzaki, J., Yamamoto, Y., Sugimoto, M., Soga, T., & Ochiya, T. (2020). Adenosine leakage from perforin-burst extracellular vesicles inhibits perforin secretion by cytotoxic T-lymphocytes. *Plos One*, *15*(4), e0231430. https://doi.org/10.1371/journal.pone.0231430

Tadokoro, H., Umezu, T., Ohyashiki, K., Hirano, T., & Ohyashiki, J. H. (2013). Exosomes derived from hypoxic leukemia cells enhance tube formation in endothelial cells. *Journal of Biological Chemistry*, *288*(48), 34343–34351. https://doi.org/10.1074/jbc.M113.480822

Takeda, H., Izumi, Y., Takahashi, M., Paxton, T., Tamura, S., Koike, T., Yu, Y., Kato, N., Nagase, K., Shiomi, M., & Bamba, T. (2018). Widely-targeted quantitative lipidomics method by supercritical fluid chromatography triple quadrupole mass spectrometry. *Journal of Lipid Research*, *59*(7), 1283–1293. https://doi.org/10.1194/jlr.D083014

Takov, K., Yellon, D. M., & Davidson, S. M. (2017). Confounding factors in vesicle uptake studies using fluorescent lipophilic membrane dyes. *Journal of Extracellular Vesicles*, *6*(1), 1388731. https://doi.org/10.1080/20013078.2017.1388731

Takov, K., Yellon, D. M., & Davidson, S. M. (2019). Comparison of small extracellular vesicles isolated from plasma by ultracentrifugation or size-exclusion chromatography: yield, purity and functional potential. *Journal of Extracellular Vesicles*, *8*(1), 1560809. https://doi.org/10.1080/20013078.2018.1560809

Taylor, D. D., & Shah, S. (2015). Methods of isolating extracellular vesicles impact down-stream analyses of their cargoes. *Methods*, *87*, 3–10. https://doi.org/10.1016/j.ymeth.2015.02.019

Théry, C., Boussac, M., Véron, P., Ricciardi-Castagnoli, P., Raposo, G., Garin, J., & Amigorena, S. (2001). Proteomic Analysis of Dendritic Cell-Derived Exosomes: A Secreted Subcellular Compartment Distinct from Apoptotic Vesicles. *The Journal of Immunology*, *166*(12), 7309–7318. https://doi.org/10.4049/jimmunol.166.12.7309

Théry, C., Regnault, A., Garin, J., Wolfers, J., Zitvogel, L., Ricciardi-Castagnoli, P., Raposo, G., & Amigorena, S. (1999). Molecular characterization of dendritic cell-derived exosomes: Selective accumulation of the heat shock protein hsc73. *Journal of Cell Biology*, *147*(3), 599–610. https://doi.org/10.1083/jcb.147.3.599

Théry, C., Witwer, K. W., Aikawa, E., Alcaraz, M. J., Anderson, J. D., Andriantsitohaina, R., Antoniou, A., Arab, T., Archer, F., Atkin-Smith, G. K., Ayre, D. C., Bach, J.-M., Bachurski, D., Baharvand, H., Balaj, L., Baldacchino, S., Bauer, N. N., Baxter, A. A., Bebawy, M., … Zuba-Surma, E. K. (2018). Minimal information for studies of extracellular vesicles 2018 (MISEV2018): a position statement of the International Society for Extracellular Vesicles and update of the MISEV2014 guidelines. *Journal of Extracellular Vesicles*, *7*(1), 1535750. https://doi.org/10.1080/20013078.2018.1535750

Trajkovic, K., Hsu, C., Chiantia, S., Rajendran, L., Wenzel, D., Wieland, F., Schwille, P., Brügger, B., & Simons, M. (2008). Ceramide triggers budding of exosome vesicles into multivesicular endosomes. *Science*, *319*(5867), 1244–1247. https://doi.org/10.1126/science.1153124

Umezu, T., Tadokoro, H., Azuma, K., Yoshizawa, S., Ohyashiki, K., & Ohyashiki, J. H. (2014). Exosomal miR-135b shed from hypoxic multiple myeloma cells enhances angiogenesis by targeting factor-inhibiting HIF-1. *Blood*, *124*(25), 3748–3757. https://doi.org/10.1182/blood-2014-05-576116

Valadi, H., Ekström, K., Bossios, A., Sjöstrand, M., Lee, J. J., & Lötvall, J. O. (2007). Exosome-mediated transfer of mRNAs and microRNAs is a novel mechanism of genetic exchange between cells. *Nature Cell Biology*, *9*(6), 654–659. https://doi.org/10.1038/ncb1596

Vallabhaneni, K. C., Penfornis, P., Dhule, S., Guillonneau, F., Adams, K. V, Mo, Y. Y., Xu, R., Liu, Y., Watabe, K., Vemuri, M. C., & Pochampally, R. (2015). Extracellular vesicles from bone marrow

mesenchymal stem/stromal cells transport tumor regulatory microRNA, proteins, and metabolites. *Oncotarget*, *6*(7), 4953–4967. https://doi.org/10.18632/oncotarget.3211

Van Niel, G., D'Angelo, G., & Raposo, G. (2018). Shedding light on the cell biology of extracellular vesicles. *Nature Reviews Molecular Cell Biology*, *19*(4), 213–228. https://doi.org/10.1038/nrm.2017.125

Vara, D., Watt, J. M., Fortunato, T. M., Mellor, H., Burgess, M., Wicks, K., Mace, K., Reeksting, S., Lubben, A., Wheeler-Jones, C. P. D., & Pula, G. (2018). Direct Activation of NADPH Oxidase 2 by 2-Deoxyribose-1-Phosphate Triggers Nuclear Factor Kappa B-Dependent Angiogenesis. *Antioxidants and Redox Signaling*, *28*(2), 110–130. https://doi.org/10.1089/ars.2016.6869

Veerman, R. E., Teeuwen, L., Czarnewski, P., Güclüler Akpinar, G., Sandberg, A., Cao, X., Pernemalm, M., Orre, L. M., Gabrielsson, S., & Eldh, M. (2021). Molecular evaluation of five different isolation methods for extracellular vesicles reveals different clinical applicability and subcellular origin. *Journal of Extracellular Vesicles*, *10*(9), e12128. https://doi.org/10.1002/jev2.12128

Vidal, M., Sainte-Marie, J., Philippot, J. R., & Bienvenue, A. (1989). Asymmetric distribution of phospholipids in the membrane of vesicles released during in vitro maturation of guinea pig reticulocytes: Evidence precluding a role for "aminophospholipid translocase." *Journal of Cellular Physiology*, *140*(3), 455–462. https://doi.org/10.1002/jcp.1041400308

Wang, J., Christison, T. T., Misuno, K., Lopez, L., Huhmer, A. F., Huang, Y., & Hu, S. (2014). Metabolomic profiling of anionic metabolites in head and neck cancer cells by capillary ion chromatography with orbitrap mass spectrometry. *Analytical Chemistry*, *86*(10), 5116–5124. https://doi.org/10.1021/ac500951v

Wang, X., Luo, G., Zhang, K., Cao, J., Huang, C., Jiang, T., Liu, B., Su, L., & Qiu, Z. (2018). Hypoxic Tumor-Derived Exosomal miR-301a Mediates M2 Macrophage Polarization via PTEN/PI3Kγ to Promote Pancreatic Cancer Metastasis. *Cancer Research*, *78*(16), 4586–4598. https://doi.org/10.1158/0008-5472.CAN-17-3841

Warburg, O, & Minami, S. (1924). Versuche an Überlebendem Carcinomgewebe. *Klin Wochenschr.*, *2*(17), 776–777. https://doi.org/10.1007/BF01736087

Warburg, Otto. (1956). On the Origin of Cancer Cells. *Science*, *123*(3191), 309–314. https://doi.org/10.1126/science.123.3191.309

Ward, P. S., Lu, C., Cross, J. R., Abdel-Wahab, O., Levine, R. L., Schwartz, G. K., & Thompson, C. B. (2013). The potential for isocitrate dehydrogenase mutations to produce 2-hydroxyglutarate depends on allele specificity and subcellular compartmentalization. *Journal of Biological Chemistry*, *288*(6), 3804–3815. https://doi.org/10.1074/jbc.M112.435495

Wei, Y., Lai, X., Yu, S., Chen, S., Ma, Y., Zhang, Y., Li, H., Zhu, X., Yao, L., & Zhang, J. (2014). Exosomal

miR-221/222 enhances tamoxifen resistance in recipient ER-positive breast cancer cells. *Breast Cancer Research and Treatment*, *147*(2), 423–431. https://doi.org/10.1007/s10549-014-3037-0

Williams, C., Palviainen, M., Reichardt, N.-C., Siljander, P. R. M., & Falcón-Pérez, J. M. (2019). Metabolomics Applied to the Study of Extracellular Vesicles. *Metabolites*, *9*(11), 276. https://doi.org/10.3390/metabo9110276

Wishart, D. S., Guo, A. C., Oler, E., Wang, F., Anjum, A., Peters, H., Dizon, R., Sayeeda, Z., Tian, S., Lee, B. L., Berjanskii, M., Mah, R., Yamamoto, M., Jovel, J., Torres-Calzada, C., Hiebert-Giesbrecht, M., Lui, V. W., Varshavi, D., Varshavi, D., … Gautam, V. (2022). HMDB 5.0: The Human Metabolome Database for 2022. *Nucleic Acids Research*, *50*(D1), D622–D631. https://doi.org/10.1093/nar/gkab1062

Xu, W., Yang, H., Liu, Y., Yang, Y., Wang, P., Kim, S. H., Ito, S., Yang, C., Wang, P., Xiao, M. T., Liu, L. X., Jiang, W. Q., Liu, J., Zhang, J. Y., Wang, B., Frye, S., Zhang, Y., Xu, Y. H., Lei, Q. Y., … Xiong, Y. (2011). Oncometabolite 2-hydroxyglutarate is a competitive inhibitor of α-ketoglutarate-dependent dioxygenases. *Cancer Cell*, *19*(1), 17–30. https://doi.org/10.1016/j.ccr.2010.12.014

Yang, H., Xie, S., Liang, B., Tang, Q., Liu, H., Wang, D., & Huang, G. (2021). Exosomal IDH1 increases the resistance of colorectal cancer cells to 5-Fluorouracil. *Journal of Cancer*, *12*(16), 4862–4872. https://doi.org/10.7150/JCA.58846

Yang, M., Soga, T., & Pollard, P. J. (2013). Oncometabolites: Linking altered metabolism with cancer. *Journal of Clinical Investigation*, *123*(9), 3652–3658. https://doi.org/10.1172/JCI67228

Yang, Y., Wang, Y., Wei, S., Zhou, C., Yu, J., Wang, G., Wang, W., & Zhao, L. (2021). Extracellular vesicles isolated by size-exclusion chromatography present suitability for RNomics analysis in plasma. *Journal of Translational Medicine*, *19*(1), 104. https://doi.org/10.1186/s12967-021-02775-9

Ye, S. B., Zhang, H., Cai, T. T., Liu, Y. N., Ni, J. J., He, J., Peng, J. Y., Chen, Q. Y., Mo, H. Y., Jun-Cui, Zhang, X. S., Zeng, Y. X., & Li, J. (2016). Exosomal miR-24-3p impedes T-cell function by targeting FGF11 and serves as a potential prognostic biomarker for nasopharyngeal carcinoma. *Journal of Pathology*, *240*(3), 329–340. https://doi.org/10.1002/path.4781

Yoo, H. C., Park, S. J., Nam, M., Kang, J., Kim, K., Yeo, J. H., Kim, J. K., Heo, Y., Lee, H. S., Lee, M. Y., Lee, C. W., Kang, J. S., Kim, Y. H., Lee, J., Choi, J., Hwang, G. S., Bang, S., & Han, J. M. (2020). A Variant of SLC1A5 Is a Mitochondrial Glutamine Transporter for Metabolic Reprogramming in Cancer Cells. *Cell Metabolism*, *31*(2), 267-283.e12. https://doi.org/10.1016/j.cmet.2019.11.020

Yoshitake, J., Azami, M., Sei, H., Onoshima, D., Takahashi, K., Hirayama, A., Uchida, K., Baba, Y., & Shibata, T. (2022). Rapid Isolation of Extracellular Vesicles Using a Hydrophilic Porous Silica Gel-Based Size-Exclusion Chromatography Column. *Analytical Chemistry*, *94*(40), 13676–13681. https://doi.org/10.1021/acs.analchem.2c01053

Yu, L., Aa, J., Xu, J., Sun, M., Qian, S., Cheng, L., Yang, S., & Shi, R. (2011). Metabolomic phenotype of gastric cancer and precancerous stages based on gas chromatography time-of-flight mass spectrometry. *Journal of Gastroenterology and Hepatology (Australia)*, *26*(8), 1290–1297. https://doi.org/10.1111/j.1440-1746.2011.06724.x

Zhang, X., Miao, R., Liu, T., Xiang, X., Gu, J., Jia, Y., Li, Z., Fu, Y., He, Y., Zhang, Y., Zhang, J., Qu, K., & Liu, C. (2019). IDH1 as a frequently mutated gene has potential effect on exosomes releasement by epigenetically regulating P2RX7 in intrahepatic cholangiocarcinoma. *Biomedicine & Pharmacotherapy*, *113*(March), 108774. https://doi.org/10.1016/j.biopha.2019.108774

Zhang, Y., Liu, D., Chen, X., Li, J., Li, L., Bian, Z., Sun, F., Lu, J., Yin, Y., Cai, X., Sun, Q., Wang, K., Ba, Y., Wang, Q., Wang, D., Yang, J., Liu, P., Xu, T., Yan, Q., … Zhang, C. Y. (2010). Secreted Monocytic miR-150 Enhances Targeted Endothelial Cell Migration. *Molecular Cell*, *39*(1), 133–144. https://doi.org/10.1016/j.molcel.2010.06.010

Zhao, H., Yang, L., Baddour, J., Achreja, A., Bernard, V., Moss, T., Marini, J. C., Tudawe, T., Seviour, E. G., San Lucas, F. A., Alvarez, H., Gupta, S., Maiti, S. N., Cooper, L., Peehl, D., Ram, P. T., Maitra, A., & Nagrath, D. (2016). Tumor microenvironment derived exosomes pleiotropically modulate cancer cell metabolism. *ELife*, *5*(e10250), 1–27. https://doi.org/10.7554/eLife.10250

Zhu, S.-K., Zhou, Y., Cheng, C., Zhong, S., Wu, H.-Q., Wang, B., Fan, P., Xiong, J.-X., Yang, H.-J., & Wu, H.-S. (2014). Overexpression of membrane-type 2 matrix metalloproteinase induced by hypoxia-inducible factor-1α in pancreatic cancer: Implications for tumor progression and prognosis. *Molecular and Clinical Oncology*, *2*(6), 973–981. https://doi.org/10.3892/mco.2014.357

Abbreviation

Lipids

Cer : ceramide

DAG : diacylglycerol

ePC : alkyl-acyl phosphatidylcholine

ePE : alkyl-acyl phosphatidylethanolamine

FFA : free fatty acid

HexCer : hexosylceramide

LPC : lysophosphatidylcholine

LPE : lysophosphatidylethanolamine

MAG : monoacylglycerol

PA : phosphatidic acid

PC : phosphatidylcholine

PE : phosphatidylethanolamine

PG : phosphatidylglycerol

PI : phosphatidylinositol

pPC : alkenyl-acyl phosphatidylcholine

pPE : alkenyl-acyl phosphatidylethanolamine

PS : phosphatidylserine

SM : sphingomyelin

TAG : triacylglycerol

Others

2-HG : 2-hydroxyglutaric acid

2-PG : 2-phosphoglyceric acid

3-PG : 3-phosphoglyceric acid

5-FU : 5-fluorouracil

ADP : adenosine diphosphate

AGO2 : argonaute-2

AJS : agilent jet stream

Ala : alanine

AML : acute myelogenous leukemia

Arg : arginine

Asn : asparagine

Asp : aspartic acid

ATCC : american type culture collection

ATP : adenosine triphosphate

AURKB : aurora kinase B

beta-Ala : beta-alanine

BSA : bovine serum albumin

c-Src : cellular proto-oncogene tyrosine-protein kinase Src kinase

CA9 : carbonic anhydrase 9

CAFs : cancer-associated fibroblasts

CCD : charge coupled device

CD9 : cluster of differentiation 9

CD41d : cluster of differentiation 41d

CD63 : cluster of differentiation 63

CD81 : cluster of differentiation 81

cDNA : complementary deoxyribonucleic acid

CE-MS : capillary electrophoresis-mass spectrometer

CTP : cytosine triphosphate

Cys : cysteine

D-2-HG : D-enantiomer 2-hydroxyglutaric acid

D-PBS : Dulbecco's phosphate-buffered saline

DAD : diode array detector

DEA : diethanolamine

DMEM : Dulbecco's modified eagle medium

DNA : deoxyribonucleic acid

ELISA : enzyme-linked immuno-sorbent assay

ER : endoplasmic reticulum

ESCRT : endosomal sorting complex required for transport

ESI : electrospray ionization

EV : extracellular vesicle

F6P : fructose 6-phosphate

FBS : fetal bovine serum

G6P : glucose 6-phosphate

GABA : gamma-aminobutyric acid

GC/MS : gas chromatography/mass spectrometry

GDP : guanosine diphosphate

Gln : glutamine

Glu : glutamic acid

GLUT1 : glucose transporter 1

Gly : glycine

Gly-Gly : glycylglycine

Gly-Leu : glycylleucine

GM130 : golgin A2

GTP : guanosine triphosphate

HDL : high density lipoprotein

HESI : heated electrospray ionization

HIF : hypoxia inducible factor

HILIC : hydrophilic interaction chromatography

HMDB : human metabolome database

HPLC : high-performance liquid chromatography

HRP : horseradish peroxidase

HSP90B1 : heat shock protein 90 beta family member 1

HSPA5 : heat shock protein family A (hsp70) member 5

HT29-CD63-Nluc : HT29 ectopically expressing CD63-Nanoluc

IC-MS : ion chromatograph-mass spectrometer

ICAM-1 : intercellular adhesion molecule 1

IDH : isocitrate dehydrogenase

IgG : immunoglobulin G

Ile : isoleucine

ILVs : intraluminal membrane vesicles

IMMT : inner membrane mitochondrial protein

ISEV : international society for extracellular vesicles

KDMs : histone lysine demethylases

KOH : potassium hydroxide

L-2-HG : L-enantiomer 2-hydroxyglutaric acid

LC-MS : liquid chromatograph-mass spectrometer

LDL : low density lipoprotein

Leu : leucine

mAU : milli arbitrary unit

MeOH : methanol

miRNA : micro ribonucleic acid

MRM : multiple reaction monitoring

mRNA : messenger ribonucleic acid

MS : mass spectrometry or mass spectrometer

MVBs : multivesicular bodies

MYC : myc proto-oncogene protein

NF-κB : nuclear factor-kappa B

NMR : nuclear magnetic resonance

nSMase : neutral sphingomyelinase

NTA : nanoparticle tracking analysis

P2RX7 : purinergic receptor P2X 7

PC1 : first principal component

PC2 : second principal component

PCA : principal component analysis

PCR : polymerase chain reaction

PES : poly ether sulfone

PHDs : prolyl hydroxylases

Phe : phenylalanine

PRM : parallel reaction monitoring

Pro : proline

PVDF : poly vinylidene fluoride

RCF : relative centrifugal force

RLU : relative light unit

RNA : ribonucleic acid

RPL27 : ribosomal protein L27

RPMI : Roswell Park memorial institute

S7P : sedoheptulose 7-phosphate

SCF : supercritical fluid

SD : standard deviation

SEC : size-exclusion chromatography

sEVs : small extracellular vesicles

SFC : supercritical fluid chromatography

SFC-QqQMS : supercritical fluid chromatography-triple quadrupole mass spectrometer

SFC-MS : supercritical fluid chromatograph-mass spectrometer

TCA : tricarboxylic acid

TEM : transmission electron microscopy

TETs : ten-eleven translocations

TF : tissue factor

Thr : threonine

TIM4 : T-cell immunoglobulin and mucin domain-containing protein 4

Tomm20 : translocase of outer mitochondrial membrane 20

TP : thymidine phosphorylase

Trp : tryptophan

TSG101 : tumor susceptibility 101

TSPAN8 : tetraspanin 8

UC : ultracentrifugation

UCA1 : urothelial cancer associated 1

UDP : uridine diphosphate

UMP : uridine monophosphate

UTP : uridine triphosphate

Val : valine

VLDL : very low density lipoprotein

WCL : whole cell lysate

WT : wild type

α-KG : α-ketoglutaric acid

Supplementary material

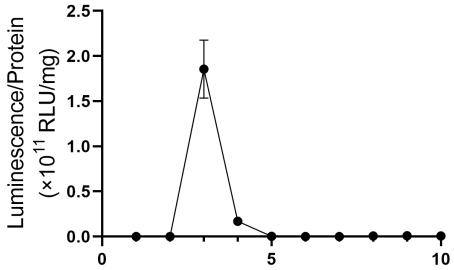

Figure S3-1. The relationship between proteins and CD63 in sEVs isolation using SEC.

The relationship between proteins and CD63 when one fraction is collected every 2.5 minutes using SEC. The vertical axis indicates the amount of CD63 per mg of protein. CD63 was quantified using Nanoluc-based luminescence.

Table S2-1. List of metabolites detected only in sEVs.

Metabolite	KEGG Pathway
Inosine	Purine metabolism
N,N-dimethylglycine	Glycine, serine, and threonine metabolism
Cytidine	Pyrimidine metabolism
Uridine	Pyrimidine metabolism
Guanosine	Purine metabolism
Citrulline	Arginine biosynthesis
Hypoxanthine	Purine metabolism
Gly-Leu	—
Xanthine	Purine metabolism
Hexylamine	—
2-Deoxyribose 1-phosphate	Pyrimidine metabolism, Pentose phosphate pathway

Table S2-2. The KEGG pathways associated with top 20 hydrophilic metabolites in cells and sEVs under normoxia.

	Cells		sEVs	
Rank	Metabolite	KEGG pathway	Metabolite	KEGG Pathway
1	Phosphorylcholine	Glycerophospholipid metabolism, Choline metabolism in cancer	Phosphorylcholine	Glycerophospholipid metabolism, Choline metabolism in cancer
2	Glutathione (reduced)	Glutathione metabolism, Cysteine and methionine metabolism	Glycerophosphorylcholine	Glycerophospholipid metabolism, Choline metabolism in cancer
3	Glu	Alanine, aspartate, and glutamate metabolism	Arg	Arginine and proline metabolism
4	Ethanolamine phosphate	Glycerophospholipid metabolism	Glu	Alanine, aspartate, and glutamate metabolism
5	Glycerophosphorylcholine	Glycerophospholipid metabolism, Choline metabolism in cancer	Lys	Lysine biosynthesis
6	Asp	Alanine, aspartate, and glutamate metabolism	Ethanolamine phosphate	Glycerophospholipid metabolism
7	Gln	Alanine, aspartate, and glutamate metabolism, Central carbon metabolism in cancer	Inosine	Purine metabolism
8	Gly	Glycine, serine, and threonine metabolism	UDP-*N*-acetylglucosamine	Amino sugar and nucleotide sugar metabolism
9	Pro	Arginine and proline metabolism	ADP	Oxidative phosphorylation, Purine metabolism
10	Lactic acid	Glycolysis, Gluconeogenesis, Central carbon metabolism in cancer	Gln	Alanine, aspartate, and glutamate metabolism, Central carbon metabolism in cancer
11	ATP	Oxidative phosphorylation, Purine metabolism	Glucose 1-phosphate	Glycolysis, Pentose, and glucuronate interconversions
12	Gly-Gly	—	Ala	Alanine, aspartate, and glutamate metabolism, Cysteine and methionine metabolism
13	Asn	Alanine, aspartate, and glutamate metabolism	GDP	Purine metabolism
14	*N*-Acetylaspartate	Alanine, aspartate, and glutamate metabolism	UMP	Pyrimidine metabolism
15	UDP-N-acetylglucosamine	Amino sugar and nucleotide sugar metabolism	*N*,*N*-dimethylglycine	Glycine, serine, and threonine metabolism
16	UTP	Pyrimidine metabolism	UDP-glucose	Pentose and glucuronate interconversions
17	Citric acid	Citrate cycle (TCA cycle), Central carbon metabolism in cancer	Gly	Glycine, serine, and threonine metabolism
18	Creatine	Glycine, serine, and threonine metabolism, Arginine and proline metabolism	Cytidine	Pyrimidine metabolism
19	beta-Ala	beta-Alanine metabolism, Propanoate metabolism	Uridine	Pyrimidine metabolism
20	Malic acid	Citrate cycle (TCA cycle), Central carbon metabolism in cancer	UDP	Pyrimidine metabolism